NOVEL METHODS FOR

REGISTRATION OF BINARY IMAGES

A Thesis

Presented in Partial Fulfillment of the Requirements for

the degree Of Ph.D in the

Graduate School of The University of Sheffield

by

Panagiotis Kotsas, M.Sc.

* * * * *

The University of Sheffield

2014

Ph.D Committee

Approved by:

____

Adviser
Department of Automatic Control and
Systems Engineering

THESIS ABSTRACT

THE UNIVERSITY OF SHEFFIELD
GRADUATE SCHOOL

NAME: Kotsas, Panayiotis **YEAR:** 2014

DEPARTMENT: Automatic Control and Systems Engineering **DEGREE:** Ph.D

ADVISER'S NAME: Tony J. Dodd

TITLE OF THESIS: Novel Methods for Registration of Binary Images

A novel signal intensity independent technique for two and three-dimensional image registration based on binary areas and lines was developed and tested using T1- , T2-weighted Magnetic Resonance image, CT and SPECT studies of the head. The 3D method uses the fuzzy c-means classification algorithm for outlining the registrable areas and then minimizes iteratively the mean squared value of the voxel per voxel weighted ratio of the two trilinearly interpolated cubic voxel volumes. Numerous experiments were performed for 2D and 3D rigid registration using binary areas, for non rigid registration using an elastic model, for 2D registration using projective geometry with 1D lines, for 3D registration using projective geometry with binary 2D areas, for hierarchical registration of MR , CT and SPECT images, for registration of reduced dimension images using the common cut registrable area. The experiments showed that: the method gives average accuracy better than 0.5 degrees and 0.5 voxels, does not converge to local minima, compares favorably to Mutual Information methods, it is not affected by noise and can be implemented as surface based, it minimizes interpolation for 2D registration using 1D projections, it is signal intensity independent, it can be implemented with reduced dimension line cut images.

To my family

ACKNOWLEDGEMENTS

My appreciation goes to Dr Tony J. Dodd who helped me correct and put together the Ph.D. document. I also want to express my thanks to the other members of the Department of Automatic Control and Systems Engineering for offering me a comfortable working program.

I want to express my gratitude to Dr. David W. Piraino whose enthousiastic guidance, innovative spirit, and engineering insight, inspired me throughout the course of this work. My appreciation goes also to Dr. J.Fredrick Cornhill for his very useful suggestions and comments. I also want to thank Ms. Christine Kabrera whose comments improved dramatically this document. Very important was the help that I received during the data collection procedures from Mr. Vassilis Gougoulidis and Mr. Dominik Meyer, I am thankful to them. The conversion of the ACR-NEMA 2.0 imaging format was made possible due to the use of the STACR utility, programmed and provided to me by Dr. Rim Cothren from the Department of Biomedical Engineering of the Cleveland Clinic Foundation, I am grateful to him. I would also like to express my gratitude to all the members of the Graduate Studies Committee of the Department of Biomedical Engineering of the Ohio State University for giving me the opportunity to study in the United States. Finally, my most sincere gratitude goes to my son Dimitris, my wife Vangelio, my parents and my sister Popi for encouraging me.

TABLE OF CONTENTS

CHAPTER I

INTRODUCTION

1.1 Medical image registration

In the field of digital image processing, image registration is the process of using electronic hardware to geometrically align two images so that corresponding voxels/pixels can be superimposed on each other. The necessity of the image registration step can be assessed if you consider two images of the same subject taken under different imaging conditions in space and time. The adjustments needed to be made prior to the comparison of the two images are included in the image registration process. These adjustments comprise a set of image processing methods which include thresholding, segmentation, fuzzy classification, geometrical aligning in rigid and non rigid form. The dimension space of the adjustments could be 1D, 2D or 3D. The speed of the image registration algorithms defines the time variable related to the shape and volume of the object to be registered. There are several applications of image registration [1]. Examples include remote sensing, medicine, cartography, and computer vision.

In the medical field, image registration is used for diagnostic purposes when images of the same anatomical structure must be superimposed on each other. Medical imaging modalities (Computed Tomography, Magnetic Resonance, Positron Emission Tomography, Single Photon Emission Computed Tomography) provide information that illustrates human brain anatomy and function. This information is often complementary and its correlative use can improve diagnostic accuracy. Registration methods are used for combining computer tomography (CT) and magnetic resonance imaging (MRI) data to obtain more complete information about the patient, for monitoring tumor growth, for treatment verification, for comparison of the patient's data with anatomical atlases [1]. Bone calcifications are seen best on CT images, while soft tissue structures are differentiated better by MR [2]. Registration techniques make it possible to superimpose features from one image study over those of another image study from a different modality. These techniques can also be applied to studies of the same modality taken at different times so that point-by-point arithmetic operations such as image averaging, subtraction and correlation can be performed [3]. In cases of mental diseases the registration techniques apply to patients under extreme stress where the single examination within the MR machine is not always feasible. The head of the patient even with the use of a mask is not always still during the examination. The medical staff has to choose the correct images or transfer the exam when the patient is tranquilized which is a source of fear.

Image registration is often a necessary procedure. It is used to merge images from different imaging modalities and different examination dates and therefore it is useful for diagnosis and assessment of disease progression or remission. Different imaging modalities provide complementary information and when the images are aligned and merged, this information is added to give a more clinically useful result. In another type of application the progression of a disease over time can be assessed by registering images of the same patient from two different examination dates. For example, after registration, measurements of a tumor growth can be made.

According to Evans et al. [4], image registration has found use in the areas of:

1) disease diagnosis
2) longitudinal monitoring of disease progress or remission
3) preoperative evaluation and neurosurgical planning
4) image guided neurosurgery
5) radiotherapy and radiosurgery treatment planning
6) functional neuroanatomy of sensorimotor and cognitive processes
7) morphometric analysis of neuroanatomic variability.

For example, the merging of fine anatomic detail from MR images of the brain with functional PET images allows the measurement of regional cerebral function [5]. Likewise, MR and CT images describe complementary morphologic features.

In recent years there has been a rapid growth of neurological applications of medical image registration with applications that address both diagnosis and therapy. Registration is progressively playing a larger role in image interpretation in many different procedures.

In this thesis a novel approach to image registration based on binary image information drawn from medical images is presented. We have categorized the image registration methods and the categories are presented in the next section with various image registration criteria.

1.2 Categories of image registration methods

1.2.1 Categories based on theoretical criteria

The majority of image registration methods are based on the use of a similarity/disparity criterion which, when the two images are brought to register, is maximized/minimized. Numerical analysis techniques are used to maximize/minimize the similarity/disparity criterion. There are many different criteria, with Mutual Information (MI) being the standard since it is quite accurate for rigid body registration and does not require any image segmentation prior to registration.

Image registration is an active research field and in recent years image registration methods have evolved from the research setting, to being incorporated into clinically useful software tools [6]. The image registration methods can be in general divided into rigid and non-rigid. Rigid registration techniques adjust for rotations and translations only (six parameters for the 3D case). This is the case with rigid brain scans. Non-rigid techniques assume a nonlinear transformation model and can adjust for image warping. Warping occurs usually due to the soft tissue deformations of the body organs between different scans [6]. Medical image registration techniques are also categorized according to the type of features they use for registration. Surface-based techniques rely on the characteristics of the surface of the registrable objects while volume-based techniques use the full volume information. West et al [7] define as volume-based "any technique which performs registration by making use of a relationship between voxel intensities within the images and as surface-based, any technique which works by minimizing a distance measure between two corresponding surfaces in the images to be matched". According to Slomka et al. [6] volume- or voxel-based techniques are more robust and accurate because they do not rely on the preprocessing of the images for being accurate. This is especially the case for the MI methods. These methods rely on maximizing the amount of information sharing between the two images to be registered. According to Bardera [8] "MI methods have become a standard reference due to their accuracy and robustness." In Liao et al [9] surface matching and MI methods are compared and the conclusion is that the surface matching registration algorithms could be followed by a few iterations of a MI algorithm for better accuracy. Improvement of the standard MI algorithms is an active research field and the effort is to use a combined approach that does not rely on voxel values only, but incorporates geometrical or regional features for computation of the MI [8,10,11,12,13].

The type of problem which is solved by the registration algorithm is another categorization criterion. The methods may be suitable for image-to-image space registration (3D-3D, 2D/3D) or physical to image space registration. 3D-3D methods register image volumes to image volumes (MR-MR, CT-MR, (positron emission tomography) PET-MR, Ultrasound-MR) [6,7,14]. 2D/3D registration techniques register, for example, one or more intraoperative X-ray projections of the patient and the preoperative 3D volume [15,16]. Physical to image space registration is similar to 2D/3D registration but may use interventional techniques like bone-implanted markers for patient to image registration [17].

In this thesis we follow a novel approach to the medical image registration problem. We propose, test and compare to the standard MI methods a method which uses binary projections of the 2D or 3D images for the computation of the registration function.

Several methods for medical image registration have been proposed. There are device-based methods and feature-based methods. The device-based methods use head-holding devices that keep the patient's head at a fixed orientation and/or external fiducial markers visible in both image sets. The fiducial marker coordinates are used to estimate the geometric transformation that establishes a one-to-one mapping between the two image spaces. These methods are non-automated, technically demanding and require a significant amount of effort at the time of each scan [18,19]. Furthermore they have been found to be less accurate than feature-based techniques. Strother et al. [20] compared the accuracy of a fiducial marker system with the accuracy of feature-based techniques and reported that “it is not possible to fix the head accurately enough relative to external fiducial markers to obtain registration results as good as those obtained by non-fiducial techniques.”

Feature-based methods use the anatomic information inherent in the two image sets. These techniques follow a general methodology with four steps [39]:

a) extraction of features in each image

b) pairing of these features

c) choice of geometric transformation and estimation of its parameters

d) application of this transformation.

Feature-based techniques do not require any special procedures or devices at imaging time and may be applied retrospectively [18,19]. The extraction of the anatomic features can be performed either manually with the assistance of an expert user [21] or automatically. For example, in the interactive method developed by Kapouleas et al. [21], the user is asked to specify the interhemispheric fissure plane in three dimensions for both image volumes by specifying its endpoints in every axial MR section. The planes are then used to align the image volumes. The disadvantages of this method are that it requires a large amount of time from the user (1 hour per registration case) and also that the registration accuracy is affected by the user’s performance.

Three different types of automated feature-based techniques can be defined when they are classified according to the type of the anatomic features they use [22]. Correlation methods make use of the voxel intensity distributions; the principal axes method makes use of the spatial moments of the three-dimensional volumes or surfaces; and the surface fitting method uses the anatomic surfaces in the two image volumes. Automated registration methods can also be categorized according to their ability to perform cross-modality image registration. Correlation methods are not able to register image studies from different modalities because the signal intensity distributions differ. Principal axes and surface fitting methods use the shape characteristics of the two image volumes that are not affected by the difference in signal intensity distributions and therefore these two methods are able to perform cross-modality registration.

Another classification criterion is the dimensionality of the registration problem. Two-dimensional registration methods assume only in-plane displacements and adjust for one rotational and two translational parameters, whereas three-dimensional methods adjust for three rotational and three translational parameters. For example, in the case of digital subtraction angiography, a major problem concerns the movements of the patient, which diminish the benefit of the subtraction procedure [23]. X-ray images capture in-plane motion and therefore the registration problem is two-dimensional. On the other hand, the motion of the patient's head inside the MR imaging machine is captured by the three-dimensional imaging system and therefore the registration algorithms that deal with MR data are three-dimensional.

The way that the geometric transformation parameters are estimated can also be used to discriminate registration methods. The principal axes method gives a closed form solution to the registration problem, whereas the correlation and surface fitting methods solve the problem iteratively.

1.2.2 2D/3D Image registration

2D/3D registration is a special case of medical image registration which is of particular interest to surgeons. According to [15] "the 2D/3D registration can be a means to noninvasively register the patient to an image volume used for image-guided navigation by finding the best match between one or more intra-operative X-ray projections of the patient and the preoperative 3-D volume". Applications of 2D/3D registration are [15] radiotherapy planning and treatment verification, spinal surgery, hip replacement, neurointerventions and aortic stenting.

With the help of 2D/3D registration methods surgical robots may be programmed using a pre-surgical 3D dataset and a set of intraoperative fluoroscopic X-ray images. In this way, there is no need for fiducial markers. Gueziec et al [25] use such an approach for CT-X-ray registration with the use of the bony anatomy for robot navigation. Specific applications for spinal surgery are presented by Kraats et al [15], Tomasevic et al [151], Penney et al [152], Russakov et al [26]. They use vertebrae bodies, spine segments or spine phantoms and register CT/MR volumes to intra-operative X-Ray images.

In a neuroradiological context Vermandel et al [27] present a method for 2D/3D medical image registration which facilitates the use of Digital Subtraction Angiography (DSA) images for treatment and diagnosis. They report that their method can be used during the treatment of Aneurysms. Aneurysms, after their initial treatment have to be followed up for several years with the use of Magnetic Resonance Angiography(MRA)/DSA images. The matching procedure is usually "mental" but an automatic 2D/3D registration method would facilitate the matching and give a "more objective and more accurate monitoring of the pathology". A similar imaging procedure with the use of MRA/DSA images is followed for the treatment planning of arteriovenous malformations. These images are obtained with a stereotactic frame. According to [27] 2D/3D registration could "enable to avoid the stereotactic X-ray examination by using the first DSA examination obtained during the diagnosis step".

A similar application of 2D/3D registration is presented by Byrne et al [28]. The only difference is that they register 3D DSA with 2D DSA images.

In a radiological context, Baert et al [29] use 2D/3D registration methods for guide wire display in endovascular interventions. They report that "during endovascular interventions, it is important for the radiologist to accurately know the 3D position of the guide wire at any time during the procedure". The problem they try to solve with the 2D/3D registration method is the establishment of the position of the guide wire relative to the 3D imaging system. They try two approaches in order to meet this goal. In both approaches they use a pre-calibrated motorized X-ray angiography system to get a 3D reconstruction of the vasculature immediately prior to the intervention. The guide wire is tracked in the biplanar fluoroscopic images and its position is reconstructed in 3D. The main difficulty is that "in order to produce a 3D reconstruction of the guide wire and relate it to the 3D coordinate system of the 3D vascular data, accurate knowledge of the C-arm geometry is required". In the first approach the system geometry is estimated in a pre-calibration step that only has to be carried out once. The disadvantage of the method is that "to maintain the relation between the 3D vascular data and the projection images, the patient should be stabilized or tracked during the intervention." In the second approach 2D/3D registration methods are used to relate the 3D vascular data to projection images. This is called image based calibration.

A similar type of application in neurosurgery is presented by Mc Laughlin et al [30] and Masutany et al. [31]. According to [30] "the registration of 2D/3D data sets is important in minimally invasive neurointerventions, such as the coiling of brain aneurysms or glueing of arteriovenous malformations (AVM)". During such interventions a catheter is guided through the brain vasculature using 2D X-ray images. In order to navigate and position the catheter accurately a pre-operative MRA 3D scan is registered to the 2D X-ray images. Various methods for 2D/3D medical image registration exist. According to Kraats et al [15] they can be divided into feature based, signal intensity based, gradient based and hybrid. The results presented usually estimate the accuracy of the registration methods by comparing it with a gold standard. We will present a demo in order to show a 3D medical imaging tool for manipulation of stereo and 3D medical images using 2D images. The main tool that will be presented is a head tracker for manipulation of 3D medical images in mono or stereo mode that can be used by a surgeant or physician to take in a hands-free way different mono or stereo views of volumetric medical image data. Two different kind of tools will be presented. The tools created by the Medical Image Processing Group of the University of Pennsylvania [32] are being distributed with the 3D Viewnix Medical Image Processing Software System and also the tools for stereo and 3D medical image processing written at the Information Processing Laboratory and incorporated in the 3DViewnix System using the X- Windows based libraries provided by MIPG. A short description of the tools presented is presented in chapter 4: (for tools provided by the MIPG some of the images and text are based on the 3DViewnix tutorial and user manual).

1.2.3 Non Rigid Registration

The non rigid registration approach deals with the warping met in images and cannot be faced with the translational and rotational adjustment of the rigid case. The methods are divided into parametric and non parametric [33]. The effort of the parametric methods is to reduce the number of degrees of freedom for the definition of the energy term of the registration problem. Instead of defining a displacement vector for each vector parametric methods define a set of basis functions (like B-Splines) which deal with the non rigid registration problem. The functions may have global or local support and define the limitations on the solution of the problem. The application of global models is more limited to the accuracy of the solution of the problem. Non parametric methods do not apply parametrization of the registration energy function. The registration function is continuous and a regularization term is applied at the model. In another approach called the demons method a low pass filter is applied to the displacement. This approach maintains better the information required after the registration is applied compared to global parametric methods. In this thesis we will present a method for non-rigid registration using a local parametric method for binary images derived from warped medical images of the head. This is a result based approach which will show that the registration method is able to adjust for large non rigid transformations.

1.3 Our approach for image registration

The necessity of image registration can be assessed if you consider images of the same subject taken under different imaging conditions in space and time. The adjustments needed to be made prior to the comparison of the two images are included in the image registration process. There are several applications of image registration. Examples include remote sensing, medicine, cartography, and computer vision.

In medicine the information of images from different modalities is often complementary and its correlative use can improve diagnostic accuracy. With image registration it is possible to superimpose features imaged by studies from different modalities. In recent years there has been a rapid growth of neurological applications of medical image registration for both diagnosis and therapy. Image registration is an active research field and in recent years image registration methods have evolved from the research setting, to being incorporated into clinically useful software tools. As described in section 1.2 image registration methods can be categorized according to the :

- Similarity function they use
- Iterative or closed form solution
- Rigid or Non Rigid
- Type of feature used for registration
- Type of problem solved with regards to dimensionality
- Device based and feature based

The goal of this work is to develop and test a registration solution that will be able to address different forms of the registration problem using a common registration logic. The common logic is to use a simple registration criterion which utilizes minimal information. Mutual information methods as they have been implemented in the State of the Art do not differentiate in application the quality of the information systems that should be used. High quality information applications must be imposed with Mutual Information in order to avoid war like solutions which can occur in hospitals in developing countries in medical imaging. This is not always possible.

We also implement a novel and easy to understand iteration loop which, in comparison to other minimization techniques, makes it easier to register images with less information used. In this context, the motivation is the need to produce a well engineered registration system of methods for 3D to 3D rigid body binary image based registration (volume and projection based), 2D/3D binary area based registration and non rigid body binary area based registration. By well engineered we mean that we will be able to address the main registration algorithm problems which are accuracy, convergence, time and comparisons with other methods. For accuracy we want to research the goodness of the registration algorithm convergence criterion in relation to the accuracy desired and the data set used. We found that the method gives registration accuracy below 0.5 degrees and 0.5 voxels for rigid registration independent of the signal intensities information.

For convergence in the case of binary projections the method converges to stable final positions independent of the initial misregistration. For time the method is generally fast. For example we are able to find out how many iterations have to be taken for the registration algorithm to converge. The application of 2D registration using 1D xy projections to rectangular shapes is faster than Mutual Information methods. For medical images the method has similar time performance with the Mutual Information Methods but gives much less burden to the cpu for the computations. Compared to Mutual Information methods the method performs more accurate and robust for rigid registration and does not converge to local minima for rigid and non rigid registration.

The Novel contributions of this thesis are:

- We introduce a registration function which works efficiently with volumes, areas (large or small), rigidly or non rigidly, with 1D (lines) and 2D (area) projections. The weigthed ratio image criterion improved the Woods ratio registration criterion.
- We introduce a Novel algorithm which iteratively deregisters and brings back into registration the images using the Chebyshev polynomial functions. The algorithm

improved in application the Powell or the simulated annealing method because it does not converge with local minima. Convergence in some types of registration problem is faster than mutual information methods. The method converges in rectangular frames of images faster than the mutual information method.

- We use classification and segmentation methods in order to exploit the areas of image with greater information content. Concentrating on the areas of interest is an idea which comes from wavelet compression methods and makes the method more able to work with artifacts and noise.
- Accuracy with the use of projections is better than Mutual Information methods. We have made comparisons with the Mutual Information method and found that the accuracy is better than 0,5 degrees and 0,5 voxels. This result stands even with the use of reduced dimension images. We have applied the method hierarchically and with the use of reduced dimension images and we were able to maintain accuracy in a large number of experiments.
- The volume based 3D registration method works efficiently with the presence of noise. This is because because the main information content which relates to the registration function is from the region of interest.
- The area based technique has been applied for rigid and non rigid registration. In non rigid registration the order of the Chebyshev points computation can be changed locally is small local areas and give controlled registration results.
- The method with 1D lines projections is faster than Mutual information for square and rectangular objects since only x and y projections are used. The method for medical images has improved the principal axes method.

1.4 Overview of the thesis

The rest of this thesis presents 2D rigid registration of MR scans using binary areas, 3D registration using binary volumes, 2D registration using 1D binary projections, 3D registration of MR volumes using 2D binary projections, 2D registration of reduced dimension images using 1D binary projections, 2D/3D alignment of stereoscopic images using a binary 2D area on the forehead, and non-rigid registration of binary area images.

In Chapter 2 we provide the theoretical literature aspects of the thesis. We have focused on the theory regarding the similarity functions which are used in order to solve the image registration problems. We are also presenting recent applications of image registration and the way they are implemented in everyday clinical practice.

In Chapter 3 the algorithm for medical image registration with the use of binary images and volumes is presented. The chapter contains the description of the fuzzy classification algorithm, the logic of the registration function, the iteration loop and the protocols for the experiments in order to evaluate the accuracy.

In Chapter 4 we present the experimental results of the algorithm in Chapter 3. We have performed a large number of experiments and put the algorithm in the stress of testing with reduced resolution. We have also focused on the worst case results and found that the method is accurate within 1 degree and 1 voxel.

In Chapter 5 we present methods for registration with the use of binary 1D and 2D projections. Using 1D lines leaves the image information content intact. 2D projections prepare the algorithm for use with the 2D-3D registration type of problems.

In Chapter 6 the technical description of the performance of the method when it is implemented in digitized radiography, hierarchically, non rigidly and with reduced dimension images is presented. These are applications of various registration problems of the head and the knee in their initial form.

Finally in Chapter 7 we present the conclusions and the discussion for future work.

CHAPTER 2

THEORETICAL ASPECTS OF LITERATURE IN IMAGE REGISTRATION

Medical imaging modalities (Computed Tomography, Magnetic Resonance, Positron Emission Tomography, Single Photon Emission Computed Tomography) provide information that illustrates human brain anatomy and function. This information is often complementary and its correlative use can improve diagnostic accuracy. For example, the merging of fine anatomic detail from MR images of the brain with functional PET images allows the measurement of regional cerebral function [5]. Likewise, MR and CT images describe complementary morphologic features. Bone calcifications are seen best on CT images, while soft tissue structures are differentiated better by MR [2].

Medical image registration is the procedure of geometrically aligning two image volumes so that voxels representing the same anatomical structure may be superimposed one on another [20]. Registration techniques make it possible to superimpose features from one image study over those of another image study from a different modality. These techniques can also be applied to studies of the same modality taken at different times so that point-by-point arithmetic operations such as image averaging, subtraction and correlation can be performed [3].

The categorization of medical image registration methods has been presented in chapter 1. The literature focuses on the solution of a wide range of problems for the solutions to be applied for 2d/3d, rigid, non rigid image registration. Most of the methods used are utilizing a registration function that will be used by the algorithm in order to bring the images into register. These methods are known as feature based techniques. The theoretical aspects that relate to the feature based techniques registration functions selection will be discussed in this chapter. The information content of the images and how can it be utilized and ranked is also a subject of the registration function selection procedure. Signal based methods use the full information content of the images but have drawbacks with regards the reliability and the application to multimodal image registration. Surface based methods have significant merit mainly because of the high sophistication of the techniques but are viable to noise. The use of the joint histogram which is a binary image is giving the Mutual Information methods the ability to work with noisy images without classification.

The rest of this chapter will provide an overview of the main existing automated, feature-based registration techniques. The principles, the accuracy and the literature applications of the correlation, surface fitting, principal axes and mutual information methods will be presented.

2.1 Correlation methods

Correlation methods register medical images by maximizing a similarity or minimizing a disparity criterion between the images. The similarity or disparity criterion used is signal intensity based, and it is maximized or minimized iteratively. Correlation methods are limited in their application because they require that the images be from the same modality. Some of the criteria proposed [23,34] require that the signal intensity distributions be exactly the same. When this does not happen, signal intensity scaling is considered as an additional parameter to be adjusted within the iteration loop. A correlation criterion that was applied by Woods et al. [35,36] for MR-PET image registration is the ratio image uniformity criterion. This application involves a preprocessing step during which the images are segmented to create the same types of anatomic regions and therefore the same signal intensity distributions. Various criteria have been proposed in the literature. The most important ones are:

a) Cross-correlation coefficient [37]
b) Stochastic sign change [23,34]
c) Maximum region overlap [38,39]
d) Ratio image uniformity [35,36]

The methods that are based on correlation criteria is an active research field. In [40] the sum of absolute differences of the pixel signal intensity values is used for 2D/3D registration. 2D to 3D registration matches two dimensional images (generated artificially or using medical procedures like histological section images) to three dimensional volume images (using MRI). Deformations due to tissue shift , breathing or heart motion make the problem non rigid and challenging. The authors [40] use a graph approach with Markov Random Fields which register in plane the 2D image non rigidly and locate the plane that the 2D image corresponds in the 3D volume using a regularization term. The non rigid registration is performed using the sum of absolute differences similarity measure. The regularization term works by using the distances of points after imposing the co-planar constraint in order to maintain the form of the grid. The results for registrations show errors of less than 0.74 degrees and 1 mm.

2.1.1 Cross-correlation coefficient

The cross-correlation coefficient for two images A and B is given by [37]:

$$r = \frac{\sum_i (\mathrm{A}_i - \overline{\mathrm{A}})(\mathrm{B}_i - \overline{\mathrm{B}})}{\sqrt{\sum_i (\mathrm{A}_i - \overline{\mathrm{A}})^2 \sum_i (\mathrm{B}_i - \overline{\mathrm{B}})^2}} \tag{2.1}$$

where i is an index to the image A and image B voxels and $\overline{\mathrm{A}}, \overline{\mathrm{B}}$ are the mean intensity values of the images over the whole voxel area. Junck et al. [37] use this coefficient for two-dimensional alignment of PET scans. They show that the maximum location of the cross-correlation coefficient is the same as the maximum location of the cross-product coefficient $\sum_i \mathrm{A}_i\ \mathrm{B}_i$. Therefore they maximize the criterion by computing the cross-product value for the whole range of the geometric transformation parameters using steps of $\Delta\vartheta = 1$degree for rotations and $\Delta\chi = \Delta y = 1$voxel for translations. To achieve better accuracy, they fit a quadratic function in $\Delta\chi$,Δy and $\Delta\vartheta$ to the cross-product data and find its peak. The peak position is recalculated after each translational and rotational correction of one image relative to another. The accuracy of the method is defined as the standard deviations of the transformation parameters among five different levels of the patient's head: 0.54 mm for x and y translations and 0.8 degrees for xy plane rotation [37].

2.1.2 Stochastic Sign Change

The stochastic sign change criterion proposed by Venot et al. [23] is defined as "the number of sign changes in the sequence of the values of the difference image." In order to understand the rationale of the use of this similarity measure, consider two images A(i,j) and B(i,j) ,where i and j are the indexes to the image voxels as a two dimensional array, of the same object and the same modality that are registered to each other. If we assume that the signal intensity distributions are identical, then the difference image D(i,j)=A(i,j)-B(i,j) will take values equal to the noise measurement differences. If we also consider the noise as additive, zero mean with a symmetric density function, then we find that the difference image values are either positive or negative and there are many sign changes in the sequence of D(i,j) because there is an equal probability of 0.5 for each sign + or -. When the two images are not registered, the difference image takes values equal to the differences of the signal intensity distributions. These differences are greater than the noise measurement differences, and therefore the sign changes number reduces. The maximization of the number of sign changes can be performed iteratively using the Simplex optimization technique [34,41].

It is obvious that the method may fail when the signal intensity distributions are not strictly identical. Gerlot-Chiron and Bizais [38,39] reported that "computing the number of sign changes in the difference image corresponds to computing the number of registered pixels only if the expected difference is zero for these pixels." Venot et al. [23] and Herbin et al. [34] solved this problem by using intensity scaling as an additional parameter to be adjusted by the method.

The Sign Change criterion was applied by Venot et al. [23] for two-dimensional translational adjustment of X-ray digitized images for improving the quality of subtraction angiographic images. It was also applied by Herbin et al. [34] for rotational and translational adjustment of digitized video medical images. In both of these studies, no quantitative measure of the accuracy of the method is given. Results are given only for a few example registration cases. In such a case of translational adjustment of x-ray images presented by Venot et al. [23], the Sign Change criterion was compared to the Correlation Coefficient criterion and was found to be more accurate.

2.1.3 Maximum Region Overlap

The Maximum Region Overlap criterion was introduced by Gerlot-Chiron and Bizais [38,39]. It aims at maximizing the overlap of the registrable areas in the two images. The method is based on the idea that the histogram of the difference image exhibits a low signal-intensity peak caused by the registered voxels in the two images. The shape of this peak is related to noise statistical properties. The area of this peak becomes maximum when the two images are registered. The algorithm aims at maximizing the peak area of the histogram, which is computed for all the possible values of the geometric transformation parameters using a matched filter:

$$RO(p)=\sum_{i=-n}^{n} a(i)\, h(i+p) \qquad (2.2)$$

where a(i) is a Gaussian matched filter impulse response $G(0,\sigma)$, h is the histogram distribution of intensity in the difference image and p is the location of the peak of the registered voxels area of the histogram. The filter was chosen to be Gaussian because noise can be considered Gaussian in most medical imaging applications [38,39].

According to Gerlot-Chiron and Bizais [38], the method can be considered as a generalization of the Sign Change criterion for the case that the signal-intensity distributions in the two images are not identical. The method was used for two-dimensional translational adjustment of lung scintigrams. In order to test the performance of the method, white and colored noise was added to the images. The error was estimated as the difference of the applied geometric transformation from the estimated one. The errors were zero for both cases of white and colored additive noise.

2.1.4 Ratio image uniformity

The ratio image uniformity criterion was introduced by Woods et al. [35,36]. To align the two images, the algorithm calculates the ratio of one image to the other on a voxel-by-voxel basis and then iteratively minimizes the variance of this ratio. The method is based on the ideal assumption that in the case that the images are registered, the values of the voxels in one image, can result by multiplying the voxels in the other image with a constant multiplicative factor. When the images are not registered, the value of the multiplicative factor varies from voxel to voxel, creating a large variance of the ratio image values.

The method uses an iteration loop based on derivatives to minimize the variance of the ratio image, which is defined as the registration function. With each iteration, the first partial derivative of the registration function with respect to each of the transformation parameters is calculated. The parameter with the largest first partial derivative is adjusted. The second partial derivative with respect to the selected parameter is then used to estimate the value of the parameter at which the first partial derivative will be zero with the Newton-Raphson method [41]. This value is used in the next iteration. Convergence is reached when all of the first partial derivatives get values below a threshold value.

The ratio image uniformity method was applied by Woods et al. [35] for alignment of functional PET three dimensional images. As mentioned above, a modified version of the algorithm [36] was applied for MR-PET registration. The investigators used the post-registration distance of external fiducial markers as a measure of the positional errors resulting from the registration procedure. They reported that the positional errors are less than 1.745 mm for PET-PET registration and less than 3 mm for PET-MR registration. These results are verified by Strother et al. [20], who applied the method for MRI-MRI, PET-MRI and PET-PET registration. They reported positional errors at the range of 1 voxel.

2.2 Surface fitting method

Surface matching methods register images by using the anatomic surface models of the two images. The most important method in this category is the surface fitting method developed by Pelizzari et al. [22,42] at the University of Chicago. The method is referred to as the "head and hat" method because it fits a set of points ("hat") extracted from contours in one image to a surface model ("head") extracted from contours in the other image . The surfaces are obtained by outlining contours on the slices of each image set, either manually or by using a semiautomatic edge detection algorithm . The head surface model is generated by the image that covers the larger area of the head or by the image with the higher resolution if the coverage of the head is comparable. The mean squared distance between the hat points and the head surface is minimized iteratively using a non-linear least-squares search technique introduced by Powell [41]. The distance is computed between the hat point and the intersection point of the head surface and the line that connects the hat point with the centroid of the head surface. A linear interpolation step between the head surface contours is needed for the computation of the intersection point. The iteration loop adjusts for xy,yz,zx plane rotations, x,y,z axes translations and x,y,z axes linear scaling. The algorithm allows operator intervention to prealign the surfaces to prevent the search from converging to a local minimum. The problem of local minima is inherent in non-linear least-squares minimization techniques [41].

The method was applied by Pelizzari et al. [42] for registration of CT, MR, and PET images. It was also modified to perform registration of image space to physical space [22]. This application involves the use of a digitizer that is able to acquire a three dimensional model of the patient's skin surface. The skin surface model is then registered to the image generated surface. The surface fit method has been used also by several other groups [43,18,44,20] who tried to evaluate its accuracy. Based on these studies the following points are of interest:

- For registration of MRI-PET images, the translational errors were found to be less than 2 mm in each direction and the rotational errors less than 2 degrees for each angle [18,44].

- For registration of MR to patient surface, the positional error is in the range of 3-8 mm [22].
- Missing data do not affect the accuracy of the method. For brain coverage as low as 40%, the registration position error remained less than 2mms in each direction [43].
- The degree of initial misangulation does not affect the accuracy of the method [43].
- The processing time is between 3 and 11 minutes, depending on the number of iterations [43].

In [153] the surface fitting methods are reported as a preprocessing step for signal intensity based criteria.

2.3 Principal axes method

The principal axes transformation is known from the theory of rigid bodies. A rigid body may be located using the position of the center of its mass and the orientation of its principal axes with respect to its center of mass [45]. The principal axes are the axes of symmetry of the rigid body and form an orthogonal coordinate system with origin the center of mass of the rigid body. To register two images using the principal axes, the following steps are used [45]:

Step 1: The two images are segmented and the object surfaces are defined using an automated [46] or manual [43] segmentation scheme. Two different implementations of the method exist. One uses the full volumes for the computation of the principal axes transformation and the other uses only the surface outlines.

Step 2: The centers of mass of the two volumes or surfaces are computed for the two images to be registered using the formula:

$$[\bar{x}, \bar{y}, \bar{z}] = \mathrm{Mean}[x, y, z] \tag{2.3}$$

where x,y,z are the integer coordinates of an image voxel that belongs to the signal area or to the surface outline, the symbol Mean indicates the arithmetic mean over the set of all voxels in each image volume or surface, and $\bar{x}, \bar{y}, \bar{z}$ denote the coordinates of the center of mass.

Step 3: The centers of both volumes or surfaces are translated to the origin of the center of mass coordinate system using the translational adjustment formula:

$$[x', y', z'] = [x, y, z] - [\bar{x}, \bar{y}, \bar{z}] \tag{2.4}$$

Step 4: The moments and products of inertia are computed as:

$$[I_{xx}, I_{yy}, I_{zz}] = \text{Mean}[x'^2, y'^2, z'^2] \tag{2.5}$$

$$[I_{xy}, I_{xz}, I_{yz}] = \text{Mean}[x'y', x'z', y'z'] \tag{2.6}$$

and the inertia matrix for each of the volumes or surfaces is formed as:

$$\mathbf{I} = \begin{bmatrix} I_{xx} & I_{xy} & I_{xz} \\ I_{yx} & I_{yy} & I_{yz} \\ I_{zx} & I_{zy} & I_{zz} \end{bmatrix} \tag{2.7}$$

with $I_{xy} = I_{yx}$, $I_{yz} = I_{zy}$, $I_{xz} = I_{zx}$.

Step 5: The inertia matrices $\mathbf{I}_{1,2}$ for the two volumes or surfaces are expressed as a similarity transformation:

$$\mathbf{I}_i = \mathbf{S}_i \, \boldsymbol{I} \, \mathbf{S}_i^T \text{ with } i = 1,2 \tag{2.8}$$

where ***I*** represents the inertia matrix as it is computed in the principal axes coordinate system and the rotation matrix $\mathbf{S}_i$ is the matrix of eigencolumns determined from $\mathbf{I}_i$.

Step 6: Rotational adjustment is performed using the rotation matrix $\mathbf{S}_1 \mathbf{S}_2^T$ and the rotation formula:

$$\mathbf{I}_2 = \mathbf{S}_2 \, \mathbf{S}_1^T \, \mathbf{I}_1 \, \mathbf{S}_1 \, \mathbf{S}_2^T \tag{2.9}$$

The principal axes method has been used by various research groups, with variable results. Alpert et al. [45] used the method for three-dimensional alignment of MR data of the brain. They estimate the rotational or translational errors as the difference of the applied transformation parameter to the computed one. They reported that when the full volumes are used for the computation of the principal axes transformation, the rotational errors are less than 0.5 degrees and the translational errors less than 0.1 mm. When the surfaces are used, the errors are three to six times greater. Slomka et al. [46] used this method for three-dimensional alignment of SPECT image volumes of the heart. Their method failed to produce good rotational accuracy and they advise that it should be used as a preprocessing step to a more robust registration scheme. Toga and Banerjee [3] compared the accuracy of the method to the cross-correlation coefficient for two-dimensional registration of SPECT image scans of the brain and reported that the principal axes method often resulted in poor accuracy compared to cross-correlation based methods. They also reported that when the initial rotational error is more than 90 degrees, the method tends to register the images with 180 degrees rotational mismatch. Rusinek et al. [43] compared the performance of the method with the surface fitting algorithm for three-dimensional registration of MR images of the head. That group used the post registration distance of external fiducial markers as a measure of positional error and reported that the average errors are 1.3 mm for implementation of the method using full volumes and 4.7 mm for implementation of the method using surface outlines. These errors are 4 to 12 times greater than the errors produced by the surface fitting algorithm. In the same study it was shown that the principal axes algorithm tends to produce large rotational errors for missing brain data and that the accuracy diminishes with larger initial misangulations. The advantages of the method are its simplicity and its speed.

2.4 Mutual Information

Mutual Information for medical image registration is presented in [47]. It is a measure of registration based on entropy. Entropy is the measure of uncertainty of a message in a communication channel. Mutual information is based on the fact that when two images are registered the joint histogram shows clusters of overlapping similar intensities with sharp edges. The joint histogram binary image is used for extraction of the mutual information theory measure which is the reduction of the uncertainty of image B when the image A is known and they are aligned. Maximization of mutual information occurrs when the images are aligned to each other. Mutual information has the following properties:

- It is symmetric. Registering A to B is the same with registering B to A.
- The information that an image A contains about itself is equal to the information (entropy) of image A.
- The information the images contain about each other can never be greater than the information in the images themselves.
- The uncertainty about A cannot be increased by learning about B.
- When A and B are not in any way related , no knowledge is gained about one image when the other is given.

Mutual information can be equivalently expressed as:

$$\begin{aligned} \mathbf{I(A;B)} &= \mathbf{H(A) - H(A \mid B)} \\ &= \mathbf{H(B) - H(B \mid A)} \\ &= \mathbf{H(A) + H(B) - H(A,B)} \\ &= \mathbf{H(A,B) - H(A \mid B) - H(B \mid A)} \end{aligned} \tag{2.10}$$

Where H(A) and H(B) are the marginal entropies, H(A|B) and H(B|A) are the conditional entropies, and H(A,B) is the joint entropy of A and B. Normalized variants of the mutual information I are provided by the coefficients:

$$\begin{aligned} \mathbf{C_{AB}} &= \mathbf{I(A;B)/H(B)} \\ \mathbf{C_{BA}} &= \mathbf{I(A;B)/H(A)} \end{aligned} \tag{2.11}$$

The Mutual Information method is used currently for rigid and non rigid registration. In [48] Mutual Information is the choice of preference for multimodal image registration. The computation of Mutual Information is reported as time consuming and as converging to local maxima. The computation of MI is based on the computation of the joint histogram which is computationally expensive. Hierarchical methods at 3 resolutions are used for the computation of the joint histogram. The paper proposes the varying sampling of the histogram with higher resolutions at areas of the image with higher information content. The convergence algorithm is based in an away to close stage approach with Powell method for the first stages and simulated annealing for the final stages. Simmulated annealing is computationally expensive for the whole registration procedure. It takes a lot of time to avoid local maxima. It is based on the heating and controlled cooling of the probability variables. It is a method for avoidance of local defects in the algorithm. Three dimensional CT, MR and PET images are used for registration examples with accuracy within the range of 1 voxel. The experiments were performed at Vanderbilt University.

The method is implemented in parallel for non rigid registration. In [49] non rigid image registration is solved using an elastic model of the object which is imaged. The model includes a regularization term which assures for the smoothness of the transformation of the final solution. The solution of the non rigid problem is performed with the solution of a partial differential equation with the finite elements method. The problem is scalable with respect to the number of variables that can be processed by the computer in order to produce the final solution. The authors agglomerate the solution of the problem by dividing the image matrix into sub-matrixes and processing each sub-matrix on a different processor. They impose rigidity on sub-matrixes that image bone and other rigid structure reducing the problem into areas that contain non rigid structures. The parallel method is called the total – FETI method.

Mutual Information belongs in the class of methods that use probability models. In [50] probabilistic methods are used for non rigid registration and longitudinal testing of

Alzheimer Disease patients. The approach of the author is data driven and introduces the reader in the notion of regularization for non rigid registration. The setup is the doctor collecting data with the elderly patient being inside the MR machine. The model created applies regularization of the data collected using a registration prior and taking into account the noise model. Smoothing filtering is also applied to alleviate the artifacts from the data collection. The study of Alzheimer's disease is longitudinal with time and the author has developed tests to classify the healthy and the diseased subjects. In a more region specific study ensembles of areas that are affected by the disease are studied in order to decide the tissue changes of specific brain areas over time.

2.5 Survey of medical image registration

A survey of medical image registration methods is presented in [51]. There are 3 main components in image registration techniques. Other than the similarity function the transformation, and the optimization steps characterize the image registration technique. There are several types of transformation [52-56] that are used in image registration. These are rigid [57], affine [58], projective [59] , curved [60] and non rigid [61]. For non rigid registration, B splines [62] with local support are used usually with models of elastic registration. The elastic deformable model [63-67] guarantees the promptness of the solution. The optimization procedures used are the downhill simplex method [68], the Powell's direction set method [69] and first derivative based methods such as conjugate gradient [70] and Levenberg-Marquardt method [71]. Multi scale and multiresolution optimization techniques give a faster and more robust convergence toward the solution. Custom made techniques which have the characteristic of fast multiscale convergence are also acceptable.

The registration techniques are also divided to monomodal and multi modal. Monomodal techniques refer to one imaging modality (e.g only MRI) whereas multimodal to registration of MR to CT and generally to registration of images from different modalities.Another categorization refers to intersubject and intrasubject registration methods. The intersubject methods use data from different patients (including Atlas based methods [72-78]) whereas intrasubject methods use methods from the same patient over time.

The registration methods are also divided according to the part of the body which is registered. There are methods for the head [79-83] , the brain [84-88] , the retina [89-93], dental [94-98], the thorax (breast and cardiac) [99-103] the abdomen [104-106] , the liver [107-109], the kidney [110-112], the prostate [113-115], the spine and the vertebrae [116-119] and the limbs [120-122].

2.6 Conclusions

Medical image registration literature focuses on the solution of a wide range of problems for the solution to be applied for 2D/3D, rigid, non rigid image registration. We have presented the main categories of feature based techniques.

Correlation methods register medical images by maximizing a similarity or minimizing a disparity criterion between images. The similarity or disparity criterion used is signal intensity based , and it is maximized or minimized iteratively. The methods that are based on correlative criteria is an active research field. The cross correlation techniques use signal intensities have been reported to work well with monomodality image registration but the have recently incorporated in the solution of 2D to 3D registration, rigid and non rigid problems. The errors reported are less than 0.74degrees and 1mm. The ratio image uniformity criterion was introduced by Woods et al [35,36]. To align the two images , the algorithm calculates the ratio of one image to the other on a voxel per voxel basis and then iteratively minimizes the variance of this ratio. The method is based on the ideal assumption that in the case that the images are registered, the values of the voxels in one image , can result by multiplying the voxels in the other image with a constant multiplicative factor.

Surface matching methods register images by using the anatomic surface models of the two images. The surface matching methods have a high degree of sophistication but due to the sensitivity to noise they have been reported to work as preprocessing step to signal intensity based methods.

The principal axes transformation is known from the theory of rigid bodies. A rigid body may be located using the position of the center of its mass and the orientation of its principal axes with respect to its center of mass [45]. The principal axes method is simple and fast and for this reason the are presented as a method of reference. They also have the characteristic of using axes as means of registration which is similar with the 1D projections used for the 2D registration in this thesis.

The Mutual Information is a measure of registration based on Entropy. Mutual Information is based on the fact that when two images are registered the joint histogram shows clusters of overlapping similar intensities with sharp edges. The Mutual Information method is in the general class of probabilistic models based methods and are used for rigid, non rigid and 2D to 3D registration. They have been implemented in parallel for non rigid registration.

In the next sections we will present the main characteristics of the method presented in this thesis. The method has been originally developed using the idea of the amplifier on the ratio image in order to enhance the ratios between signal and background voxels. It exploits both edges like the case of Mutual Information with the joint histogram and areas or volumes.

For the programming of this new method we are following the implementation of the Woods [35,36] ratio image registration criterion. This criterion is considered the predecessor of the Mutual Information methods. We set the ratios between the signal and background pixels or voxels to a standard infinite like value and we programmed the area based binary methods which can be found in Chapter 3 and 4. We use lines for projective geometry of ratios and we improved the principal axes method and got better results in accuracy comparing to the Mutual Information method (Chapter 5). We cat the images at levels of straight lines (Woods is also providing curved cuts) and we managed to maintain the accuracy (as seen in Chapter 6). We have also programmed and tested a custom made iteration loop which works well in multiresolutions(Chapter 6).

CHAPTER III

NOVEL APPROACH TO MEDICAL IMAGE REGISTRATION USING BINARY AREAS AND VOLUMES

As described previously, two different approaches to the solution of the problem of medical image registration exist: the iterative approach represented by the correlation, mutual information and surface matching methods and the analytic approach represented by the principal axes method. The subject of this thesis is the development of a new iterative method for two and three-dimensional image registration. The method that will be presented in this chapter is based on the weighted ratio image criterio. The ratio image criterion was originally presented by Woods et al [35,36] and is considered a reference method in medical image registration. We are implementing the criterion in a novel way and the first change we have made is to set the ratios between signal and background voxels to a standard high value. This approach creates binary areas in the ratio image which are used for registration, improving the performance of the method for rigid registration. As Chapter III will show, with the modifications made to the criterion together and the new way that it is minimized, the method can no longer be characterized as correlational. In medical image registration research in order to produce a method you need to invent a registration function and program a literature or custom made iteration loop. According to [1] evaluating the accuracy by deregistering and then registering with known parameters is a valid research method. We have programmed a custom based iteration loop and applied experiment protocols to test the accuracy of the method in multiple experiments. A total of 200 two-dimensional and 240 three-dimensional registration experiments were performed using patient data from the database of the Cleveland Clinic Foundation. The purpose of this chapter is to present the algorithm used for these experiments. We will present the processing steps, the classification and interpolation methods, the registration function, the iteration loop and the protocol for the experiments.

3.1 Processing steps of the method

To register two three-dimensional studies, the method uses the following processing steps:

A.Fuzzy c-means classification

Each of the scans of the two studies is classified with the use of the fuzzy c-means classification algorithm as presented by Bezdek et al. [123]. Three clusters are used and a threshold for each scan is computed by taking the mean value of the centers of the two lowest clusters. This threshold is the value that separates the signal from the background area for each scan. The lowest of all the thresholds computed for each study is considered the global threshold for this study. No thresholding operation is performed at this point.

B. Interpolation

The two studies are interpolated using a trilinear interpolation routine to create the cubic voxel volumes. This step is necessary because of the different resolution in the xy plane and the z axis used in the acquisition of three-dimensional medical image data.

C. Threshold Comparison

All the voxel values of the two volumes are compared to the global thresholds.
Voxels that have signal intensities lower than the corresponding global threshold are set to zero.

D. Iteration loop –Minimization of registration function

Finally, an iteration loop based on Chebyshev's approximation theory [41] is used to minimize the registration function, which is defined as the mean squared value of the average weighted ratio $\tilde{R}$ of the two volumes:

$$E\left(\tilde{R}^2\right) \quad \text{with} \quad \tilde{R} = \frac{1}{2} * \left(weighted(\frac{A}{B}) + weighted(\frac{B}{A}) \right) \tag{3.1}$$

where A and B are the two volumes. The ratios of the two volumes are computed on a voxel per voxel basis and weighting is performed by setting the voxel ratios with background voxels in the denominator to a standard high value. All the other voxel ratios are not affected and generally have low values.

In the next sections of this chapter, the basic theory and formulas relating to the steps outlined above will be presented in detail. A block diagram of the registration method is shown in figure 1.

3.2 Fuzzy c-means classification

The fuzzy c-means classification algorithm has been used in this thesis for the computation of the thresholds that define the surfaces in the two studies to be registered. The choice of this classification method was based on the results presented by Bezdek et al. [123] and Hall et al. [124], who applied the algorithm to T1 weighted and T2 weighted MRI technique images. The algorithm for the implementation of this classification method is also presented in [123] and is briefly outlined below.

The purpose of the fuzzy c-means algorithm is to compute, for a given data set x[1...n], the optimal values of the centers V[1...c] of c clusters, by using the c fuzzy memberships assigned to each data element u[1...n,1...c] and by minimizing the fuzzy within-groups sum-of-squared-errors function, which is defined as:

$$J(u,x)= \sum_{k=1}^{n}\sum_{i=1}^{c}(u[i,k])^{m} D(x[k],V[i]) \qquad (3.2)$$

where D can be considered as the Euclidean distance of the data element x[k] from the center V[i] and m is a weighting exponent on each fuzzy membership. According to Bezdek and colleagues[51], J(u,x) can be minimized if and only if:

$$u[i,k]=\left[\sum_{j=1}^{c}\left(\frac{D(x[k],V[i])}{D(x[k],V[j])}\right)^{\frac{2}{(m-1)}}\right]^{-1} \qquad \text{for all i,k} \qquad (3.3)$$

and

$$V[i]=\frac{\sum_{k=1}^{n}(u[i,k])^{m}x[k]}{\sum_{k=1}^{n}(u[i,k])^{m}} \qquad \text{for all i=1...c.} \qquad (3.4)$$

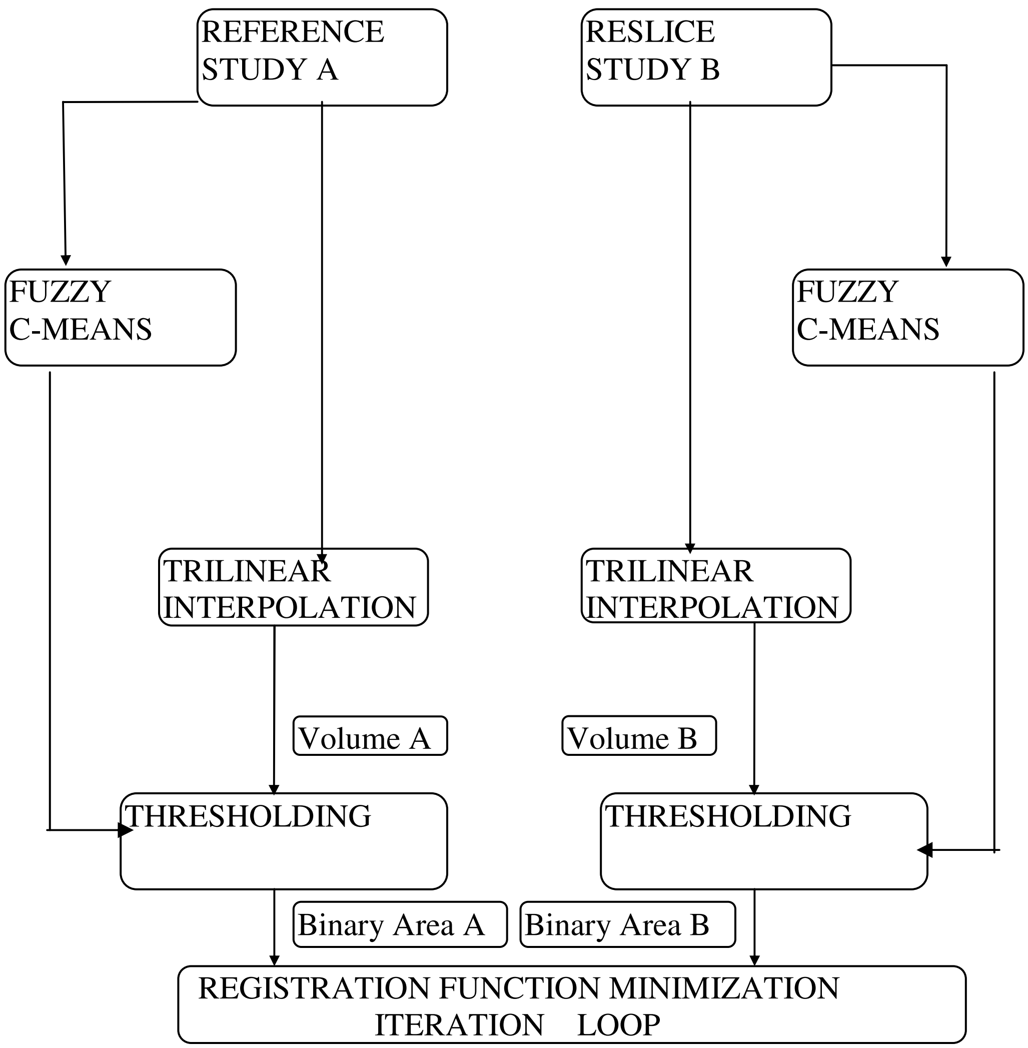

Figure 1: Block diagram of the registration algorithm. The four processing steps, fuzzy c-means classification, interpolation, thresholding and the registration function minimization loop are seen in this diagram.

The minimization can be performed using the following steps :

Step 1: Initialize the number of clusters c, the fuzzy memberships array u[1...n,1...c], the weighting exponent m>1, the maximum number of iterations T and the error tolerance e>0. For this thesis the number of clusters is provided by the user; the membership array is initialized with crisp memberships so that each voxel has one of the c memberships equal to 1 and all the others equal to zero, m is set to 1.1, T to 100 and e to 1.

Step 2: Compute the initial values of the c cluster centers using (3.4).

Step 3: For t=1,2,...T, compute memberships using (3.3) and update the cluster centers array V^{t+1} using (3.4).

Step 4: Compute $E^{t} = D(V_{t+1}, V_{t})$

Step 5: If $E^{t} < e$ stop , else next t.

The generalization of this algorithm assigns vectors instead of arithmetic values to each voxel and it was used by Bezdek's group for classifying MR images using both T1 and T2 imaging sequences.

For the application of the algorithm in this thesis, a hierarchical form of the algorithm was programmed in C and implemented. In this implementation the user is able to apply the algorithm hierarchically to analyze further the highest cluster. For example, if the user chooses two levels of hierarchy with two and three clusters for each level, then the fuzzy c-means with two clusters will first be applied to all the voxels of the image and then the voxels that belong to the defuzzified highest cluster will be further analyzed with three clusters. Defuzzification is performed by using the mid distance of the centers of sequential clusters as a threshold. When one level of hierarchy is used, the method is equivalent to the fuzzy c-means algorithm as presented in [123]. An example application of the fuzzy c-means to a proton density MR scan is shown in figure 2. The left image is the original MR scan, the center image is the c-means classified and defuzzified scan with one level and three clusters, and the right image is the c-means classified and defuzzified scan with one level and 7 clusters.

(a) (b) (c)

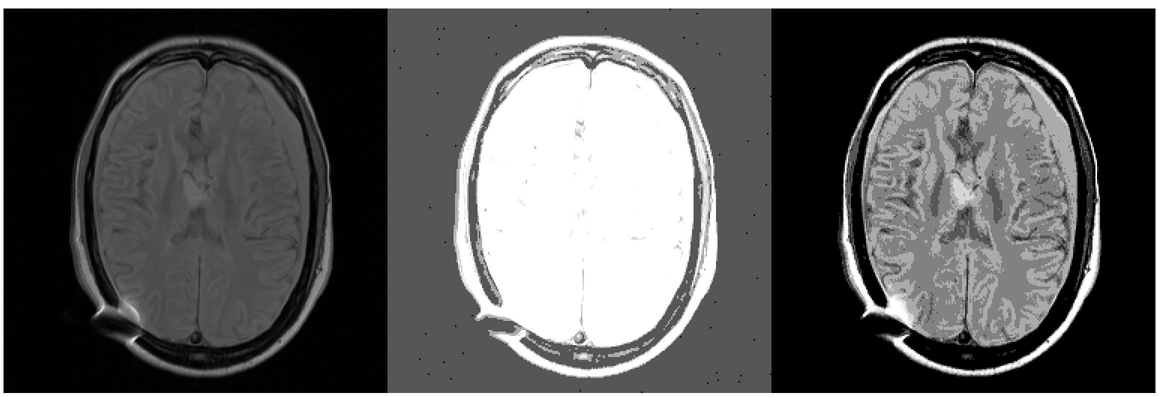

Figure 2: Application of the fuzzy c-means to an MR scan. Left (a): the original scan. Center (b): the c-means classified and defuzzified scan with c=3. Right (c): the c-means classified and defuzzified scan with c=7.

3.3 Trilinear interpolation

The second step of the registration method is to create the cubic voxel volumes using a trilinear interpolation routine. The formulas used for trilinear interpolation were based on the bilinear interpolation formulas presented in [124]. The interpolation procedure is as follows (we use the algorithmic formulation as it has been implemented with C programming):

Let's consider a three-dimensional study with size LxMxN voxels and voxel size XsxYsxZs mm with Xs=Ys < Zs and L=M. The interpolation parameters along the three dimensions will be X_interp=1, Y_interp=1, Z_interp=Zs/Xs. The interpolated cubic voxel volume resulting from this study will have a size of LnewxMnewxNnew with Lnew=L*X_interp, Mnew=M*Y_interp, Nnew=N*Z_interp. For each voxel (xnew,ynew,znew) in this volume, a signal intensity value G is computed using the formula:

$$G(x,y,z)=a*x+b*y+c*z+d*x*y+e*x*z+f*y*z+g*x*y*z+h \quad (3.5)$$

with x=xnew/X_interp, y=ynew/Y_interp, z=znew/Z_interp. The parameters a,b,c,d,e,f,g,h are computed by using the signal intensities G1-G8 of the eight voxels of the original study that form a cube around the (x,y,z) point. So if xint=(int)x, yint=(int)y and zint=(int)z, we have the system of 8 equations with eight unknowns a-h:

$$G1=G(xint,yint,zint) \quad (3.6)$$

$$G2=G(xint+1,yint,zint) \quad (3.7)$$

$$G3=G(xint,yint+1,zint) \quad (3.8)$$

$$G4=G(xint+1,yint+1,zint) \quad (3.9)$$

$$G5=G(xint,yint,zint+1) \quad (3.10)$$

$$G6=G(xint+1,yint,zint+1) \quad (3.11)$$

$$G7=G(xint,yint+1,zint+1) \quad (3.12)$$

$$G8=G(xint+1,yint+1,zint+1) \quad (3.13)$$

The solution of this system gives:

$$g=A+B+F-(C+D+E) \quad (3.14)$$

$$d=C-(A+B)-g*zint \quad (3.15)$$

$$f=E-B-g \quad (3.16)$$

$$e=D-A-g \quad (3.17)$$

$$a=A-d*yint-e*zint-g*yint*zint \quad (3.18)$$

$$b=B-d*xint-f*zint-g*xint*zint \quad (3.19)$$

$$c=H-e*xint-f*yint-g*xint*yint \quad (3.20)$$

$$h=G1-a*xint-b*yint-c*zint-d*xint*yint-e*xint*zint-f*yint*zint-g*xint*yint*zint \quad (3.21)$$

with :

A=G2-G1, B=G3-G1, C=G4-G1, D=G6-G5, E=G7-G5, F=G8-G5, H=G5-G1

Figure 3 shows the surface rendering of a trilinearly interpolated MR volume with interpolation parameters 1:1 along the x and y axes and 5:0.9 along the z axis.

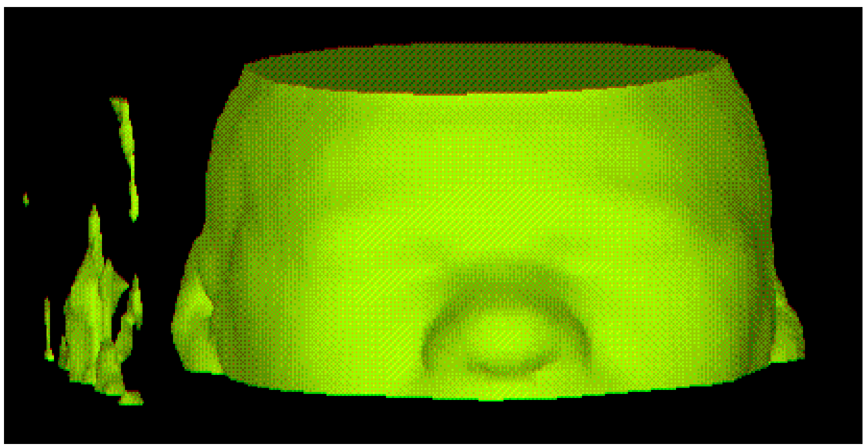

Figure 3: Surface rendering of a trilinearly interpolated cubic voxel volume. Interpolation parameters are 1:1 along the x and y axes and 5:0.9 along the z axis.

3.4 Registration function - Iteration loop

As mentioned previously, the registration algorithm aims at minimizing the mean squared value of the average weighted ratio of the two images. The way that the registration function is computed and minimized will be presented now in greater detail.

Consider two three-dimensional digital images $A[i,j,k]$ and $B[i,j,k]$ with i:1...L, j:1...M, k:1...N. Using these images two ratios can be defined, the ratio R_1 of image A to image B with $R_1[i,j,k] = \frac{A[i,j,k]}{B[i,j,k]}$ and the ratio R_2 of image B to image A with

$R_2[i,j,k] = \dfrac{B[i,j,k]}{A[i,j,k]}$. Let's define now as S an LxMxN image that results from A or B by keeping nonzero values only for the signal voxels and as G an LxMxN image that results from A or B by keeping nonzero values only for background voxels whose intensities are due to noise. The following equations stand $\forall$ i:1...L, j:1...M, k:1...N:

$$S[i,j,k] \neq 0 \Leftrightarrow G[i,j,k] = 0 \tag{3.22}$$

$$A[i,j,k] = S_A[i,j,k] + G_A[i,j,k] \tag{3.23}$$

$$B[i,j,k] = S_B[i,j,k] + G_B[i,j,k] \tag{3.24}$$

$$R_1[i,j,k] = \frac{S_A[i,j,k] + G_A[i,j,k]}{S_B[i,j,k] + G_B[i,j,k]} \tag{3.25}$$

$$R_2[i,j,k] = \frac{S_B[i,j,k] + G_B[i,j,k]}{S_A[i,j,k] + G_A[i,j,k]} \tag{3.26}$$

The weighted ratios $\tilde{R}_1$ and $\tilde{R}_2$ can now be defined as:

$$\tilde{R}_1\,[\mathrm{i,j,k}] = \begin{cases} \mathrm{R}_1\,[\mathrm{i,j,k}] \text{ when } \mathrm{S_B}[i,j,k] \neq 0 \\ \\ \mathrm{C} \qquad \text{when } \mathrm{S_B}[\mathrm{i,j,k}] = 0 \end{cases} \tag{3.27}$$

$$\tilde{R}_2\,[\mathrm{i,j,k}] = \begin{cases} \mathrm{R}_2\,[\mathrm{i,j,k}] \text{ when } \mathrm{S_A}[i,j,k] \neq 0 \\ \\ \mathrm{C} \qquad \text{when } \mathrm{S_A}[\mathrm{i,j,k}] = 0 \end{cases} \tag{3.28}$$

$\forall$ i:1...L, j:1...M, k:1...N where C is a constant ratio with an amplified standard high value.

The function that is minimized iteratively is the mean squared value of the mean weighted ratio, that is :

$$E(\tilde{R}^2) \text{ with } \tilde{R}[i,j,k] = \frac{\tilde{R}_1[i,j,k] + \tilde{R}_2[i,j,k]}{2} \quad \forall \text{ i:1...L, j:1...M, k:1...N} \qquad (2.29)$$

Figure 4 illustrates the meaning of the above relationships. The first row shows two MR scans that are rotated to each other by 30 degrees. The second row left shows the two scans superimposed on each other and the second line right gives a mapping of the different types of areas that can be found in the mean weighted ratio image $\tilde{R}$. In the white area, the weighted ratios $\tilde{R}_1$ and $\tilde{R}_2$ are computed using signal voxels only, whereas in the gray area, one of the ratios is computed using background voxels in the denominator and this ratio is set to a standard high value. It is obvious that the gray area does not exist for the correct registration position. For this position, the registration function gets its minimum value.

The iteration loop used for the minimization of the registration function is programmed with the following rules:

1.One of the six possible geometric transformation parameters (three rotations around the three axes and three translations along the three axes) is adjusted with each iteration. For the testing performed for this thesis, the order was set to be the rotations first, followed by the translations. The reason for this order selection is that the centroid registration of the two volumes could be considered as a first step of the registration method. This step was omitted, so that the translational displacements imposed can be considered errors from the centroid registration procedure.

2. One of the two volumes is defined as the reference volume and the other as the reslice volume, which is to be aligned to the reference. Since the registration function is symmetric, the choice of the reference volume affects only the sign of the final adjustment values computed by the method.

(a) (b)

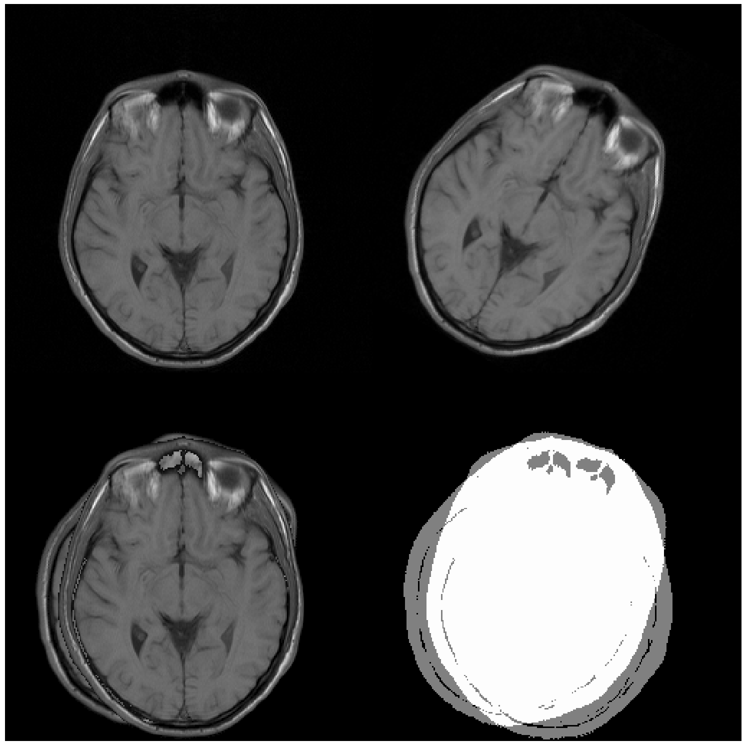

(c) (d)

Figure 4: Illustration of the different image areas used by the algorithm for the computation of the registration function. First row left and right : two scans (a) and (b) rotated to each other by 30 degrees. Second row left (c) and right (d): The two scans when superimposed give two different types of area. In the white area the registration function is computed with the use of signal voxels only, whereas in the gray area both signal and background voxels are used.

3. For each iteration the registration function is computed for n=4 Chebyshev points per 36 transformation units. The transformation units are degrees for rotations and voxels for translations. The Chebyssev points used are[24] :

$$x_k = 18\cos\left(\frac{\pi\left(k-\frac{1}{2}\right)}{n}\right) \qquad \text{k=1,...,n} \tag{3.30}$$

For all other points in the range of the 36 transformation units, the registration function is approximated using the Chebyshev approximation formula:

$$f(x) \approx \left[\sum_{k=0}^{n-1} c_k T_k(x)\right] - \frac{1}{2}c_0 \tag{3.31}$$

$T_k(x)$ is the Chebyshev polynomial of degree k and is given by the explicit formula:

$$T_k(x) = \cos(k \arccos(x)) \tag{3.32}$$

which can be given explicitly in a polynomial form as [41]:

$$T_0(x) = 1 \tag{3.33}$$

$$T_1(x) = x \tag{3.34}$$

$$T_2(x) = 2x^2 - 1 \tag{3.35}$$

$$T_3(x) = 4x^3 - 3x \tag{3.36}$$

$$T_4(x) = 8x^4 - 8x^2 + 1 \tag{3.37}$$

$$\ldots$$

$$T_{n+1}(x) = 2xT_n(x) - T_{n-1}(x) \qquad \text{n} \geq 1 \tag{3.38}$$

The coefficients c_k are the Chebyshev coefficients and are defined by

$$c_k = \frac{2}{n}\sum_{l=1}^{n} f(x_l)T_k(x_l) \qquad \text{k=0,...,n-1} \tag{3.39}$$

where x_l are the Chebyshev points.

The minimum of the approximated registration function is considered as the adjustment value for the geometric transformation parameter.

4. A transformation parameter is determined to have converged when it completes two iterations that give adjustment values less than one transformation unit.

5. A maximum number of eight iterations per transformation parameter is allowed. If the parameter has not converged after eight iterations, the adjustment value is considered to be the average of the adjustment values given by the seventh and eighth iteration. In this study we found that in all the cases of non-convergence, the adjustment values oscillated around the correct registration position with amplitudes greater than one transformation unit.

The results from the application of the above algorithm will be presented in the next chapters.

3.5 Protocol for 2D experiments - "20 displacement" technique

The MR data used came from 10 different patients with various diseases. The data had the following characteristics:

- The patients had repetitive MR examination at two different times. The examination data can be found in Appendix A.
- For each time, T1- and T2-weighted axial interleaved studies that corresponded to the same position of the patient's head were performed.
- All the studies had 19 scans.
- All the studies had xy-plane resolution of 0.9 mm and z-axis resolution of 5 mm.

Using this data, a total of 200 two-dimensional experiments for alignment of a T2 to a T1 axial scan were performed using the algorithm described in sections 3.1 to 3.4. These experiments will be referred to as "20 displacement" experiments and were conducted according to the following rules:

a) In order to avoid being data per patient specific, for each patient the tenth scan of each of the T1 and T2 studies of the first examination time were used.

b) The T1 scan was used as the reference scan. The T2 scan was considered the reslice scan. The latter was rotated and translated using a standard set of 20 two-dimensional geometric transformations and then registered to the reference scan, giving 20 registration experiments per patient. The geometric transformations parameters were randomly selected using a random number generator in the range of -45 to +45 degrees for the xy rotation and -30 to +30 voxels for x and y translations. The translations were rounded to the nearest integer for reasons that relate to the implementation of the geometric transformations routine; these will be explained later in this chapter. The resulting “20 displacement” set is shown in table 1.

c) All the experiments were performed at full resolution. The size of the scans in voxels was 256x256 and the voxel size was 0.9 mm.

d) The Absolute Error (AE) per transformation parameter was defined as the absolute difference of the adjustment value from the applied transformation parameter value. The xy rotation AE for each transformation was defined as the Absolute Rotational Error (ARE) for the transformation and was computed in degrees. The Absolute Translational Error (ATE) per transformation was computed in millimeters by averaging the x and y translation AEs in voxels and then by multiplying the average value with the voxel size (0.9 mm). The Average Absolute Rotational Error (AARE) per patient was defined as the average of the AREs from all the transformations. Similarly, the Average Absolute Translation Error (AATE) per patient was defined as the average of the ATEs from all transformations.

Table 1 : Geometric transformation set used for the two-dimensional "20 displacement" registration experiments.

Transformation #	xy - rotation (degs)	x-translation(voxs)	y-translation(voxs)
1	-40.08	7	0
2	21.37	-9	-19
3	-16.18	-10	-11
4	-34.80	-5	2
5	-2.67	10	27
6	-32.64	-6	-20
7	-14.40	-17	12
8	-36.15	0	-16
9	33.23	-26	0
10	20.60	16	-23
11	-25.82	24	-25
12	-37.63	-23	-7
13	8.17	26	-13
14	7.09	12	-8
15	-44.71	0	29
16	24.54	29	2
17	-36.06	-5	16
18	-28.42	-19	9
19	15.82	13	16
20	0.35	-5	17

3.6 Protocol for 3D experiments

The three-dimensional registration accuracy of our method was tested using the data described in the previous section with a total of 240 three dimensional registration experiments. Two types of three-dimensional experiments were performed: The "10 displacement" experiments, a three-dimensional version of the "20 displacement" experiments, and the "different times" experiments. For the "10 displacement" experiments the following rules were used:

a) For each patient the T1 and T2 studies of the first examination date were used.

b) The T1 study was used as the reference study.The same study was also rotated and translated using a standard set of 10 three dimensional geometric transformations and then registered to the reference study, giving 10 T1-T1 three-dimensional registration experiments per patient. The T2 study was also rotated and translated using the same three-dimensional geometric transformation set and then registered to the reference study, giving 10 T1-T2 three-dimensional registration experiments per patient. The rotational parameters of the geometric transformation set were randomly chosen within the limits of the adjustment values that were obtained from registration of patient data from different times. The translational parameters were kept within lower limits than those resulting from "different times" experiments, because they simulate centroid registration errors. The limits used were -30 degrees to +30 degrees for xy rotation, -10 degrees to +10 degrees for yz and zx rotations, -10 to +10 mm for x and y translations and -5 to +5 mm for z translation. The translations were converted to voxels by dividing the millimeters with the cubic voxel size and quantizing to the nearest integer. The resulting set of the 10 three-dimensional geometric transformations is shown in table 2.

c) All the experiments were performed at half resolution using a voxel size of 1.8 mm.

d) The Absolute Error (AE) per transformation parameter was defined as the absolute difference of the adjustment value from the applied transformation parameter value. The average of the AEs for xy, yz, zx rotations was defined as the Absolute Rotational Error (ARE) per transformation and was computed in degrees. The Absolute Translational Error (ATE) per transformation was computed in millimeters by averaging the x, y and z translation AEs in voxels and then by multiplying the average value with the voxel size (1.8 mm). The Average Absolute Rotational Error (AARE) per patient was defined as the average of the AREs from all the transformations. Similarly, the Average Absolute Translation Error (AATE) per patient was defined as the average of the ATEs from all transformations.

The “different times” experiments were performed in the following way:

a) For each patient the T1 study of the first examination date and the T1 and T2 studies of the second examination date were used.

b) The T1 study of the first examination date was considered as the reference study. The T1 and T2 studies of the second examination date were considered as the reslice studies and were both registered to the T1 study of the first examination date.

c) The experiments were performed first at half and then at full resolution, giving four “different times” registration experiments per patient.

Table 2: Geometric transformation set used for the “10 displacement” registration experiments

Transformation #	**xy rotation (deg)**	**yz rotation (deg)**	**zx rotation (deg)**	**x translation (mm)**	**y translation (mm)**	**z translation (mm)**
1	-10.26	-6.94	-9.3	-9.2	-3.6	-3.98
2	12.42	2.32	-3.7	-4.6	-9.6	-2.02
3	-8.58	-4.38	1.9	8.4	6.9	-4
4	19.26	-7.2	-1.9	-1.66	-8	1.97
5	-26.58	-6.3	-2.16	-3.2	-7.6	0
6	7.56	2.1	-7.6	0	-6.08	0.8
7	-5.82	-2.2	2.8	-8.4	-5.72	2
8	-5.04	4.2	-4.04	4.2	3	-2
9	-15.66	-5.14	6.04	8	-6.04	1.6
10	-9.24	6.44	-6.7	-0.5	1.48	3.2

3.7 Nearest neighbor - Quantization effects

As already noted in the interpolation and iteration loop sections, the registration algorithm moves the reslice image at positions that are defined by the Chebyshev points, computes the registration function values for these points and then extrapolates its values for all the other points using the Chebyshev approximation formulas. The implementation of this algorithm requires the use of a geometric transformation routine that incorporates a trilinear interpolation step that will ensure the floating point operations. For all the testing performed for this thesis, a geometric transformations routine that follows the nearest-neighbor rule for coordinate computations was used. This choice was based solely on the non-time-efficient programming of a combined geometric transformation and trilinear interpolation routine.

The effects of this choice on the performance of the algorithm are as follows:

a) When rotations are present, the nearest-neighbor approach generates voxels within the signal area for which no values are computed. These voxels are crucial to the performance of the algorithm because they are considered as background points. The solution to this problem was given by putting an additional loop at the end of the geometric transformation routine that detects these voxels and computes a value for them by interpolating linearly between the neighboring voxels. Figure 5 illustrates this effect for the case of a two-dimensional image. The left image (5a) is the original MR scan. The center image (5b) is the scan rotated by 30.5 degrees with the nearest-neighbor artifact present. The right image (5c) shows the same rotated scan after interpolation.

b) When translations are present, the effects of the quantization imposed by the nearest-neighbor approach are more serious. First, the translation points for which the computation of the registration function is done are not the Chebyssev points but the nearest integers to these points. Second, the adjustment value for each translation iteration loop is not the minimum of the registration function but the nearest- nteger to this minimum. We were not able to define the effect of these two events on the accuracy of the method for translational adjustments. For this reason, in all the experiments performed for this thesis, the comparisons relating to the accuracy of the method use only the rotational errors.

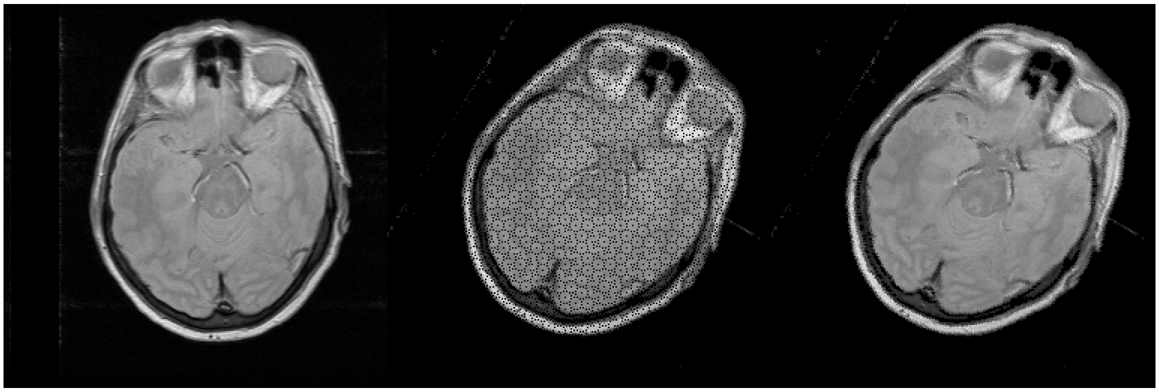

(a) (b) (c)

Figure 5: Use of the linear interpolation for the implementation of the geometric transformations. Left (a): original MR scan. Center (b): MR scan rotated by 30.5 deg using the nearest-neighbor rule for the geometric transformations. Right (c): MR scan rotated by 30.5 deg after the implementation of linear interpolation.

3.8 Conclusions

The subject of this thesis is the development of a novel iterative method for two and three dimensional image registration. The processing steps of the method use a fuzzy c-means classification algorithm, a trilinear interpolation routine, a thresholding routine, and an iteration loop based on Chebyshev's approximation theory. Fot the application of fuzzy c-means in this thesis an hierarchical form of the algorithm has been programmed. In order to create the cubic voxel intensities we programmed a trilinear interpolation routine. Thresholding is performed with the use of the centroids of the clusters computed by the fuzzy c-means classification. We programmed a novel iteration loop which works like the Powell method and also deregisters and and brings back orderly the images using the Chebyshev polynomials in a similar way to simulated annealing theoretical paradigm.

Using the algorithm for image registration , a total of 200 two dimensional experiments for alignment of a T2 to a T1 axial MR scan were performed. The use of the binary areas allowed us to make use of an experimental protocol for numerous image registration experiments. A standard experimental protocol with standard geometric transformations with a wide range of values was developed for the evaluation of the method. The three dimensional registration accuracy of the method was tested with a total of 240 three dimensional registration experiments. A protocol for the three dimensional experiments also includes a standard set of transformations with wide range of values in the 3D space. In the following chapter we will present the results obtained for volumes and areas as the main registration feature.

CHAPTER IV

EXPERIMENTAL RESULTS FOR MEDICAL IMAGE REGISTRATION USING BINARY AREAS AND VOLUMES

We have presented in Chapter 3 the ratio image registration method with weighting performed in order to set the ratios with background voxels in the denominator to a standard high value. These ratios create ratio images with binary areas which when minimized bring the images into register. We have shown that the method comprises of interpolation of the data, fuzzy c-means classification, thresholding, registration function computation and iteration loop. The changes made to the algorithm allowed us to program and test the method with a high number of registration experiments. We have presented the data we used to perform the experiments and in sections 3.5 and 3.6 the protocols for the 2D and 3D experiments.

In this chapter we will present the experimental results of the method for medical image registration which was applied to solve the problem of registration of MR images of the head using binary areas and volumes. A total of 200 two-dimensional and 240 three-dimensional registration experiments were performed using patient data from the database of the Cleveland Clinic Foundation. The purpose of this chapter is to present a synopsis of the results obtained by performing these experiments. We also give the procedures followed at the Department of Musculosceletal Radiology of the Clevaland Clinic Foundation which is a high quality working environment in an area similar to downtown Cleveland.

In the first part of this Chapter we will show how the parameters of the registration function and the iteration loop were selected. Then we will give a two dimensional registration example, a summary of the results, procedures for two and three dimensional experiments, an evaluation of the method ,and finally the results of the application of the method for non rigid registration using B-splines with local support.

4.1 Two-dimensional results - "20 displacement" technique

4.1.1 Choice of the number of Chebyshev points

We have performed extensive experiments in order to define the number of Chebyshev points that should be used for 2D and for 3D experiments. For all the two-dimensional experiments performed, the number of Chebyssev points was set to n=10 for 36 transformation units. This value was decided by applying the "20 displacement" technique experiment for patient 1 for n=4,5,...,10 and using only the geometric transformations 1-10. The Average Absolute Rotational Error for each value of n is given in table 3. It was less than 1 degree for $n \geq 8$. Using these results, the value of n was set to 10.

Table 3: Average Absolute Rotational Errors for the two-dimensional T1-T2 MR image registration case for patient 1 and various numbers of Chebyssev points n for 36 transformation units.

Chebyssev points n	4	5	6	7	8	9	10
AARE (degrees)	3.85	3.47	3.01	1.27	0.21	0.36	0.17

4.1.2 Choice of the registration function - Variance versus mean squared value

As described in Chapter III, the registration function is defined as the mean squared value of the average weighted ratio of the two images. The initial implementation of the method used a different registration function - the variance of the average weighted ratio. The variance of the ratio is also the correlational criterion that Woods et al. [35,36] use to align images. The mean squared value was chosen for two reasons:

a) The variance function provides a small value for the correct registration position but its global minimum is for the position in which no overlap between the two images exists for which it becomes zero.

b) The registration accuracy with the mean squared value as the registration function was found to be better than with the variance. This was tested for the two-dimensional case by applying the “20 displacement” experiment for patient 1 with both the variance and the mean squared value, using only the first 10 of the 20 geometric transformations. The Absolute Rotational Error for these 10 cases with the use of the variance function varied between the values of 0.1 and 1.03 degrees (average 0.35 degrees), whereas with the use of the mean squared value, the error varied between 0.02 degrees and 0.6 degrees (average 0.17 degrees). It must be noted, however, that with the use of variance in no case were the eight iterations reached for the adjustment of any geometric transformation parameter, whereas with the mean squared value, this happened once for xy rotation, three times for y translation and four times for x translation. The Average Absolute Translational Errors were 0.9 mm for the mean squared value and 0.63 mm for the variance.

4.1.3 A two-dimensional registration example

To illustrate the registration procedure, a two-dimensional registration “20 displacement” experiment will be given in terms of the registration function curves, as they are extrapolated for the xy plane rotation parameter and for each iteration. The experiment uses the transformation number 12 and data from patient 1. The thresholds used for the two scans were computed by applying the fuzzy c-means to the two scans and were 381 for the T1 and 120 for the T2 scan. Figure 6 shows the two scans before and after registration. The top left image (a) is the T1 reference scan, the top right image (b) is the T2 reslice scan before registration and the bottom left image (c) is the reslice scan after registration. The errors computed for this experiment were 0.05 deg for xy rotation and 0 voxels for x translation and 2 voxels for y translation. Figures 7 to 9 show the variance curves with each iteration for rotational adjustment. The minimum values marked on the curves are the adjustment values that the algorithm uses to register the two images. The total adjustment is 37.68 deg, which corresponds to an error of 0.05 deg.

4.1.4 Summary of the results from 200 two-dimensional experiments

A total of 200 "20 displacement" experiments were performed using the data from the 10 patients. Table 4 gives a summary of the Average Absolute Errors per patient. It can be seen that the Average Absolute Rotational Error varies between 0.16 and 0.38 degrees (average 0.23 degrees), whereas the Average Absolute Translational Error varies between 0.32 and 1.01 mm (average 0.79 mm).

(a) (b)

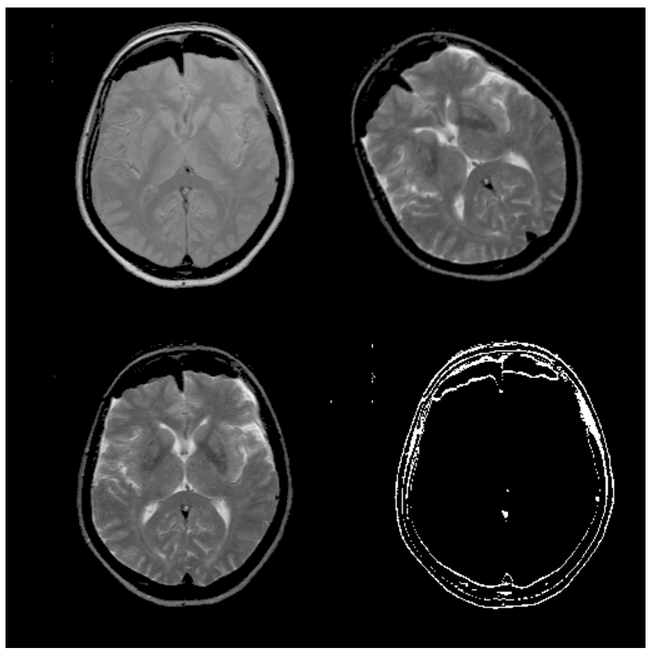

(c) (d)

Figure 6: "20 displacement" T1-T2 registration example. Reference and reslice scans before and after registration. Top left (a): Reference T1 MR scan. Top right (b): Reslice T2 MR scan before registration. The two scans are rotated by 37.63 deg and translated by 23 voxels along the x-axis and 7 voxels along the y-axis. Bottom left (c): Reslice scan

after registration. The registration error is 0.05 deg for xy rotation, 0 voxels for the x translation, and 2 voxels for the y translation. Bottom right (d): the white areas show the areas of non-overlap of the two scans after registration.

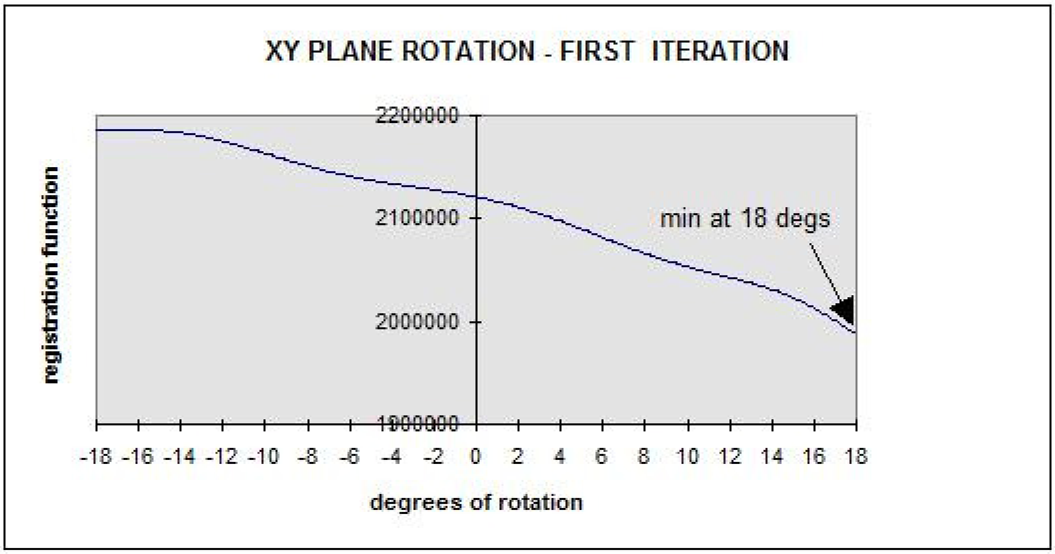

(a)

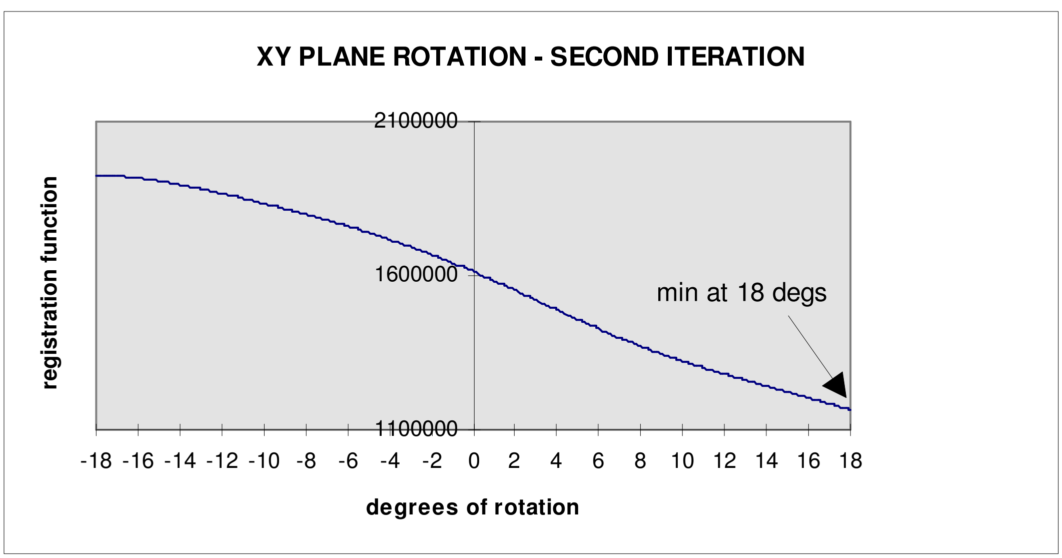

(b)

Figure 7: “20 displacement” T1-T2 registration example. Registration function minimization curves. Iterations 1 (a) and 2 (b).

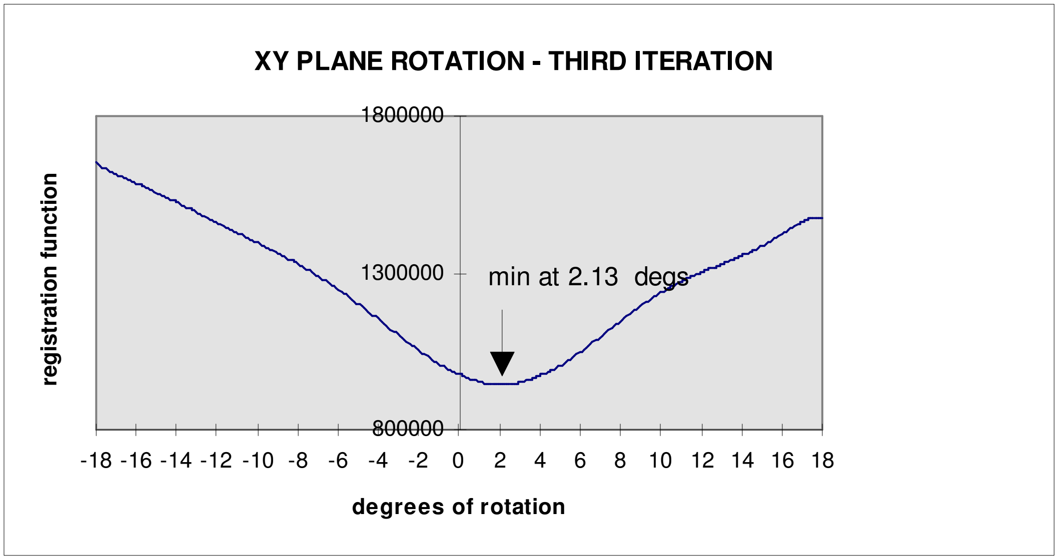

(c)

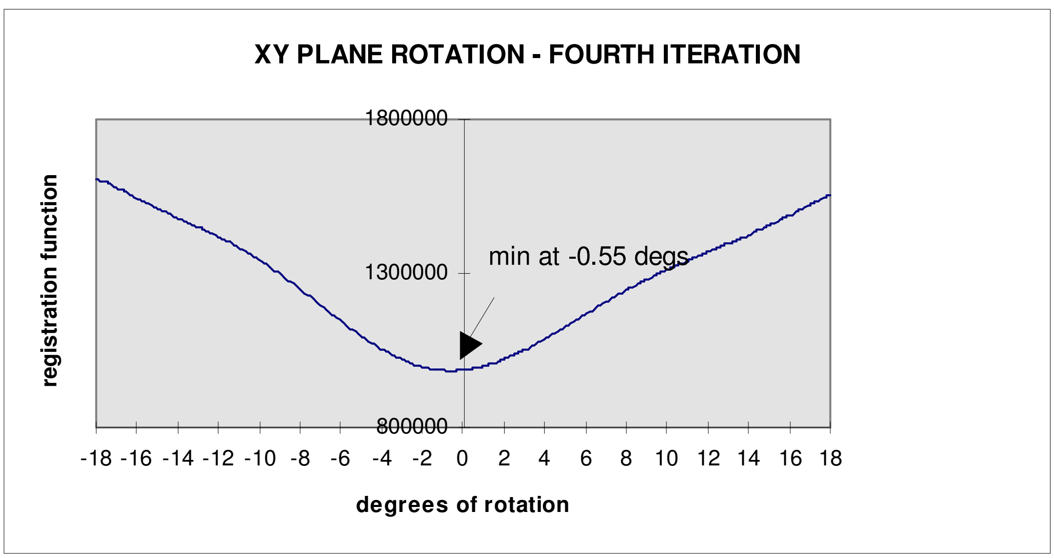

(d)

Figure 8:”20 displacement” T1-T2 registration example. Registration function minimization curves. Iterations 3 (c) and 4 (d).

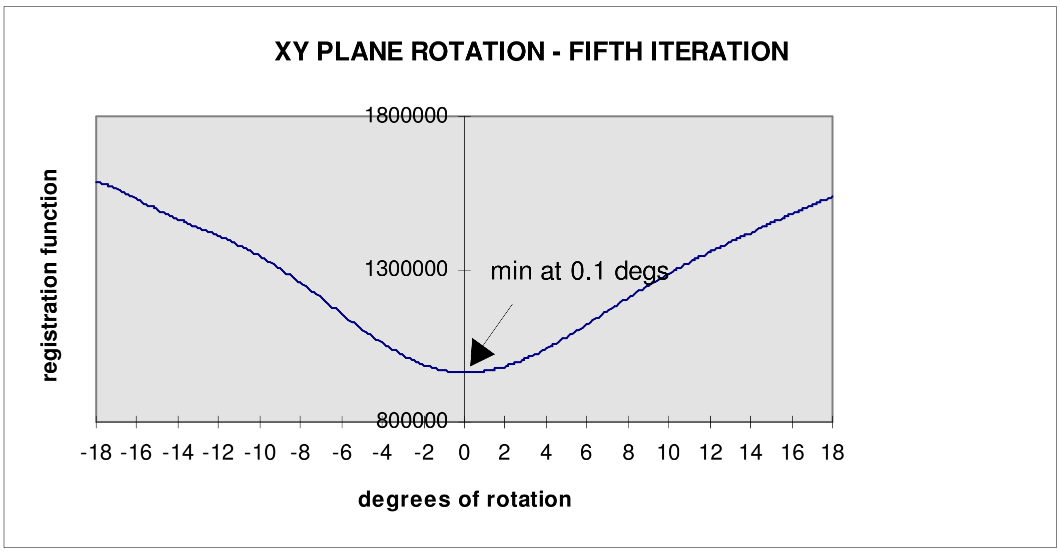

(e)

Figure 9: "20 displacement" T1-T2 registration example. Registration function minimization curve. Final iteration 5 (e).Total adjustment: 18+18+2.13-0.55+0.1 = 37.68 deg. Registration error: 37.68-37.63 = 0.05 deg

Table 4: Average Absolute Rotational and Translational Errors per patient for two-dimensional “20 displacement” registration experiments.

Patient number	**AARE (deg)**	**AATE(mm)**
1	0.18	0.9
2	0.21	0.9
3	0.38	0.78
4	0.25	0.32
5	0.16	0.45
6	0.19	0.9
7	0.22	0.9
8	0.25	0.9
9	0.19	0.9
10	0.25	1.01
Average	**0.23**	**0.79**

4.2 Three-dimensional results - “10 displacement” experiments

As mentioned earlier in section 3.6, the “10 displacement” technique was used for performing 200 three-dimensional registration experiments for T1-T1 and T1-T2 MR data registration. For all these experiments, n=4 Chebyssev points for 36 transformation units were used because this value was found to give rotational errors less than 1 degree. This section will summarize the results obtained from these experiments. The 10 T1-T2 registration cases with the highest Absolute Rotational Errors will first be presented.

Then the worst case will be selected and the whole registration procedure will be described and given in terms of surface renderings with the relative positions of the two volumes. Finally, a statistical description of the results will be given. Full results from all the "10 displacement" experiments can be found in Appendix A. They include the errors computed for each experiment and for each geometric transformation parameter.

4.2.1 Worst-case analysis

Table 5 shows the 10 worst "10 displacement" T1-T2 registration cases in terms of the Absolute Rotational Errors computed for these cases. The first column shows the order of the case with case 1 corresponding to the experiment with the highest ARE. The second and third columns show the patient and the geometric transformation numbers. The fourth column shows the ARE values for each case, and the fifth column shows

Table 5: Absolute Rotational Errors for the 10 worst cases of T1-T2 "10 displacement" registration experiments.

Case	Patient	Transformation	ARE (degrees)	AARE (degrees)
1	3	5	0.89	0.46
2	6	5	0.80	0.45
3	3	3	0.79	0.46
4	10	3	0.75	0.49
5	6	3	0.70	0.45
6	8	4	0.70	0.44
7	4	3	0.69	0.27
8	8	10	0.66	0.44
9	3	4	0.65	0.46
10	1	4	0.61	0.36

the Average Absolute Rotational Error for the patient of the second column. The worst case corresponds to patient 3 and transformation 5, which gave an ARE value of 0.89 degrees, 0.43 degrees higher than the AARE value for patient 3.

Table 6 shows the errors for all the transformation parameters and iterations for the worst-case experiment. The first column shows the iteration numbers with iteration number 0 corresponding to the initial misalignments imposed by transformation 5. Columns 2 to 7 show the errors for each iteration and transformation parameter. The last row of the table shows the final adjustment errors. The application of the maximum iteration rule affected the adjustment errors for the xy rotation and the y translation that did not converge after eight iterations. The values of table 6 can be compared with the values of table 7, which gives the average absolute errors per iteration for all the T1-T2 "10 displacement" registration experiments that used transformation 5. This comparison shows that for the worst case there is a slowing in the rhythm of reduction of the absolute error with each iteration. This is most obvious for the xy rotation, which gives an absolute error less than 1 degree for the first time on the eighth iteration. In no other case in all the T1-T2 "10 displacement" registration experiments did a transformation parameter give error less than one transformation unit so late in the registration procedure. A similar behavior is observed for the xy rotation in the corresponding T1-T1 "10 displacement" experiment. Another interesting observation can be made when the same values with table 7 are computed for the T1-T1 registration experiments (table 8) and the absolute differences of the values of tables 7 and 8 are computed (table 9).

It can be seen that the differences in the errors per iteration are always less than one transformation unit with an average value less than 0.5 transformation unit and the differences in the final adjustment are also less than 0.5 transformation unit. This result shows that our method is not affected by the differences in the signal intensities between the two studies and can thus be considered surface based. More results that justify this characterization will be given later in this chapter.

Table 6 : Errors for each iteration for the worst-case T1-T2 “10 displacement” registration experiment. In bold the values of maximum iteration rule for xy rotation and y translation caused y the even number of Chebyshev points.

Iteration number	**xy rotation error (degrees)**	**yz rotation error (degrees)**	**zx rotation error (degrees)**	**x translation error (voxels)**	**y translation error (voxels)**	**z translation error (voxels)**
0	-26.58	-6.3	-2.16	-2	-4	0
1-6	-22.86	-3.03	-1.26	-1	2	0
7-12	-19.71	0	-0.36	2	-1	0
13-18	-16.11	0.11	-0.36	-2	-1	0
19-24	-12.63	-0.78	-0.36	1	1	0
25-30	-9.7	-0.78	-0.36	0	-2	0
31-36	-5.54	-0.78	-0.36	0	0	0
37-42	**-2.5**	-0.78	-0.36	0	**-1**	0
43-48	**-0.59**	-0.78	-0.36	0	**0**	0
Max iteration rule	**-1.54**	-0.78	-0.36	0	**0**	0

Table 7: Average Absolute Errors for each iteration of transformation 5 and all patients for T1-T2 "10 displacement" registration experiments. 1.8 mm is the voxel size.

Iteration number	xy rotation error (degrees)	yz rotation error (degrees)	zx rotation error (degrees)	x translation error (mm)	y translation error (mm)	z translation error (mm)
0	26.58	6.3	2.16	2*1.8	4*1.8	0
1-6	21.2	1.7	0.69	0.6*1.8	2.2*1.8	0.1*1.8
7-12	14.65	0.88	0.88	1.5*1.8	1*1.8	0.1*1.8
13-18	8.8	0.36	0.64	0.5*1.8	0.6*1.8	0.2*1.8
19-24	4.59	0.64	0.52	0.7*1.8	0.6*1.8	0.2*1.8
25-30	2.28	0.33	0.65	0.3*1.8	0.5*1.8	0.2*1.8
31-36	1.24	0.52	0.5	0.2*1.8	0.3*1.8	0.2*1.8
37-42	0.51	0.37	0.49	0.2*1.8	0.4*1.8	0.2*1.8
43-48	0.44	0.5	0.49	0.2*1.8	0.2*1.8	0.2*1.8
Max iteration rule	0.55	0.5	0.49	0*1.8	0.2*1.8	0.2*1.8

4.2.2 Worst T1-T2 "10 displacement" registration case

As stated in the previous section, the worst case for T1-T2 "10 displacement" registration corresponds to patient 3 and transformation 5. The errors after each iteration for this case were given in table 6 and the ARE was computed to be 0.89 degrees, which was 0.43 degrees higher than the AARE value for the same patient and all 10 transformations of table 2. In this section the whole registration procedure for this case will be presented in detail and will also be depicted with surface renderings of the two volumes before and after registration.

For the worst-case experiment, the T1-T2 interleaved study of patient 3 of the first examination date (November 3, 1994) was used. This study constituted of 19 T1 and 19 T2 scans with voxel size 0.9x0.9x5 mm. The files were transformed from ACR-NEMA 2.0 format to the Cleveland Clinic Foundation Biomedical Engineering Department BIP format using the STACR utility of the BIP library. The info on the voxel size was extracted from the header of the BIP files, the raw data were also extracted, the T1 scans were separated from the T2 scans and saved as two different studies in the IMPACT raw format that is read by the all the three-dimensional image processing programs written for this thesis. This format saves the MR scans as short raw images with a header of 6144 bytes. The size of the image data is 256x256 voxels and two bytes per voxel are used. The names of the files are descriptive and follow a standard naming format. The first character of the file name is the "i" referring to the IMPACT format followed by the patient number, the date of the examination, the number of the ACR-NEMA study and the type of the IMPACT study, the increasing number of the scan in this study and finally the ".ima" ending. For example, the name "ipat03_nov94_std0t1_10.ima" refers to an IMPACT image that corresponds to the tenth T1 scan of the first MR T1-T2 interleaved study, performed to patient 3 in November 1994. All the scans of the two IMPACT studies are saved to a standard directory "~/3d/data" from which all the three-dimensional image processing utilities read the input files. The user defines the input files by providing the standard part of the two file names, which for this example were “ipat03_nov94_std0t1_” and “ipat03_nov94_std0t2_”, and also the numbers of the first and last scan of the two studies, which for a study with 19 scans would be 1 and 19.

Table 8: Average Absolute Errors for each iteration of transformation 5 and all patients for T1-T1 “10 displacement” registration experiments. 1.8 mm is the voxel size.

Iteration number	xy rotation error (degrees)	yz rotation error (degrees)	zx rotation error (degrees)	x translation error (mm)	y translation error (mm)	z translation error (mm)
0	26.58	6.3	2.16	2*1.8	4*1.8	0*1.8
1-6	21.44	1.76	0.63	0.7*1.8	2.1*1.8	0*1.8
7-12	13.97	0.85	1	1.9*1.8	0.6*1.8	0*1.8
13-18	9.44	0.6	0.47	0.8*1.8	0.3*1.8	0*1.8
19-24	4.63	0.52	0.97	0.6*1.8	0.5*1.8	0*1.8
25-30	2.24	0.33	0.51	0.5*1.8	0.3*1.8	0*1.8
31-36	0.97	0.27	0.48	0.4*1.8	0.3*1.8	0*1.8
37-42	0.58	0.26	0.44	0.3*1.8	0.3*1.8	0*1.8
43-48	0.34	0.26	0.33	0.3*1.8	0.3*1.8	0*1.8
Max iteration rule	0.4	0.32	0.34	0.1*1.8	0.1*1.8	0*1.8

Table 9: Absolute differences of the errors given in tables 7 and 8. 1.8 mm is the voxel size.

Iteration number	**xy rotation error (degrees)**	**yz rotation error (degrees)**	**zx rotation error (degrees)**	**x translation error (mm)**	**y translation error (mm)**	**z translation error (mm)**
0	0	0	0	0*1.8	0*1.8	0*1.8
1-6	0.24	0.06	0.06	0.1*1.8	0.1*1.8	0.1*1.8
7-12	0.68	0.03	0.12	0.4*1.8	0.4*1.8	0.1*1.8
13-18	0.64	0.24	0.17	0.3*1.8	0.3*1.8	0.2*1.8
19-24	0.04	0.12	0.45	0.1*1.8	0.1*1.8	0.2*1.8
25-30	0.04	0	0.14	0.2*1.8	0.2*1.8	0.2*1.8
31-36	0.27	0.25	0.02	0.2*1.8	0*1.8	0.2*1.8
37-42	0.07	0.11	0.05	0.1*1.8	0.1*1.8	0.2*1.8
43-48	0.1	0.24	0.16	0.1*1.8	0.1*1.8	0.2*1.8
Max iteration rule	0.15	0.18	0.15	0.1*1.8	0.1*1.8	0.2*1.8
Average	0.27	0.12	0.15	0.19*1.8	0.13*1.8	0.18*1.8

The first program to be applied in this example registration procedure was the fuzzy c-means hierarchical algorithm. The algorithm was applied sequentially to all the scans of the two studies. For each study the classification program was executed as follows:

The user was noted to provide two identification numbers of the first and second study. Since one study was processed with each execution of the program the same identification, for example, "ipat03_nov94_std0t1_", was used for both studies. The study to be processed had 19 scans and when the numbers of the first and last scan for the two studies were requested, the numbers 1-10 and 11-19 were given. In this way all the scans of the IMPACT study "ipat03_nov94_std0t1_" were processed in the order 1,11,2,12,3,13.... The reason for this special type of input used by the classification algorithm is that the hierarchical form of the c-means was programmed for processing of MR FLAIR image data that are acquired in the Department of Radiology of the Cleveland Clinic Foundation; these image studies have to be read in an interleaved way. The next information that the user was asked to provide was the prefix of the names of the classified image files which were saved with a name, using this prefix followed by a number that showed the order by which the scans had been processed. Consequently the user gave the number of levels of the hierarchical scheme, which for this case was 1 and the number of clusters for the first level, which was 3. After all this information was provided, the classification program processed all the scans of the IMPACT study "ipat03_nov94_std0t1_" and computed the centers of the three clusters for each scan. These centers were then used to compute the thresholds for each scan by taking the average of the two lowest clusters centers. The same procedure was then repeated for the IMPACT study "ipat03_nov94_std0t2_". The thresholds computed for the two studies of the worst-case example are shown in Table 10. The lowest of the thresholds for each study was considered as the global threshold of the study and appears in the same table in boldface characters.

The next step of the method was to enter the main registration procedure. The user defined the two studies to be registered by giving the identification numbers of the two studies, which for this case were “ipat03_nov94_std0t2_” for the reslice study and “ipat03_nov94_std0t1_” for the reference study. The user was then asked to provide some initial estimates for the geometric transformation parameters needed for registration. For the case of the “10 displacement” experiments, where the two studies correspond to the same position of the head, the estimates given in this point of the procedure are used to deregister the two volumes. Therefore for this experiment the rotational and translational parameters of the transformation 5 were given. Then the user was asked to provide the voxel size parameters, which were 0.9 mm for the xy plane resolution and 5 mm for the z axis thickness. Since half resolution is used for all the “10 dispacement” experiments, the xy plane resolution was multiplied by two. Using this xy plane resolution as the cubic voxel size, the translations, given in millimeters, were transformed into voxel numbers using the nearest integer approach. The trilinear interpolation routine was then applied to the two studies to create the cubic voxel with dimensions 1.8x1.8x1.8 mm. The size of the volumes created was 128x128xZ with Z=18x(5/1.8)=50. An empty area on the top and the bottom of each volume was also created by inserting (int)(5/1.8)+1=3 layers of zero valued cubic voxels. The purpose was to reduce the truncation of the edges of the volume, which when the volume is rotated, exceed the image area.

Table 10: Thresholds computed with the use of the fuzzy c-means for all the scans of the two studies of the worst-case T1-T2 “10 displacement” registration experiment.

Scan number	**T1 study thresholds**	**T2 study thresholds**
1	410	143
2	396	138
3	383	128
4	376	130
5	369	135
6	372	130
7	500	245
8	540	250
9	535	256
10	544	258
11	434	265
12	325	265
13	354	260
14	350	238
15	362	154
16	370	143
17	350	116
18	316	101
19	**265**	**75**

After the two cubic voxel volumes were created, the main registration procedure started. First the global thresholds that were computed with the fuzzy c-means were used to set the background voxels to zero. The registration function minimization iteration loop was then applied. Six buffers that summate the adjustment values for each of the six rotational or translational parameters were defined; their values were used to transform the reslice volume. This operation for the first iteration deregistered the two volumes with the rotational and translational parameters of transformation 5. For each of the next iterations the adjustment values were the ones computed by the iteration loop; these were used to register the two volumes. All the transformations were performed to the reslice volume, with center of rotations its centroid, which was computed before the iteration loop and was updated according to the translations applied to this volume. As noted in Chapter II, one geometric transformation parameter was adjusted with each iteration and the adjustment value was computed by taking the minimum of the registration function approximated from n=4 Chebyssev points for 36 transformation units. After all the transformations converged or the maximum iteration limit was reached, the final adjustment was applied to the reslice volume and the two volumes were saved. Figures 10 to 12 show the surface renderings with the relative position of the two volumes of the worst-case example before and after registration. For these illustrations the two volumes were enhanced using three-dimensional median filtering and then rendered using an AVS commercial isosurface renderer software package. We rendered the surface of the 3D image considered as the reference image. We also rendered the surface of the 3D image considered as reslice before and after registration. The rendering of the reference shows the same orientation with the reslice image after registration.

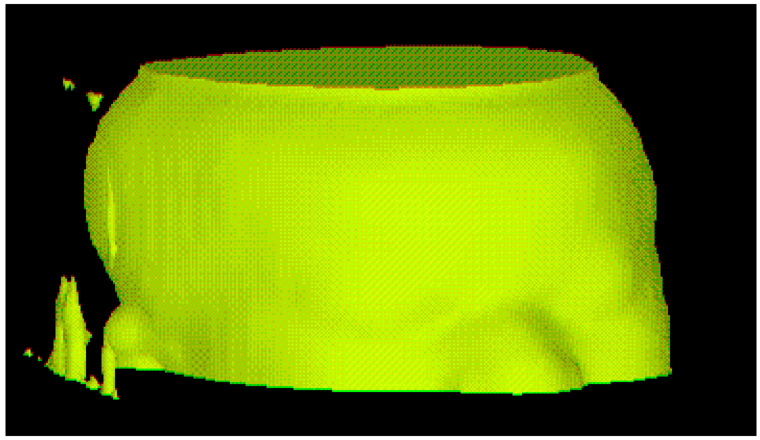

Figure 10: T1-T2 registration example. Surface rendering of the reference T1 image volume for the worst-case T1-T2 “10 displacement” registration experiment.

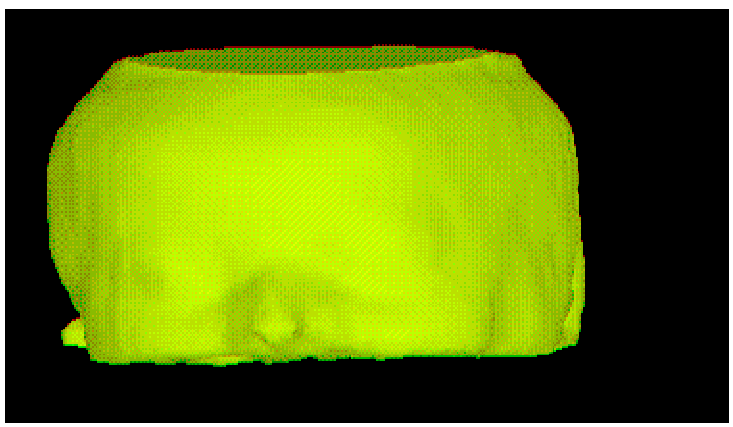

Figure 11: T1-T2 registration example. Surface rendering of the reslice T2 image volume for the worst-case T1-T2 “10 displacement” registration experiment before registration.

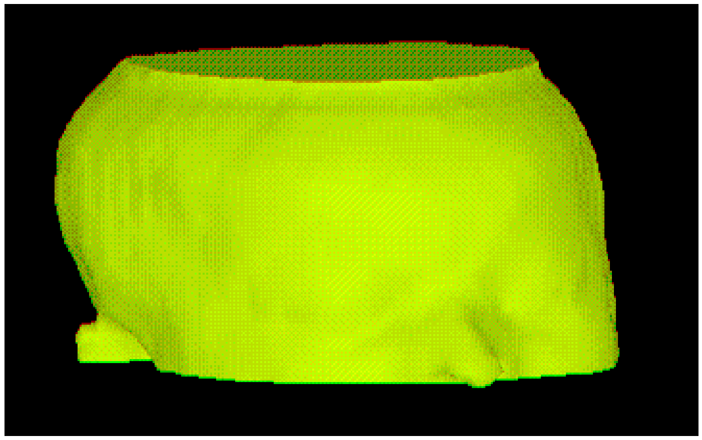

Figure 12: T1-T2 registration example. Surface rendering of the reslice T2 image volume for the worst-case T1-T2 "10 displacement" registration experiment after registration to volume of figure 10.

4.2.3 Summary of the results from 200 "10 displacement" 3D experiments

A total of 200 "10 displacement" experiments were performed for T1-T1 and T1-T2 three-dimensional registration. Tables 11 and 12 give a summary of the average absolute errors per patient for "10 displacement" registration. Table 11 shows that for T1-T1 registration the Average Absolute Rotational Error per patient varied between 0.17 and 0.42 degrees with an average value of 0.24, whereas the Average Absolute Translational Error per patient varied between 0 and 0.03 voxels with an average value of 0.02. Table 12 shows the same errors for the T1-T2 "10 displacement" experiments. The average values are 0.36 for AARE (range, 0.23 to 0.49 degrees) and 0.2 voxels for AATE (range, 0.03 to 0.53 voxels).

Table 11: Average Absolute Rotational and Translational Errors per patient for "10 displacement" T1-T1 registration experiments. 1.8 mm is the voxel size.

Patient	**AARE (degrees)**	**AATE (mm)**
1	0.24	0.03*1.8
2	0.23	0.03*1.8
3	0.42	0.03*1.8
4	0.17	0*1.8
5	0.18	0*1.8
6	0.35	0*1.8
7	0.21	0*1.8
8	0.2	0*1.8
9	0.26	0.03*1.8
10	0.18	0.03*1.8
Average	**0.24**	**0.02*1.8**

Table 12: Average Absolute Rotational and Translational Errors per patient for "10 displacement" T1-T2 registration experiments. 1.8 mm is the voxel size.

Patient	**AARE (degrees)**	**AATE (mm)**
1	0.36	0.2*1.8
2	0.24	0.2*1.8
3	0.46	0.13*1.8
4	0.27	0.13*1.8
5	0.37	0.03*1.8
6	0.45	0.23*1.8
7	0.32	0.33*1.8
8	0.44	0.03*1.8
9	0.23	0.13*1.8
10	0.49	0.53*1.8
Average	**0.36**	**0.2*1.8**

It can be seen that no significant loss in accuracy is measured when going from T1-T1 to T1-T2 registration. This result shows, once more, that our method is surface based. Tables 13 and 14 show the same results as they are computed per geometric transformation and for all patients. It can be seen that the initial misalignment imposed does not affect the registration accuracy of the method.

4.3 3D results - "different times" experiments

In addition to the "10 displacement" experiments, 40 "different times" registration experiments were performed. These experiments were T1-T1 or T1-T2 and aimed at:

- investigating the surface matching nature of the method
- identifying the effect of different imaging resolutions to the registration algorithm.

The main results obtained from these experiments will be presented in the next sections.

4.3.1 Half resolution "different times" experiments

The half resolution "different times" experiments were performed to identify changes in the behavior of the registration algorithm between T1-T1 and T1-T2 registration. This was done by measuring the differences in the adjustment values computed by the algorithm for each iteration. The results from these measurements are shown in tables 15 to 18. Table 15 shows the final adjustments per patient for the 10 "half resolution" T1-T1 "different times" experiments. Table 16 shows the same result for the T1-T2 experiments and table 17 shows the absolute differences in the adjustment values of the two previous tables. The differences in rotational parameters vary between 0 and 1.57 degrees with average values 0.28 degrees for xy rotation, 0.32 degrees for yz rotation and 0.33 degrees for zx rotation. The differences in translational parameters vary between 0 and 1 voxel with average values of 0.4 voxels for x translation, 0.5 voxels for y translation and 0.4 voxels for z translation. Table 18 shows the absolute differences in the adjustment values per iteration for the worst-case patient 3.

The same trend can be seen, since the rotational adjustment differences are less than 0.34 degrees and the translational adjustment differences are less than 1 voxel. Both of these results show clearly that the performance of the method is not affected by the differences in signal intensity and therefore the method can be implemented as surface based.

Table 13: Average Absolute Rotational and Translational Errors per transformation for "10 displacement" T1-T1 registration experiments. 1.8 mm is the voxel size.

Transformation	**AARE (degrees)**	**AATE (mm)**
1	0.22	0*1.8
2	0.19	0.03*1.8
3	0.2	0*1.8
4	0.32	0.1*1.8
5	0.32	0.03*1.8
6	0.27	0*1.8
7	0.22	0*1.8
8	0.24	0*1.8
9	0.27	0*1.8
10	0.2	0*1.8
Average	**0.24**	**0.02*1.8**

Table 14: Average Absolute Rotational and Translational Errors per transformation for "10 displacement" T1-T2 registration experiments. 1.8 mm is the voxel size.

Transformation	**AARE (degrees)**	**AATE (mm)**
1	0.29	0.13*1.8
2	0.3	0.3*1.8
3	0.47	0.13*1.8
4	0.41	0.2*1.8
5	0.48	0.2*1.8
6	0.3	0.17*1.8
7	0.38	0.17*1.8
8	0.34	0.2*1.8
9	0.32	0.23*1.8
10	0.35	0.17*1.8
Average	**0.36**	**0.2*1.8**

Table 15: Final adjustment values per patient for half resolution "different times" T1-T1 registration experiments. 1.8 mm is the voxel size.

Patient number	**xy rotation (degrees)**	**yz rotation (degrees)**	**zx rotation (degrees)**	**x translation (mm)**	**y translation (mm)**	**z translation (mm)**
1	-2.36	-1.7	-0.33	-4*1.8	-4*1.8	0*1.8
2	5.96	-0.67	1.3	3*1.8	1*1.8	0*1.8
3	-2.92	-1.57	-0.22	-1*1.8	0*1.8	0*1.8
4	-1.91	-0.33	-0.22	-1*1.8	-2*1.8	0*1.8
5	-4.61	0.33	1.12	-2*1.8	0*1.8	-1*1.8
6	2.02	-0.67	0	-15*1.8	-2*1.8	-1*1.8
7	-10.01	0.45	-0.45	-2*1.8	2*1.8	-1*1.8
8	-5.73	-1.68	0	5*1.8	8*1.8	0*1.8
9	0.45	0.11	0.11	-1*1.8	0*1.8	0*1.8
10	-4.61	0.33	0.11	0*1.8	0*1.8	0*1.8

Table 16: Final adjustment values per patient for half resolution “different times” T1-T2 registration experiments. 1.8 mm is the voxel size.

Patient number	**xy rotation (degrees)**	**yz rotation (degrees)**	**zx rotation (degrees)**	**x translation (mm)**	**y translation (mm)**	**z translation (mm)**
1	-1.91	-1.68	-0.11	-4*1.8	-4*1.8	0*1.8
2	5.96	-0.33	1.12	2*1.8	1*1.8	-1*1.8
3	-2.58	-1.91	-0.22	-1*1.8	-1*1.8	1*1.8
4	-2.02	0.45	-0.33	-1*1.8	-1*1.8	0*1.8
5	-4.38	0	1.25	-2*1.8	-1*1.8	0*1.8
6	1.79	-0.78	-1.57	-14*1.8	-3*1.8	-2*1.8
7	-10.23	0.45	-0.78	-3*1.8	1*1.8	-1*1.8
8	-5.96	-1.12	-0.22	4*1.8	8*1.8	0*1.8
9	0.33	1.12	0.33	-1*1.8	0*1.8	0*1.8
10	-5.51	0.67	0.45	0*1.8	0*1.8	0*1.8

Table 17: Absolute differences of the adjustment values of tables 15 and 16. 1.8 mm is the voxel size.

Patient number	xy rotation (degrees)	yz rotation (degrees)	zx rotation (degrees)	x translation (mm)	y translation (mm)	z translation (mm)
1	0.45	0.02	0.22	0*1.8	0*1.8	0*1.8
2	0	0.34	0.18	1*1.8	0*1.8	1*1.8
3	0.34	0.34	0	0*1.8	1*1.8	1*1.8
4	0.11	0.12	0.11	0*1.8	1*1.8	0*1.8
5	0.23	0.33	0.13	0*1.8	1*1.8	1*1.8
6	0.23	0.11	1.57	1*1.8	1*1.8	1*1.8
7	0.22	0	0.33	1*1.8	1*1.8	0*1.8
8	0.23	0.56	0.22	1*1.8	0*1.8	0*1.8
9	0.12	1.01	0.22	0*1.8	0*1.8	0*1.8
10	0.9	0.34	0.34	0*1.8	0*1.8	0*1.8
Average	0.28	0.32	0.33	0.4*1.8	0.5*1.8	0.4*1.8

Table 17 shows that there is good behavior of the algorithm when signal intensity changes for patients imaged with different modalities. The absolute differences in the final adjustment values are below the 1 voxel size of 1.8mm. The patient data were acquired with different MR imaging methods (T1 and T2 weighted) and were stored with the patients id number at the database of the Cleveland Clinikc Foundation. For rotational and translational adjustment the differences are below the value of 0.5(degrees or voxels).

Table 18: Absolute differences of adjustment values per iteration for patient 3 between T1-T1 and T1-T2 half resolution "different times" registration experiments. 1.8 mm is the voxel size.

Iteration number	**xy rotation (degrees)**	**yz rotation (degrees)**	**zx rotation (degrees)**	**x translation (mm)**	**y translation (mm)**	**z translation (mm)**
1-6	0.34	0.23	0.11	0*1.8	1*1.8	0*1.8
7-12	0	0.22	0	1*1.8	1*1.8	1*1.8
13-18	0	0.34	0	0*1.8	1*1.8	0*1.8
19-24	0.34	0.34	0	0*1.8	1*1.8	1*1.8
Average	0.17	0.28	0.03	0.25*1.8	1*1.8	0.5*1.8

Table 18 shows the dynamic behavior of the algorithm with regards to the number of iterations and the change of signal intensity for patient 3 and T1 to T2 weighted MRI imaging taken from the database of the Cleveland Clinic Foundation. The good behavior during the registration procedure stands throughout the registration iteration loop.

4.3.2 Full resolution "different times" experiments

The same experiments outlined in the previous section were performed again at full resolution and the results were compared to the results at half resolution. The purpose was to identify the effect of different imaging resolutions on the registration algorithm. Table 19 shows the absolute differences in the final adjustment values between half and full resolution for each patient for T1-T1 registration, and table 20 shows the same result for T1-T2 registration. The average rotational differences are below 0.51 degrees. Tables 21 and 22 show the absolute differences in the adjustment values for each iteration for the worst-case patient. The average rotational differences are less than 0.64 degrees. Translational differences are higher because of the reduced effect of quantization for higher imaging resolutions. Based on these results, it can be shown that a resolution of 1.8 mm/voxel is sufficient for the registration method and that higher resolution does not seem to improve the registration accuracy.

Table 19: Absolute differences of the final adjustment values per patient between full and half resolution “different times” T1-T1 registration experiments. 0.9 mm is the voxel size.

Patient	xy rotation (degrees)	yz rotation (degrees)	zx rotation (degrees)	x translation (mm)	y translation (mm)	z translation (mm)
1	0.45	0.77	0.22	0*0.9	1*0.9	0*0.9
2	0.11	0.67	0.1	1*0.9	1*0.9	0*0.9
3	1.24	0.11	0.11	0*0.9	0*0.9	0*0.9
4	0.11	0.66	0.56	0*1.9	2*0.9	1*0.9
5	0.23	0.66	0.8	2*0.9	1*0.9	0*0.9
6	0.9	0	1.12	1*0.9	0*0.9	0*0.9
7	0.34	0.12	0.11	1*0.9	1*0.9	1*0.9
8	0.66	0	0.9	2*0.9	1*0.9	1*0.9
9	0.78	0.11	0.45	1*0.9	1*0.9	2*0.9
10	0.11	0.12	0.11	0*0.9	1*0.9	2*0.9
Average	0.49	0.32	0.45	0.8*0.9	0.9*0.9	0.7*0.9

Table 19 shows that there is good behavior of the algorithm when resolution changes for patients of the same T1 weighted MRI modality. The absolute differences in the final adjustment values are below the 1 voxel size of 0.9 mm. The patient data were acquired at different examination times and were stored with the patients id number at the database of the Cleveland Clinikc Foundation. For rotational adjustment the differences are below 0.5 degrees whereas for translational adjustments are in the range of 0.5 to 1 voxel.

Table 20: Absolute differences of the final adjustment values per patient between full and half resolution "different times" T1-T2 registration experiments. 0.9 mm is the voxel size.

Patient number	xy rotation (degrees)	yz rotation (degrees)	zx rotation (degrees)	x translation (mm)	y translation (mm)	z translation (mm)
1	0.45	0.34	0.11	0*0.9	2*0.9	0*0.9
2	0.11	0.22	0.45	1*0.9	1*0.9	2*0.9
3	0.12	0.45	0	0*0.9	1*0.9	1*0.9
4	0.23	0.78	0.23	1*0.9	0*0.9	2*0.9
5	0	0.56	0.56	1*0.9	1*0.9	2*0.9
6	0.79	0.78	0.9	0*0.9	1*0.9	1*0.9
7	0.34	0.12	0.12	0*0.9	1*0.9	1*0.9
8	0.56	0.68	0.22	0*0.9	2*0.9	1*0.9
9	0.11	0.67	0.11	1*0.9	1*0.9	1*0.9
10	0.56	0.45	0.23	0*0.9	2*0.9	1*0.9
Average	0.33	0.51	0.3	0.4*0.9	1.2*0.9	1.2*0.9

Table 20 shows that there is good behavior of the algorithm when resolution changes for patients of T1 to T2 weighted MRI modality. The absolute differences in the final adjustment values are around the 1 voxel size of 0.9 mm. The patient data were acquired at different examination times and were stored with the patients id number at the database of the Cleveland Clinikc Foundation. For rotational adjustment the differences are about 0.5 degrees whereas for translational adjustments are in the range of 0.4 to 1.2 voxel.

Table 21: Absolute differences in adjustment values per iteration for patient 3 between full and half resolution "different times" T1-T1 registration experiments. 0.9 mm is the voxel size.

Iteration number	xy rotation (degrees)	yz rotation (degrees)	zx rotation (degrees)	x translation (mm)	y translation (mm)	z translation (mm)
1-6	0.1	0.1	0.11	0*0.9	1*0.9	1*0.9
7-12	0.34	0.34	0.11	1*0.9	0*0.9	1*0.9
13-18	0.9	0.11	0.11	0*0.9	1*0.9	0*0.9
19-24	1.24	0.11	0.11	0*0.9	0*0.9	1*0.9
Average	0.64	0.17	0.11	0.25*0.9	0.5*0.9	0.75*0.9

Table 21 shows the dynamic behavior of the algorithm with regards to the number of iterations and the change of resolution for patient 3 and T1 to T1 weighted MRI imaging. taken from the database of the Cleveland Clinic Foundation. The good behavior during the registration procedure stands throughout the registration iteration loop.

Table 22: Absolute differences in adjustment values per iteration for patient 3 between full and half resolution "different times" T1-T2 registration experiments. 0.9 mm is the voxel size.

Iteration number	xy rotation (degrees)	yz rotation (degrees)	zx rotation (degrees)	x translation (mm)	y translation (mm)	z translation (mm)
1-6	0.12	0	0.34	0*0.9	0*0.9	0*0.9
7-12	0.11	0.56	0	1*0.9	1*0.9	1*0.9
13-18	0.12	0.45	0	0*0.9	1*0.9	0*0.9
19-24	0.12	0.45	0	0*0.9	1*0.9	1*0.9
Average	0.12	0.37	0.09	0.25*0.9	0.75*0.9	0.5*0.9

Table 22 shows the dynamic behavior of the algorithm with regards to the number of iterations and the change of resolution for patient 3 and T1 to T2 weighted MRI imaging. taken from the database of the Cleveland Clinic Foundation. The good behavior during the registration procedure stands throughout the registration iteration loop.

Figures 13 to 14 illustrate the "different times" T1-T1 experiment for patient 7. The T1 image volume of the first imaging date is used as the reference for this experiment. The surface rendering of this volume appears in figure 13. Figure 14 shows the scans 4, 10, and 16 of the corresponding MR study.

(a)

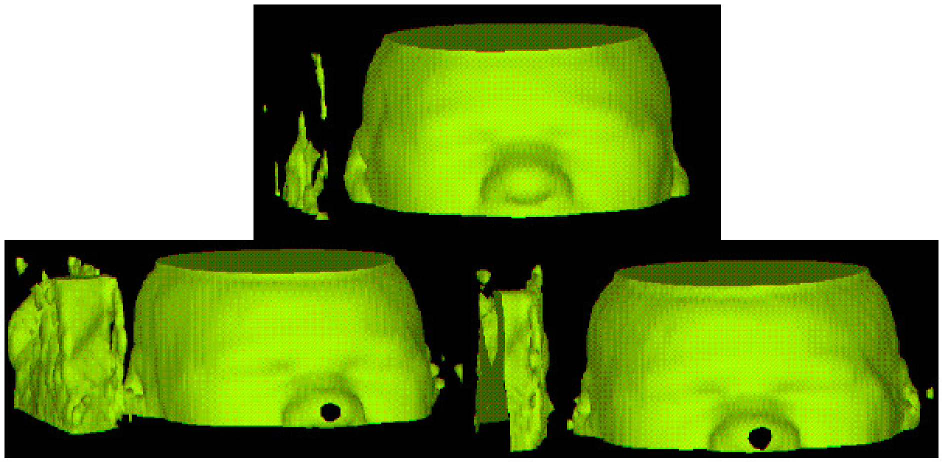

(b) (c)

Figure 13 : T1-T1 "different times" registration experiments example. Top (a): Reference T1 volume. Bottom left (b) : Reslice T1 volume before registration. Bottom right (c) : T1 volume after registration

For figure 13 we have used the AVS renderer software package to work with the MR scans from the database of the Cleveland Clinic Foundation. We have first collected the scans nd defined the reference and reslice study. We rendered with the isosurface rendering the reference study(a) and also the reslice study prior to registration(b). Then we applied the registration algorithm and created the MR scans after registration for the reslice study. Finally we rendered the reslice MR study (c). The areas of noise which remain after classification and thresholding are also rendered and it has been found that they do not affect the accuracy of the method.

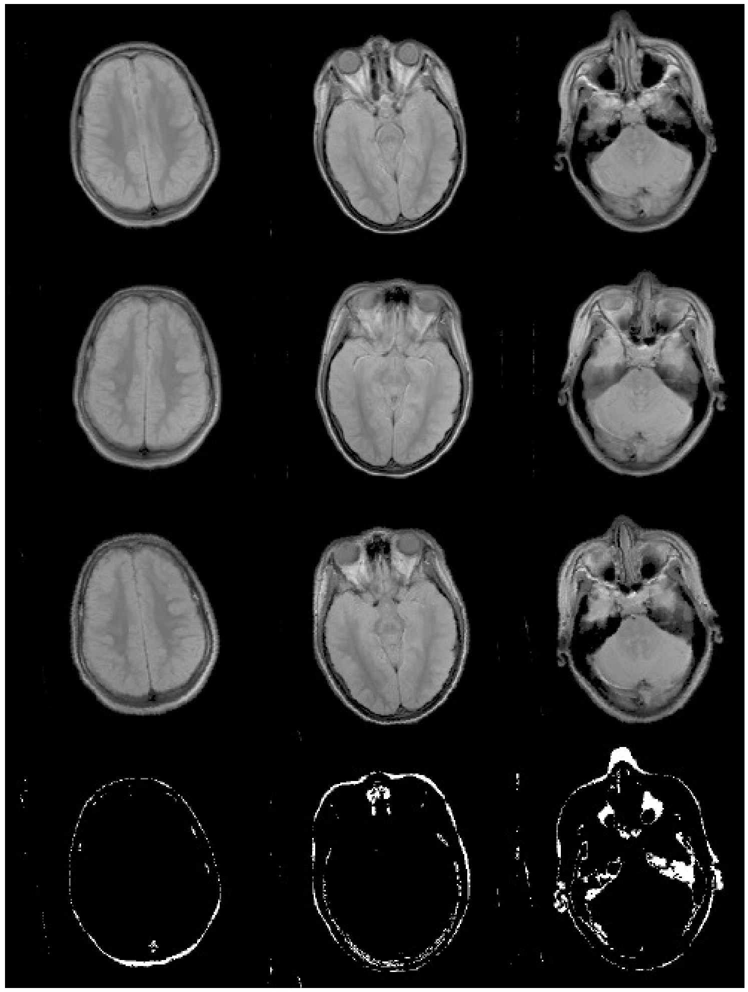

(a)

(b)

(c)

(d)

Figure 14 : Illustration of the “different times” T1-T1 three dimensional registration experiments. First row (a) : Scans #4,10,16 of the reference image study. Second row (b) : Scans #4,10,16 of the reslice image study before registration. Third row (c) : Scans #4,10,16 of the reslice image study after registration. Fourth row (d) : White areas show the areas of mismatch between the studies of rows 1 and 3.

4.4 Evaluation of the method

Using the results presented , conclusions regarding the accuracy and the surface matching nature of the method and the effect of imaging resolution will be drawn. Additionally to the evaluation of the results some more measurements that refer to the effect of non-overlapping segments in the two volumes will be presented. Finally some remarks on the ability of the method to perform non – rigid body registration will be given.

The accuracy of the method for T1-T1 and T1-T2 MR image three-dimensional registration was evaluated using the “10 displacement” technique that gave rotational and translational errors less than 1 degree and 1 voxel.

The following cautionary remarks should be noted:

a) The translational error computed by the “10 displacement” method is affected by the quantization effect due to the nearest integer implementation of the geometric transformations. The result of this effect on the error cannot be accurately estimated. The error can be corrected with the incorporation of the trilinear interpolation routine in the geometric transformations routine.

b) Both rotational and translational error estimates for the “10 displacement” technique are acquired under ideal conditions, since the rotated and translated volumes have exactly the same signal areas with the reference ones-something that can never occur in real-life experiments. Some measurements that refer to the effect of non-overlapping segments on the accuracy of the method will be presented later in this chapter.

Safer conclusions can be drawn regarding the surface matching nature of the method. Several results in the previous chapter showed that the behavior of the method is not affected by the differences in signal intensities in the two volumes. When going from T1-T1 to T1-T2 “different times” experiments, the final adjustment values and the adjustments with each iteration do not change significantly. The same holds for the errors as computed with the “10 displacement” technique: these do not deteriorate when studies of different signal intensities are registered. This result shows also either the suitability of the fuzzy c-means for surface definition with MR data or the insensitivity of the method to noise and minor surface differences. Additional studies regarding the effect of noise on the performance of the method are needed.

Deterioration in the imaging resolution was not found to affect significantly the performance of the method as measured by the rotational errors. More studies with the use of floating point operations for translations and also with volumes with voxel size of 3.6 mm should be made to investigate the extent of this effect. The ability of the method to perform well at lower resolutions is an important feature because it increases the speed of the registration procedure.

The "10 displacement" experiments were performed under ideal conditions, given that the two volumes had exactly the same signal area. To investigate the effect of non-overlapping segments on the accuracy of the method, experiments with volumes from different parts of the head were performed. These experiments used the T1 and T2 data from the first imaging date of patient 1 and geometric transformation 1. The presence of non-overlapping segments along the z dimension was assured by using scans 1-10 for the T1 study and scans (1+i) - (10+i) for the T2 study with i=0...9. All the experiments were performed at half resolution using a voxel size of 1.8 mm. The number of the experiment and the scans used for each study appear in table 23. The errors computed for each experiment and for each transformation parameter are shown in table 24. Although this result is preliminary and further analysis of the effect of non-overlapping segments effect is needed, the following two points are of interest:

a) The presence of non-overlapping segments along the z dimension affects the z-translation error, which stays constant and close to zero, whereas it should follow the increase in the extent of the non-overlapping segments. The presence of non-overlapping segments also increases the xy plane rotation error for areas of non-overlap more than 3 layers of non-cubic voxels. No effect on the x and y translation errors seems to exist.

b) Non-overlapping segments along the z axis did not affect yz, zx plane rotations. This result could be attributed to the fact that the rotation of the reslice volume is artificial and is performed after the interpolation, whereas in a real experiment, slicing and interpolation along the z axis are performed after the rotations.

More studies are needed to investigate whether the above observations are correct. As it will be shown in chapter 6 with the incorporation of projections we have managed to cut the images and create non overlapping segments and at the same time maintain the accuracy.

Table 23: Numbers of scans from each study used for the 10 non-overlapping segment experiments.

Experiment	T1 study scans	T2 study scans
1	1-10	1-10
2	1-10	2-11
3	1-10	3-12
4	1-10	4-13
5	1-10	5-14
6	1-10	6-15
7	1-10	7-16
8	1-10	8-17
9	1-10	9-18
10	1-10	10-19

Table 24: Final adjustment errors per transformation parameter for the non-overlapping segment experiments.

Exper #	xy rot (degrees)	yz rot (degrees)	zx rot (degrees)	x trans (voxels)	y trans (voxels)	z trans (voxels)
1	-1.03	0.14	-0.86	1	-1	-1
2	-0.69	0.65	-0.41	0	0	1
3	-1.59	0.93	-0.18	0	1	1
4	-3.39	0.59	-0.07	0	0	1
5	-5.08	-0.19	0.38	0	1	1
6	-6.77	-0.3	-0.52	0	1	1
7	-7.22	-0.07	-0.52	0	1	1
8	-7.78	-0.64	-0.07	0	2	1
9	-7.33	-0.3	0.71	0	2	2
10	-6.99	-0.3	0.48	0	3	2

4.5 Comparison with Mutual Information methods

We have performed a high number of experiments and we have shown [131,154] that the method:

- Gives accuracy better than 0,5 degrees and 0,5 voxels. Mutual Information Methods show accuracy more than 0,5 degrees or voxels and less than 1 in average.
- Does not stop converging because of local minima. Mutual Information methods are affected by local minima.
- After thresholding the majority of the pixels/voxels contributing to the computation of the registration function are from the signal area of the two images. For this reason, the method is not affected by noise and it can be used as a main method for image registration considering the surface as the main

characteristic. As we will show in chapter 6 the use of an amplifier of the ratios as a preprocessing step can give the impression that we do not affect the image in preprocessing with regards to background as Mutual Information methods do also.

- We have improved the Mutual Information Method throughout the chapter with the use of minimal binary information with the images.

4.6 Non-rigid body registration

Another aspect of our method that needs to be investigated is how well it can perform non-rigid body registration. The non-rigid body registration algorithm works as following:

- The signal areas are segmented from the background areas in the same way as the rigid case. It must be noted here that the threshold can be user defined and not necessarily automatically computed.

- A local elastic geometric transformation model presented in [126,127] that uses cubic B-splines is used. The local B-spline deformation model is obtained by using a scaled version of the B-splines : g(x)=x+ $\sum_{j \epsilon Ic \subset Z^N} c_j \beta_{nm}(x/h - j)$ where n ^{m} is the degree of splines used, and h is the knot spacing.

- The h parameter of the model is defined as h=32 for image dimensions 256x256 and the splines are cubic B-splines .

- The registration function is minimized iteratively in the same way as in the rigid body case with n=4 for A=18 in the range of values of the geometric transformation parameters.

One parameter is adjusted with each iteration. The effort of the parametric methods is to reduce the number of degrees of freedom for the definition of the energy term of the registration problem. Instead of defining a displacement vector for each vector parametric methods define a set of basis functions (like B-Splines) which deal with the non rigid registration problem. The functions may have global or local support and define the limitations on the solution of the problem.

For non-rigid registration the 2D form of the method has been implemented. The MR scan was transformed using the local geometric transformation model and then registered using the method.

Figure 15 shows an example of the non-rigid registration experiment. The result is after 9 iterations per parameter of the registration algorithm.

The following points are of interest:

- The ratio image uniformity method has been presented by Woods [144] for registration of warped images using a global model. We have applied the method with the binary areas using models with local support.
- The method can adjust with binary areas for large deformations and warpings.
- The registration function works at small local binary areas in the image with efficiency and does not stop to local minima.
- The order of the registration function computation at the n=4 Chebyshev points can change. (1,2,3,4) or (1,3,2,4).
- We have implemented the non rigid method with the binary projections but the method converges to local minima caused by noise points external to the signal area.
- This method has been cited in [155].

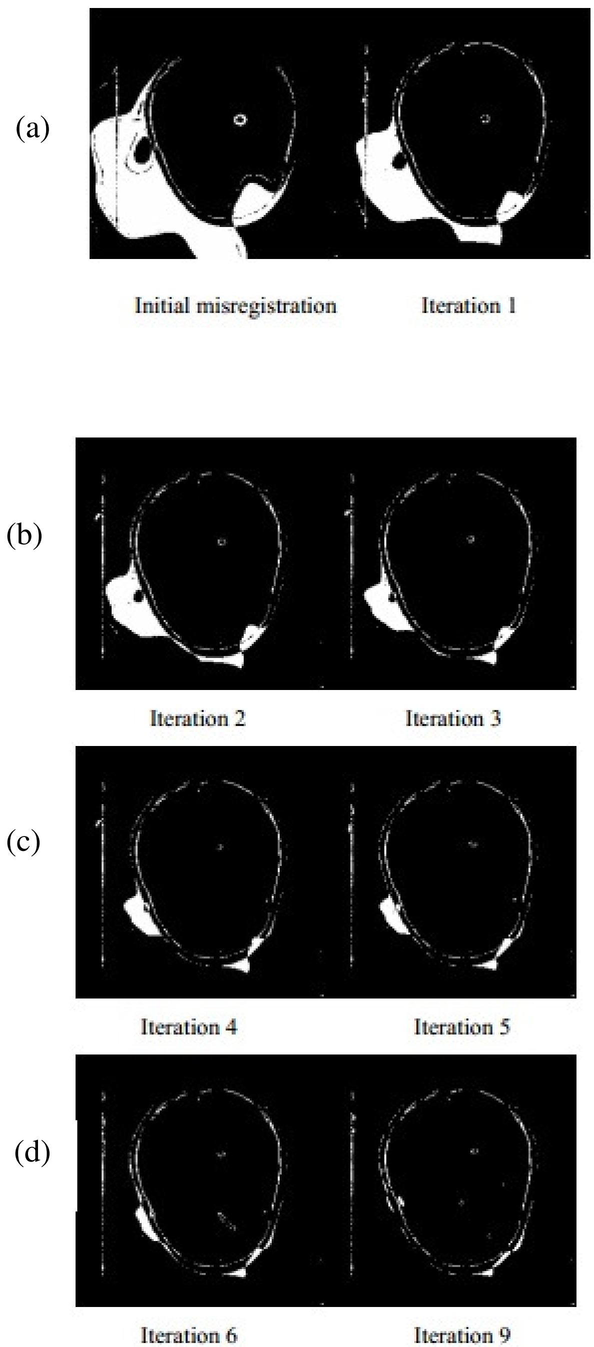

Fig.15 Areas of non overlap up to the first 9 iterations (rows a-d) show the dynamic behavior of the algorithm.

4.7 Conclusions

We have presented the main characteristics of the method for registration experiments of 2D and 3D images rigidly using binary areas and volumes.

We have chosen experimentally the number of Chebyshev points for 2D and 3D registration. We presented the registration function curves as they are extrapolated per iteration. We performed worst case registration analysis and we showed that the error is within the 1 degree and 1 voxel and below 0,5 degrees and 0,5 voxels on average. When an even number of Chebyshev points is used we apply the maximum iteration rule to define the final error which oscillates around the correct registration position. We described the main registration procedure as it was implemented in the department of Musculoskeletal Radiology of The Cleveland Clinic Foundation. We used surface renderings to present the final results of the correct registration position. WE compared half with full resolution and we found out that the method works adequately in half resolution experiments compared to full resolution ones. We performed 2D non rigid body experiments and we showed that the method works locally with large elastic deformations of binary images.

The method has the advantage compared to signal intensity methods that it is able to perform multimodality image registration. Compared to surface fitting methods the method is not affected by noise which allows the incorporation of the 2D projection algorithm into a surface fitting registration scheme. The registration function works with non rigid giving a unique solution for small areas of local effect. Compared to Mutual Information methods for rigid registration the method has been shown not to be affected by misregistrations caused by local minima and to be able to maintain an accuracy of better than 0,5 degrees and 0,5 pixels. The method has also been shown to not be affected by resolution.

CHAPTER V

RIGID REGISTRATION OF MEDICAL IMAGES USING 1D AND 2D BINARY PROJECTIONS

Image registration is a necessary procedure in everyday clinical practice. Several techniques for rigid and non rigid registration have been developed and tested and the state-of-the-art is evolving from the research setting to incorporate image registration techniques into clinically useful tools. We have presented in Chapters 3 and 4 the application of the weighted ratio criterion to binary areas and volumes. In this chapter we develop a novel rigid medical image registration technique which incorporates binary projections on line segments and 2D areas. The novelty is that the method is signal intensity independent with the computation of the projections. This technique is tested and compared to the standard Mutual Information (MI) methods. Results show that the method is significantly more accurate and robust compared to MI methods. The accuracy is well below 0.5 degrees and 0.5 mm. This method introduces two more improvements over MI methods: (1) for 2D registration with the use of 1D binary projections, we use minimal interpolation; and (2) for 3D registration with the use of 2D binary projections the method converges to stable final positions, independent of the initial misregistration.

The rest of this chapter presents 2D rigid registration of MR scans using 1D binary projections and 3D registration of MR volumes using 2D binary projections. The registration function used is the mean-squared-value of the weighted ratio of the binary projections. In the section 5.1 a connection with the literature for projection based registration is given. In the section 5.2 the basic characteristics of the projection based registration methods are given. In Section 5.3 a full set of results for 2D and 3D registration are presented together with detailed comparisons with MI methods. Finally, we discuss and draw conclusions on the proposed methods and indicate areas for future work.

5.1 Theoretical aspects of the chapter

Image registration is the process of geometrically aligning two images so that corresponding voxels/pixels can be superimposed on each other. There are several applications of image registration[1]. Examples include remote sensing, medicine, cartography, and computer vision.

The majority of image registration methods are based on the use of a similarity/disparity criterion which, when the two images are brought to register, is maximized/minimized. Numerical analysis techniques are used to maximize/minimize the similarity/disparity criterion. There are many different criteria, with Mutual Information(MI) being the standard since it is quite accurate for rigid body registration and does not require any image segmentation prior to registration.

Image registration is an active research field and in recent years image registration methods have evolved from the research setting, to being incorporated into clinically useful software tools [6]. The image registration methods can be in general divided into rigid and non-rigid. Rigid registration techniques adjust for rotations and translations only (six parameters for the 3D case). This is the case with rigid brain scans. Non-rigid techniques assume a nonlinear transformation model and can adjust for image warping. Warping occurs usually due to the soft tissue deformations of the body organs between different scans [6]. Medical image registration techniques are also categorized according to the type of features they use for registration. Surface-based techniques rely on the characteristics of the surface of the registrable objects while volume-based techniques use the full volume information. West et al [7] define as volume-based "any technique which performs registration by making use of a relationship between voxel intensities within the images and as surface-based, any technique which works by minimizing a distance measure between two corresponding surfaces in the images to be matched". According to Slomka et al. [6] volume- or voxel-based techniques are more robust and accurate because they do not rely on the preprocessing of the images for being accurate. This is especially the case for the MI methods. These methods rely on maximizing the amount of information sharing between the two images to be registered. According to Bardera [8] "MI methods have become a standard reference due to their accuracy and robustness." In Liao et al [9] surface matching and MI methods are compared and the conclusion is that the surface matching registration algorithms could be followed by a few iterations of a MI algorithm for better accuracy. Improvement of the standard MI algorithms is an active research field and the effort is to use a combined approach that does not rely on voxel values only, but incorporates geometrical or regional features for computation of the MI [8, 10, 11, 12, 13].

The type of problem which is solved by the registration algorithm is another categorization criterion. The methods may be suitable for image-to-image space registration (3D-3D, 2D-3D) or physical to image space registration. 3D-3D methods register image volumes to image volumes (MR-MR, CT-MR, (positron emission tomography) PET-MR, Ultrasound-MR [6,7,14]. 2D- 3D registration techniques register, for example, one or more intraoperative X-ray projections of the patient and the preoperative 3D volume [15,16]. Physical to image space registration is similar to 2D-3D registration but may use interventional techniques like bone-implanted markers for patient to image registration [17].

In this chapter we follow a novel approach to the medical image registration problem. We propose, test and compare to the standard MI methods a method which relies on the computation of the weighted ratio with the use of binary projections of the 2D or 3D images on lines and registrable areas.

Several techniques for signal intensity projection based image registration have been developed [128,129,130]. The most relevant work to this report is the method presented in Khamene et al [128]. In this work the registration problem is analyzed into the sub-problems of registering, using signal intensity based algorithms and criteria, the rendering projections of the two volumes along the three axes and adjusting the two volumes according to the projection-based computed registration parameters. In this work, we use a different similarity/disparity measure and a different iteration loop which have been shown to be very accurate and robust for volume based registration [131]. The similarity/disparity measure allows us to use binary (shadowing) projections and not renderings simplifying the hardware limitations for projection computation presented in Khamene et al [128].

Another projection-based technique for 3D-3D vascular registration is presented in Chan et al [129]. In this technique the 3D-3D registration problem is transformed into multiple 2D-3D vascular registration problems. The 2D images are the Maximum Intensity Projection (MIP) images (gray scale signal intensity images) which are first generated for the reference volume along the three axes. At each iteration three binary projections from the segmented binary floating volume are compared and registered to the corresponding MIPs. The similarity measure used is the sum-of-squared-differences.

A projection-based 2D-2D image registration technique in the presence of fixed pattern noise is presented in Cain et al [130]. In this method the 1D projections along the two axes are computed by accumulating pixels along the two main axes of the 2D image. The horizontal and vertical components of the shift are then computed using 1D cross-correlation. They show that the method is very robust in the presence of temporal and spatial noise and computationally efficient compared to the 2D correlation based shift estimator.

The goal of this work is to develop and test a registration solution that will be able to address different forms of the registration problem using a common registration logic. The common logic is to use a simple registration criterion which utilizes minimal information. We also implement a novel and easy to understand iteration loop which, in comparison to other minimization techniques, makes it easier to register images with less information used. In this context, the motivation is the need to produce a well engineered registration system of methods for 3D-3D rigid body registration (volume and projection based), 2D- 3D registration and non-rigid body registration. By well engineered we mean that we will be able to address the main registration algorithm problems which are accuracy and convergence. We want to research the goodness of the registration algorithm convergence criterion in relation to the accuracy desired and the data set used. For example we want to find out how many iterations have to be taken for the registration algorithm to converge.

5.2 Materials and Methods

The registration function used was first introduced for 3D rigid volume registration [131,132]. It was defined as follows: Given two superimposed non-registered images two types of areas can be identified: (1) areas where signal voxels/pixels are superimposed on other signal voxels/pixels; and (2) areas where signal voxels/pixels are superimposed on background voxels/pixels. The registration function is the mean squared value of the weighted ratio image. This ratio is computed on a voxel per voxel basis and weighting is performed by setting the ratios between signal and background voxels to a standard high value. The mean value is computed over the union of the signal areas of the two images. For the evaluation of the accuracy of the method, 3D MR images from ten patients from the database of the Cleveland Clinic Foundation were used. The images were interleaved T1-weighted and T2-weighted studies. The T2 MR study was transformed using ten arbitrary rigid 3D transformations and then registered back to the T1MR study. The experiments were performed at half resolution of 1.8mm. 3-5 iterations per geometric transformation parameter for registration are needed. The nature of the similarity criterion is multi-resolution. When the resolution is halved both the high value areas and the area over which they are averaged are equally divided. The average rotational error was found to be 0.36 degrees and the average translational error 0.36mm giving sub-voxel accuracy. In no experiment convergence to a local minimum occurred. The method performed well in the presence of high noise areas. The method was extended in [133] for 2D non-rigid body binary volume based registration using a local elastic geometric transformation model which uses cubic B-splines. The difference of this paper with the above described work [131] is that instead of the full volumes/areas, the projections only are used for the computation of the registration function.

The main steps of the method are:

- Preprocessing of the MR data
- Registration using projections

The method is applied for 2D and 3D registration and has a different form for each case.

5.2.1 2D Registration Method

The data used consist of pairs of MR scans of the head which are provided registered. The images are preprocessed in order to separate the head area from the background area and using the head area the outer contour of the head is identified. Five different pairs are used. Four of these pairs come from the Harvard medical atlas database and are provided carefully registered on the internet [134]. The atlas contains images from various modalities and clinical cases and can be navigated in a user friendly way on the internet. This data set has been used in other Image Registration research papers for evaluation of the method [135].

For 2D registration using 1D projections the scans correspond to 3D studies and the ones used were randomly selected from the cases of Acute Stroke, Multiple Embolic Infarctions, Multiple Sclerosis and Vascular Dementia. One additional scan pair consists of T1/T2 interleaved study scans from the database of the Cleveland Clinic Foundation.

The preprocessing of the 2D scans was performed using the Bioimagesuite Software of Yale University [136]. Preprocessing consists of the following steps:

- Median filtering to reduce the level of the noise with window size of 3 (this step is necessary for the Cleveland Clinic Foundation scans which are more noisy).

- C-means segmentation with 3 clusters. The purpose of the C-means algorithm is to compute, for a given data set x[1...n], the optimal values of the centers V[1...c] of k clusters, by using the c memberships assigned to each data element u[1...n,1...c] and by minimizing iteratively a within-groups sum-of-squared-errors function. It is included as a standard choice for segmentation in the Bioimagesuite Software. The value of 3 clusters was found to give better threshold for the separation of signal from background area than the value of 2 clusters. A presentation of C-means is given in [123,124]. We found through experimentation that the use of 3 clusters better outline the head area.

- Region growing for background connection and hence head area and contour extraction. We use the method included in Bioimage Suite.

The effort in the preprocessing step was to introduce minimum non-registrable areas which affect the registration accuracy. Figure 16 shows the scan pairs for the five cases and the areas of non-overlap after preprocessing. It shows scans used for the registration experiments and the non-overlap image prior to registration, showing left to right the reference image, the reslice image and the areas of non-overlap prior to the application of the initial misregistration.

(f) (g) (h)

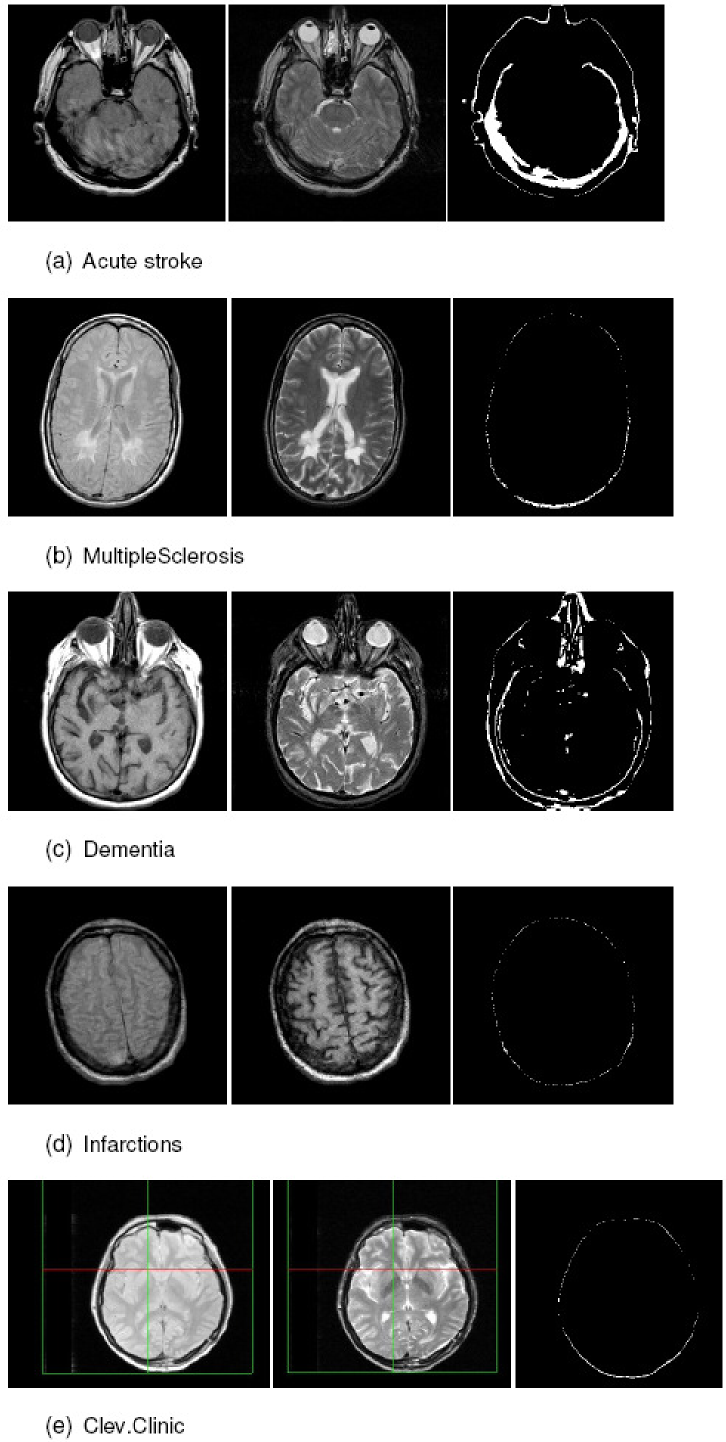

Figure 16 : Scans used for the registration experiments and the non-overlap image prior to registration, showing left to right the reference image (f), the reslice image (g) and the areas of non-overlap (h) prior to the application of the initial misregistration.

The 2D registration method works in the following way (see below Algorithms 1 and 2):

- After preprocessing, the contour pixels of the two images are projected along the x- and y-axes giving two sets of x- and y-projections. They are then rotated by $\boldsymbol{\theta}$ degrees and projected onto the x-axis giving a set of $\boldsymbol{\theta}$ degree projections. The projection of the reslice image is part of the iteration loop whereas the projection of the reference image is performed only once. Projections are incorporated into the geometric transformation function.
- The minimum and maximum values of x- and y-coordinates of the nonzero pixels of the geometrically transformed data set are computed and the 1D projections are created by padding the in-between ranges [xmin, xmax], [ymin, ymax], [xθmin, xθmax] with a standard non-zero value. The min and max values refer to the minimum and maximum projection along x, y and angular directions. The projections have double the dimension of the image in order to cope with the out-of-the-imaging area rotations and translations.
- For registration of translations the sum of x- and y-projections is used whereas for the registration of the xy-plane rotation the $\boldsymbol{\theta}$ degree projections are used. The registration function is the 1D equivalent of the volume based definition given above.
- The way that we compute the projections allows us to avoid the use of interpolation within the geometric transformations. Instead of interpolation a computation of minimum and maximum x- and y-dimensions is performed.

One of the two images is defined as the reference image. The other image is aligned to the reference and is referred to as the reslice image because in the 3D registration case it has to be resliced after alignment.

The main iteration loop is entered and one of the N=3 geometric transformation parameters is adjusted with each iteration.

For this parameter the reslice image is transformed at n Chebyshev points in the transformation units interval [-18, +18] and for these points the registration function is computed explicitly. As reported in [41] a Chebyshev approximation may be sufficient when the function is analytic and then no least-squares based function approximation is necessary. The transformation units are degrees for rotations and pixels for translations. The approximated function has a point of minimum which is considered as the adjustment value of the geometric transformation parameter. Using this value, the reslice image is transformed.

The adjustment values computed for each transformation parameter in different iterations are summed to give the final adjustment value. In Chapter 4 we have presented curves of the registration function and we showed that the point of minimum is unique. Convergence for a transformation parameter is achieved when two iterations which adjust this transformation parameter give adjustment values less than one transformation unit.

It is clear from the above that the value of $\boldsymbol{\theta}$ which registers the 2D rotation is a parameter of the algorithm. Extensive experiments showed that the value is not steady for all initial transformations and should be varied and the registration results compared in order to get the best registration result. The range of the variation of this angle used for the results in this report is 40 to 50 degrees for the usual orientation of the reference image which is parallel to the y-axis. If the reference image is significantly rotated relative to the y-axis, then a measurement of the angle of the rotation of the axis of symmetry of the image is performed and the $\boldsymbol{\theta}$ range is adjusted accordingly. Eleven angles in the range 40-50deg separated by one degree (40, 41, 42,…,50) are used to evaluate the best $\boldsymbol{\theta}$ by performing an exhaustive search of the projection angles.

Another form of the 2D registration method incorporates multiple projections for rotational adjustment into the iteration loop. In order to incorporate multiple projections a decision has to be made at each iteration about the best projection. It was found that this decision cannot be projection based. The reason for this is that the projection based sequential execution of the full algorithm is based on selecting the final best result after visual inspection of all the final results. For the automated form of the algorithm [131] the full area-based criterion was found to be robust and accurate. This criterion was used for the incorporation of multiple projections into the iteration loop.

The implementation of the incorporated projections method uses two sets of projections with each rotational iteration, one at 40-50 degrees and one at -50 to -40 degrees. The best result from these two sets is kept as the correct result. The algorithms used are:

Algorithm 1: 2D image registration using binary projections and repetitive execution

For θ = 40,50 degs with step 1deg

Step 1 : Define R as reference image and B as reslice image

Step 2: Compute x,y and θ deg projections for A

For each of xy rotation, x translation, y translation:

Step 3 : Transform B at n Chebyshev points positions.

Step 4 : For each Chebyshev point:

compute x , y and θ deg projection of B

compute the registration function

End For (Chebyshev Points)

Step 5 : Approximate using Chebyshev polynomials and compute the point of minimum

Step 6 : Adjust reslice image to the point of minimum

Step 7 : With 2 less than one adjustments per transformation exit.

End For (transformations)

End For θ

Choose the best registration of all thetas.

Algorithm 2: 2D image registration using binary projections with inclusion of theta selection in the iteration loop

Step 1 : Define R as reference image and B as reslice image

Step 2: Compute x,y and θ deg projections for R

For each of xy rotation, x translation, y translation:

For θ = [40,50]-[-50,-40] degs with step 1deg

Step 3 : Transform B at n Chebyshev points positions.

Step 4 : For each Chebyshev point:

compute x , y and θ deg projection of B

compute the registration function

End For (Chebyshev Points)

Step 5 : Approximate using Chebyshev polynomials and compute the point of minimum

Step 6 : For xy rotation compare results for thetas using the full area based registration function[17]

Step 6 : Adjust reslice image to the point of minimum

Step 7 : With 2 less than one adjustments per transformation exit.

End For theta

End For (transformations)

For the 2D case registration is performed using a two step registration procedure when the projections are not incorporated in the iteration loop. The first step of the procedure aims at bringing the two scans rotationally close as determined by the visual inspection of the result. This step is considered successful if after the step the scans are rotated to each other by less than 10 degrees.

The first step is performed in the following way: an initial registration is performed with n=5 Chebyshev points in the interval ([-18,+18]) (A=18) with projection angle θ=45. In most cases this step brings the images sufficiently close. But there are cases when this step fails to register and therefore a search in the space of [A, θ] starts in order to find the range and angle which achieve this goal. First A is increased to A=36 or A=50 and if still a failure occurs a search in the projection angle space starts with θ scanning the [40º, 50º] interval or in one case even the [-40º, -50º] interval with steps of 1 degree. Once a successful first step occurs the adjustment of this step gives the initial misalignment for the second step.

The second step uses the parameter A=9 with n=5 Chebyshev points and it performs 11 repetitive registrations in the interval [40º, 50º] with one degree step projection angle choosing at the end the result with minimum rotational error. The characteristic of the second step is that in all cases the rotational error produced by the first step is reduced and that in all cases the rotational error is less than 1 degree. In fact in most cases the error is close to zero.

The calibration is based on the fact that when the first step fails the images are misregistered by large angles. The errors are compared with the initial misregistration of the image which is known. The calibration step is not necessary when the projections are incorporated in the iteration loop where no first step is necessary since overall no local minima occur.

5.2.2 3D Registration Method

The method was also implemented for 3D-3D registration of MR volumes using 2D parallel projections. The data used for the 3D experiments also come from the Harvard Medical Atlas database (five patient cases).

The basic characteristics of the 3D registration method are (See below Algorithm 3):

- The two volumes to be registered are provided as a set of 2D scans with non-cubic voxel size of 1x1x5mm. For this reason, in order to create the cubic voxel volumes a tri-linear interpolation routine is used. For example, for a volume of 25 scans a cubic voxel volume with dimensions 256x256x120 is created.

- The two volumes are then preprocessed in order to create the binary volumes. This is done by thresholding using the k-means segmentation with 3 clusters. For the MR data used in this report this procedure gives a threshold value of around 20 (the data is unsigned char).

- The main iteration loop is then entered. With each iteration one of the six 3D transformation parameters (xy plane rotation, yz plane rotation, zx plane rotation, x-axis translation, y-axis translation, z-axis translation) is adjusted. The adjustment is according to the variance of the weighted ratio disparity measure as computed by the projections of the two volumes. The minimization method is again Chebyshev polynomial based with 5 Chebyshev points in the interval [-9, +9] for all transformation parameters.

- The full volume is transformed with all transformations and trilinear interpolation is used for the computations.

The data used for the testing of the method are from the Harvard database and specifically from the cases of Alzheimers, Aids dementia, Multiple infarctions, Acute stroke and Multiple sclerosis. The basic results are given in the following section. For the testing of the method one of the two volumes was initially de-registered using a standard set of 10 random 3D geometric transformations and then registered using the method. The errors were then computed. The 3D registration algorithm is:

Algorithm 3 : 3D registration algorithm using 2D binary projections

Step 1 : Define A as reference image and B as reslice image

Step 2: Compute x,y,z 2D binary projections for A

For each of xy rotation,yz rotation, zx rotation, x translation, y translation,z translation:

Step 3 : Transform B at n Chebyshev points positions.

Step 4 : For each Chebyshev point:

compute x , y and z projection of B

compute the registration function

End For (Chebyshev Points)

Step 5 : Approximate using Chebyshev polynomials and compute the point of minimum

Step 6 : Adjust reslice image to the point of minimum

Step 7 : With 6 less than one adjustments per transformation exit.

End For (transformations)

The above methods were compared to the Mutual Information and Normalized Mutual Information methods which are included in the Bioimage suite software package. The theoretical aspects of Mutual Information methods have been presented in Chapter 2. A good presentation can be found in Pluim et al [47]. Mutual Information is an Information Theory measure which when maximized it maximizes the amount of information, image A contains about image B, or interchangeably image B about image A. This maximization of information brings the images into register.

5.3 Experiments and Results

5.3.1 2D Experiments

Using data from the five 256x256 scan pairs described above, a total of 100 2D experiments for the alignment of differently-weighted axial MR scans were performed. These experiments were conducted according to the following rules (where all the experiments were performed at full resolution):

One of the two scans was used as the reference scan. The other scan was considered to be the reslice scan. The latter was rotated and translated using a standard set of 20 2D geometric transformations and then registered to the reference scan, giving 20 registration experiments per case. For this reason these experiments are referred to as '20 displacements' experiments. The geometric transformations parameters were randomly selected using a random number generator in the range [-45, 45°] for the *xy* rotation and [-30,30] mm for *x* and *y* translations. The 2D geometric transformation set is shown in Table 25.

For the two stage experiment we gave a different angle θ between 40 and 50 degrees, with each execution of the 2D registration algorithm. We stored the final error for each value of theta na dwe chose the smallest error as the correct registration. For the one stage registration experiments the change of thetas was incorporated in the iteration loop and the algorithm gives one final adjustment value.

Table 25: 2D geometric transformation set. The range is -45 to +45 degrees for rotations and -30 to +30 mm for translations.

Transformation number	XY rotation	X translation	Y Translation
1	-40.08	7.2	0.23
2	21.37	-9.41	-19.11
3	-16.18	-10.88	-11.62
4	34.8	-5.23	2.31
5	-2.67	10.11	27.22
6	-32.64	-6.45	-20.83
7	-14.4	-17.08	12.91
8	-36.15	0.21	-16.41
9	33.23	-26.32	0.55
10	20.6	16.71	-23.55
11	-25.82	24.21	-25.2
12	-37.63	-23.64	-7.72
13	8.17	26.23	-13.42
14	7.09	12.88	-8.11
15	-44.71	0.55	29.63
16	24.54	29.72	2.83
17	-36.06	-5.65	16.94
18	-28.42	-19.11	9.08
19	15.82	13.62	16.41
20	0.35	-5.55	17.74

Table 26 shows the average errors for the 20-displacements experiments for each of the five cases.

The processing time of the method is 1-2 seconds on a HP A6240 Intel Quad Core 2.4GHz PC with 2 GByte Ram. Of course the method can be implemented in parallel and give processing time less than 1 second.

Table 26: Mean Errors (per 20 experiments) for each of the five scan pairs of Figure 1 with repetitive execution of the full program.

	Type of MR/MR experiment	Rotational error (degrees)	Translation error (pixels)
Accute Stroke	T2/PD	0.91	0.45
Multiple Sclerosis	T2/PD	0.095	0.72
Vascular Dementia	T2/T1	0.36	0.42
Infarctions	T1/PD	0.14	0.26
Cleveland Clinic	T2/T1	0.12	0.47
Overall Average Rotational Error		**0.32**	
Overall Average Translational Error			**0.46**

When the projections are incorporated in the iteration loop the results are similar to those obtained for sequential execution of the full registration algorithm. The errors are below 1 degree for rotations and 1 voxel for translations. The advantage of the method is that it does not have to be implemented in two steps since the problem of local minima is reduced. The results per 20 experiments show in Table 27.

Table 27: Mean Errors (per 20 experiments) for each of the five scan pairs of Figure 1 with inclusion of the projection based selection into the iteration loop.

	Type of MR/MR experiment	Rotational error (degrees)	Translation error (pixels)
Accute Stroke	T2/PD	0.57	0.47
Multiple Sclerosis	T2/PD	0.31	0.71
Vascular Dementia	T2/T1	0.31	0.38
Infarctions	T1/PD	0.22	0.37
Cleveland Clinic	T2/T1	0.38	0.52
Overall Average Rotational Error		**0.35**	
Overall Average Translational Error			**0.49**

5.3.2 3D Experiments

For 3D registration the results show the ability of the method to converge to the correct registration position independent of the initial misregistration. Table 28 gives the 10 transformations used for deregistering the images. The range is between -30 to +30 degrees for rotations and -10 to +10 voxels for translations. In order to perform the experiments we execute the 3D algorithm automatically and we measure the average error per case and the number of iterations needed to converge. The algorithm converges to stable final positions and further execution does not enhance accuracy.

Table 28: 3D geometric transformation set. The range is between -30 to +30 degrees for rotations and -10 to +10 voxels for translations.

TRANSFORMATION NUMBER	XY ROT	YZ ROT	ZX ROT	X TRANS	Y TRANS	Z TRANS
1	-10.26	-6.94	-9.3	-9.2	-3.6	-3.98
2	12.42	2.32	-3.7	-4.6	-9.6	-2.02
3	-8.58	-4.38	1.9	8.4	6.9	-4.0
4	19.26	-7.2	-1.9	-1.66	-8.0	1.97
5	-26.58	-6.3	-2.16	-3.2	-7.6	0.0
6	7.56	2.1	-7.6	0.0	-6.08	0.8
7	-5.82	-2.2	2.8	-8.4	-5.72	2.0
8	-5.04	4.2	-4.04	4.2	3.0	-2.0
9	-15.66	-5.14	6.04	8.0	-6.04	1.6
10	-9.24	6.44	-6.7	-0.5	1.48	3.2

5.3.3 3D results for Acute stroke

The total average absolute error is 0.19 degrees for rotations and 0.14 voxels for translations.

For the transformation number 9 of the acute stroke case it was found that the convergence criterion of two less than one degree adjustments per transformation parameter was not adequate (gives YZ error 3.57degs) and for this reason it was increased to 6 less than one degree adjustments. This gives a total number of iterations between 44 and 53 and a YZ error for the specific case of 1.55. If allowed to proceed further the method advances slowly to the correct position. The value of six is a compromise for the necessity of producing all the results in this paper using common registration parameters.

For the acute stroke case the projection based method was compared with the full volume method[131] using the same registration parameters [n=5, A=9] but different convergence criterion since two less than one degree or voxel iterations is sufficient for full volume adjustment. The total absolute error is 0.19 degrees for rotations and 0.4 voxels for translations. The iterations needed are between 20 and 22.

5.3.4 3D results for Alzheimers

The number of iterations needed is between 43 and 51. The average error is 0.3 degrees for rotations and 0.35 voxels for translations.

5.3.5 3D results for Aids dementia

The number of iterations needed is between 42 and 50. The average error is 0.07 degrees for rotations and 0.11 voxels for translations.

5.3.6 3D results for Multiple sclerosis

The number of iterations needed is between 42 and 52. The average error is 0.11 degrees for rotations and 0.3 voxels for translations.

5.3.7 3D results for Multiple Infarctions

The number of iterations needed is between 43 and 50. The average error is 0.56 degrees for rotations and 0.44 voxels for translations.

5.4 Comparisons with other methods

In order to evaluate the performance of the method in comparison with the state-of-the-art, we performed experiments with the MI and the Normalized MI (NMI) methods using the same data. These methods are included in the Bioimage suite software and were chosen as they compare favorably to several other image registration methods. For the 2D case the main parameters of these experiments were the following:

We use the conjugate gradient method for the iteration loop with the MI methods.

We found that when using the same initial misregistration as in the projections methods both of the MI methods fail to converge to the correct registration position in several occasions. Therefore we limited these methods to an initial misregistration within the [-10,+10] units (degrees or mm).

The projection based methods are more accurate than the MI methods even when starting from a wider initial misregistration interval. Both sequential execution of the algorithm several times and incorporation of the projections in the iteration loop make the registration method more accurate than the state-of-the-art MI methods even when those methods use a favorable initial misregistration. The MI method gives an average rotational error of 0.399 degrees and an average translational error of 0.64mm. The NMI method gives an average rotational error of 0.45 degrees and an average translational error of 0.65mm. The projection method with repetitive execution of the program gives an average rotational error of 0.32 degrees and an average translational error of 0.46mm. The projection based method with inclusion of the projections within the basic iteration loop with the usage of the area for best projection selection gives an average rotational error of 0.36 degrees and an average translational error 0.49 mm. These results of all five 2D registration data sets are given in Table 29.

Table 29: Comparison results for 2D rigid registration experiments

	Normalized Mutual Information	**Mutual Information**	**Projections with Repetitive Execution**	**Projections Included in the Iteration Loop**
Average Rotational Error (degrees)	0.45	0.39	0.32	0.36
Average Translational Error (mm)	0.65	0.64	0.46	0.49

The processing time is the same for all methods: 1-2 secs on a HP A6240 Intel Quad Core 2,4GHz PC with 2 GByte Ram.

For 3D registration we compared again the projections method with the MI and NMI methods. The main parameters and results for these experiments are:

We did not need to reduce the initial misalignment for the 3D experiments. We found that with the same initial misalignment intervals as in the 3D case, the MI methods are able to converge close to the correct position. We performed a thorough analysis of the final registration error with respect to the initial rotational misregistration. For the AIDS DEMENTIA case:

For the NMI method the average rotational error is 0.57 degrees and the average translational error is 0.92mm. When the initial average rotational misregistration is greater than 5 degrees the average rotational error is 0.76 degrees and the final translational error is 1.35mm. When the initial misregistration is lower than 5 degrees the average rotational error is 0.33degrees and the average translational error is 0.4 mm.

For the MI method the average rotational error is 0.6 degrees and the average translational error is 0.93mm. When the initial average rotational misregistration is greater than 5 degrees the average rotational error is 0.77 degrees and the final translational error is 1.33mm. When the initial misregistration is lower than 5 degrees the average rotational error is 0.38 degrees and the average translational error is 0.43 mm.

Similar results were obtained for the other data cases. Table 30 summarizes the results for all cases.

Figure 17 shows the scans of the Aids Dementia case and the areas of non-overlap after a 3D registration case.

(a) (b) (c)

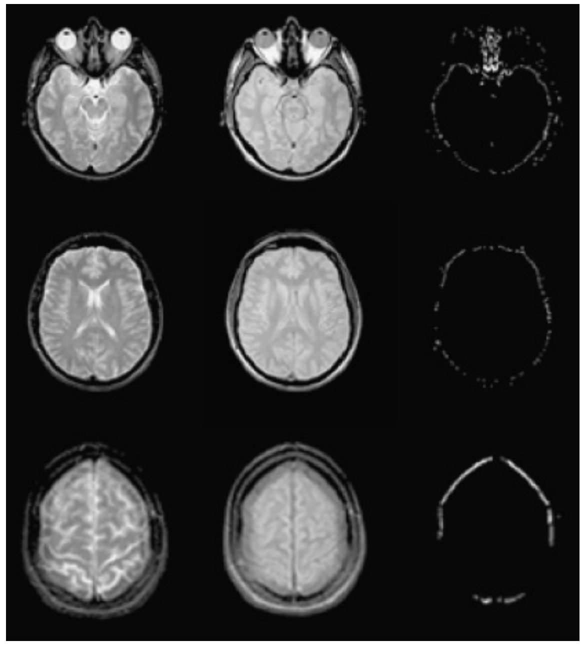

Figure 17 : Registered scans (a) and (b) columns and areas of misregistration (c) for the AIDS dementia case. The errors are *xy* rot 0.27°, *yz* rot –0.34°, *zx* rot 0°, *x* transl 0 mm, *y* trans 0 mm, *z* transl 0.05 mm.

From the above it is obvious that the accuracy of the MI methods is worse than the projection method. It is also obvious that with MI the accuracy of the method depends on the initial misalignment. This does not happen for the projection method where the accuracy is independent of the initial misregistration.

Table 30: 3D comparisons of the Mutual Information, Normalized Mutual Information and Projections methods.

	Mutual Information	**Normalized Mutual Information**	**Projections**
AIDS DEMENTIA			
rotational error	0.59deg	0.57deg	0.07deg
translational error	0.93mm	0.93mm	0.11mm
ALZHEIMERS			
rotational error	0.83deg	0.83deg	0.3deg
translational error	1.09mm	0.99mm	0.35mm
ACCUTE STROKE			
rotational error	0.7deg	0.72deg	0.19deg
translational error	1.04mm	1.08mm	0.14mm
MULTIPLE INFARCTIONS			
rotational error	0.76deg	0.72deg	0.56deg
translational error	1mm	1.04mm	0.44mm
MULTIPLE SCLEROSIS			
rotational error	0.7deg	0.67deg	0.11deg
translational error	1.03mm	1.02mm	0.3mm
AVERAGE			
rotational error	**0.71deg**	**0.7deg**	**0.24deg**
translational error	**1.02mm**	**1.01mm**	**0.27mm**

The method converges to almost stable final positions. The standard deviation of the error is around 0,3 for the 2D registration for both rotations and translations. For the 3D case it is 0,05 for rotations and 0,2 for translations.

The processing time of the projection based method at full resolution is 7-8 minutes on a HP A6240 Intel Quad Core 2,4GHz PC with 2 GByte Ram. The MI methods implemented hierarchically in the Bioimage Suite implementation take about 2 minutes.

From the above it can be seen that the 3D registration projections based method is more robust and accurate than the MI methods.

A full comparison of the Mutual Information and Normalized Mutual Information with other image registration methods may be found in [6,11,47]. Based on these papers we chose these two methods to compare with.

5.5 Discussion

We see that by using disease data with the projection methods described in this paper we get better accuracy compared to state-of-the-art methods and it is clear when the convergence occurs. It is clear because no matter what the initial misalignment is, the algorithm converges to stable final positions. Another advance made in this chapter is the fact that the proposed algorithm for 2D-2D registration uses minimal voxel interpolation. With the use of other registration functions (i.e. Sum-of-Squared-Differences, Cross Correlation, MI) the interpolation causes local minima and special techniques like high speed B-spline interpolation, low pass filtering and stochastic integration have to be used for their reduction or removal [137,138]. It was reported in a previous work [131] that with the use of full volumes, interpolation does not cause local minima to our registration method. In this work with the use of binary projections we use less information for registration, we minimize interpolation and still get a 100% convergence to the correct registration position. The preprocessing step affects more heavily the projection based method compared to the volume based method which was not affected by high noise presence. The method is generally fast and it is not converges always to the correct registration position. The preferred parameters were selected with experimentation and an effort has been made to be maintained the same since the first implementation of the algorithm.

5.6 Conclusions

A new robust method for 2D and 3D rigid registration using binary projections was developed and tested using MR scans of the head. The method for projections is signal intensity independent and it minimizes the use of interpolation in the geometric transformations algorithm.

For the 2D case the accuracy of the method is better than 1degree and 1 pixel. In most cases the error is less than 0.5 deg and 0.5 pixels. The preprocessing of the images must be careful not to produce non-registrable areas in the contours to be registered (avoid for example repetitive median filtering in one of the two images). No interpolation is necessary for 2D registration with the use of binary projections. The registration function is not dependent on signal intensity distributions. The method is directly applicable to binary images and contours. The method is fast with a typical time of 1-2sec running on an HP A6240 Intel Quad Core 2,4GHz PC with 2GByte ram.

The first results of a 3D projection based method have been given in this report. The accuracy of the method is better than 0.5 degrees for rotations and 0.5 voxels for translations. Compared to the full volume method [131] the method takes more steps to converge towards the correct registration position but remains as accurate. Minimal preprocessing of the images prior to registration is needed. The method is more accurate and robust than standard MI methods. It converges to stable final positions independent of the initial misregistration.

The MI methods rely on minimizing the spread of the joint histogram for registration. In order to register non-rigidly transformed images the method presented in this report could be adopted to work with the projections of the joint histogram instead of projections of the images and tested accordingly. Further future work will include the application of the method for 2D/3D registration.

In the next chapter we will see some applications of the method with reduced dimension images where the reference image has been cut at various levels. We will also measure the performance of the method in multiresolutions. The initial application of the method to radiograph images will be presented. Some more results for non rigid registration will be given together with a method for 2D to 3D registration using free head motion.

CHAPTER VI

IMAGE REGISTRATION APPLICATIONS

In this chapter we present techniques which have been implemented with the development of the weighted ratio image registration method and have been used for registration of bone anatomy and quantitative evaluation of changes in alignment in radiographs, for hierarchical implementation of the registration algorithm, for 2D registration of reduced dimension images with no overlapping segments using the 1D binary projections, for 2D non rigid registration and a 2D/3D registration system with free motion of the head. The application of the method in these problems can be improved in the future with more viable solutions.

In Section 6.1 we will present the first application of the weighted ratio image registration method made which was with digitized radiographs of the knee and spine. We show some early results of the method before it was applied extensively to MR images of the head.

In Section 6.2 we will give some more measurements for the performance of the algorithm at different imaging resolutions showing that the method is not affected by resolution. In this section there are also results with the application of the algorithm at different modalities (MR to CT and MR to SPECT).

In Section 6.3 we cut the reference image along straight lines and register the reslice image to the reduced dimension image. Woods [35,36] uses a computer based solution to produce more cuts for final registration including curved geometry cuts. With the straight line cuts we have managed to register the reduced dimension images at numerous experiments using an experiment protocol similar to the full area registration experiments.

In Section 6.4 we give some more results for non rigid registration. Finally in section 6.5 we give the report from the implementation of a 2D to 3D registration method with European program Panorama for free motion of the head in order to take views of 3D stereoscopic medical images in the 3D Viewnix software package environment.

6.1 2D registration of Radiographs of the knee and the spine

We present an algorithm for two-dimensional registration of musculoskeletal radiographic examinations. The technique determines a best match of bone anatomy by rotating and translating portions of digitized radiographs. For the radiographs alignment we used digitized radiographs from the database of the Cleveland Clinic Foundation.

To align the two images the algorithm iteratively minimizes the variance of the weighted ratio of the two images. Ratios between signal and background pixels are amplified using an amplifier on the ratio image. Digitized x-rays of foot and knee phantoms were used to determine if this method could align bone structures taken in different degrees of rotation and translation. Clinical examples of spinal fusion were used to compare this new automated method and traditional manual methods. Figure 18 gives an example of the amplification weighting function for the weighted ratio image registration. Figure 19 demonstrates registration of radiographs of a knee phantom taken in different degrees of rotation and translation. Figure 20 shows a method to evaluate changes in vertebral body alignment. We segmented the vertebral bodies and used the weighted ratio image registration method to register when they are in flexion and extension. These results showed promising but more studies are needed in order to assess the accuracy of the method for knee and spine registration.

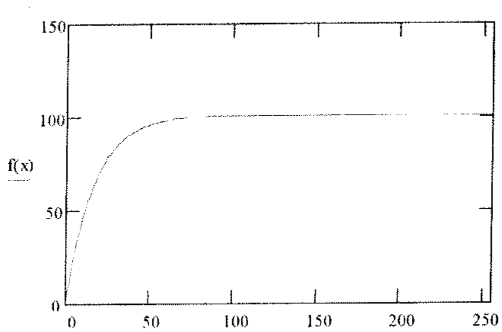

Figure 18 : Example amplification weighting function (x pixel value, f(x) amplification). We amplify the ratios between signal and background up to a standard high value.

(a) (b) (c)

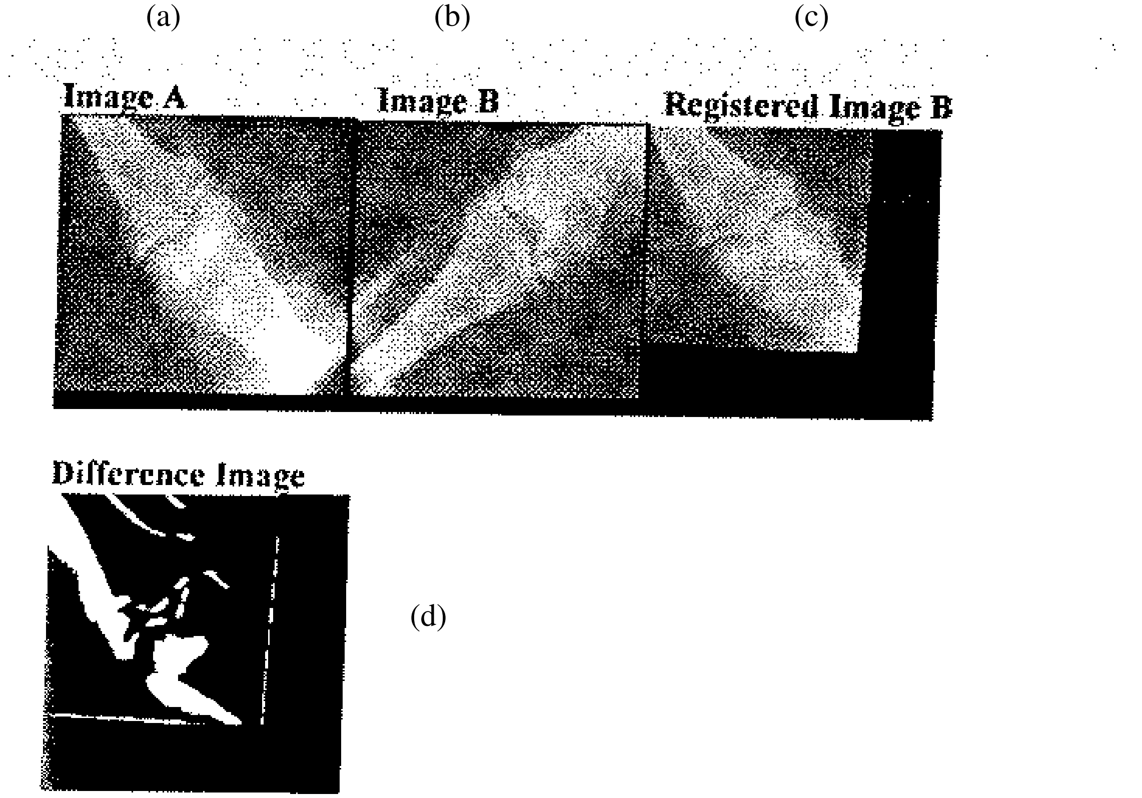

(d)

Figure 19: Original images(a-b), registered image(c) and difference image (d) of knee phantom.

(a) (b) (c)

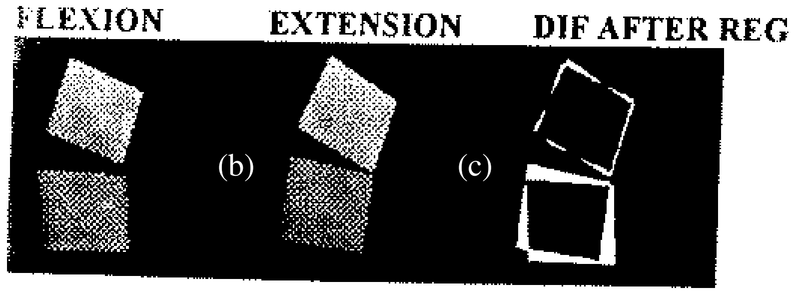

Figure 20: Outline of L4 and L5 vertebral bodies in flexion (a) and extension (b) in a patient status post attempted fusion. Registration (c) of L4 vertebral body shows motion at the L4-L5 level demonstrating incomplete fusion.

6.2 Hierarchical Implementation

The method described in Chapter 3 was applied for SPECT to MR and CT to MR 3D registration. A total of 60 3D single-resolution and 20 3D hierarchical multi resolution experiments were performed in order to estimate the accuracy of the method for cross-modality registration and test the performance of the hierarchical implementation of the method. The purpose of this chapter is to show that the method works well with different modalities and at different imaging resolutions.

6.2.1 3D SPECT-MR registration

The SPECT and T2-weighted MR data used were obtained through "The Whole Brain Atlas" web page of the Harvard Medical School (http://count51.med.harvard.edu/AANLIB/home.html). The SPECT and MR studies came from a patient with metastatic bronchogenic carcinoma and are provided registered at the whole brain Atlas web site. Each study has 24 scans.

Using this data a total of 60 three-dimensional experiments for alignment of a SPECT to an MR study were performed. These experiments were conducted according to the following rules:

a) The MR study was used as the reference study. The SPECT study was considered the reslice study. The latter was rotated and translated using a standard set of 10 three-dimensional geometric transformations and then registered to the reference study, giving 10 registration experiments. For this reason these experiments will be referred to as "10 displacements" experiments. The rotational parameters of the geometric transformation set were randomly chosen within -30 degrees to +30 degrees for xy rotation, -10 degrees to +10 degrees for yz and zx rotations, -10 to +10 mm for x and y translations and -5 to +5 mm for z translation.

b) As we have also presented in Chapter 3 the *Absolute Error (AE)* per transformation parameter was defined as the absolute difference of the adjustment value from the transformation parameter value applied. The average of the AEs for the xy, yz, zx rotations was defined as the *Absolute Rotational Error (ARE)* per transformation and was computed in degrees. The *Absolute Translational Error (ATE)* per transformation was computed in millimeters by averaging the x, y and z translation AEs in voxels and then by multiplying the average value by the voxel size (1.8 mm). The *Average Absolute Rotational Error (AARE)* per patient was defined as the average of the AREs from all transformations. Similarly, the *Average Absolute Translation Error (AATE)* per patient was defined as the average of the ATEs from all transformations.

The "10 displacements" registration experimental protocol is depicted in figure 20.

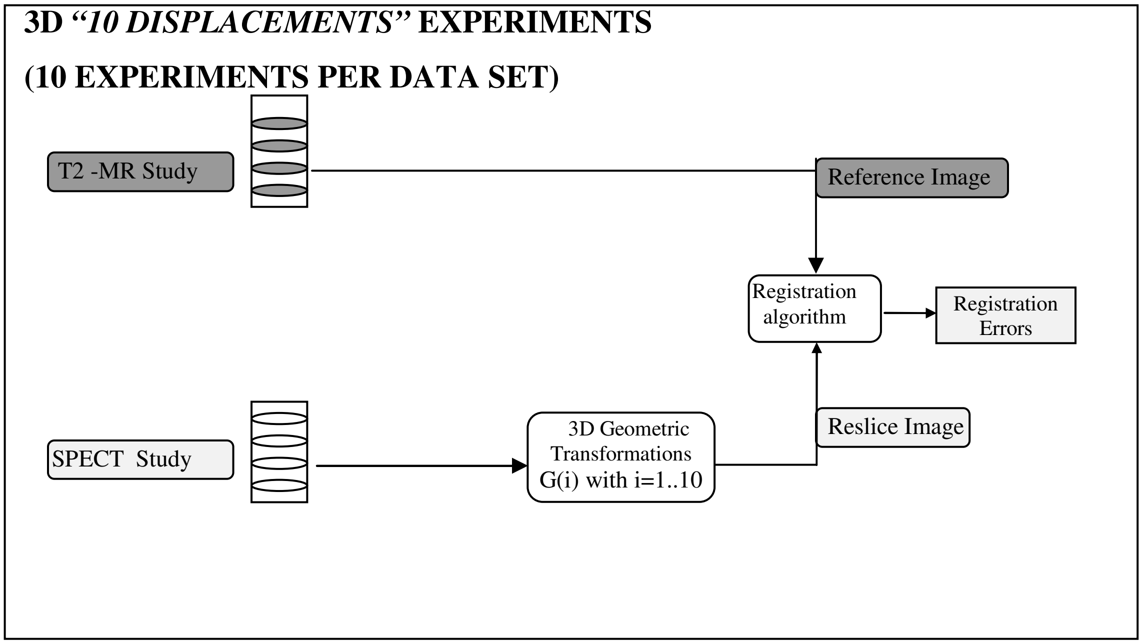

Figure 20: Experimental protocol used for the estimation of the 2D registration accuracy of the method for T1-T2 MR image registration. We apply the 3D geometric transformations to the 3D SPECT study and we bring it back to register using the registration algorithm. Finally we compute the registration errors.

The "10 displacements" experiments were first performed at 3 different resolutions (quarter, half, full) giving 30 single-resolution 3D SPECT-MR registration experiments.

The Average Absolute Rotational and Translational Errors computed at each resolution are shown in Table 31. As expected, the best accuracy is obtained at full resolution with an AARE of 0.65 deg and AATE of 0.60mm. Only for quarter resolution the errors exceeded 1 deg and 1mm.

Table 32 gives the Relative Average Processing Time for each resolution. It is computed by defining as To the time taken by the processor for each iteration of the registration algorithm at full resolution and by considering the iteration times at half and quarter resolutions to be To/8 and To/64 respectively.

Each entry of Table 37 is the average of the times computed for the 10 experiments. It can be seen that the ratio of the relative times computed for two consecutive resolution levels is close to 8. This result shows that the dynamic behavior of the algorithm, as measured by the number of iterations required for convergence, does not change with the resolution.

Table 31: Average Absolute Rotational and Translational Errors for the "10 displacements" single-resolution SPECT-MR 3D registration experiments for 3 different resolutions: quarter, half, full.

Resolution	**AARE (degrees)**	**AATE (mm)**
Quarter	1.68	1.51
Half	0.91	0.62
Full	0.65	0.60

Table 32: Relative Average Processing Time for the "10 displacements" single-resolution SPECT-MR 3D registration experiments for 3 different resolutions: quarter, half, full.

Resolution	**APT/To**
Quarter	0.26
Half	2.17
Full	19.3

The "10 displacements" experiments were repeated using the hierarchical form of the registration algorithm. The CONV parameter of the program, which defines the number of less-than-1-unit (degree or mm) iterations required for convergence of the transformation parameters (rotations and translations), was modified in order to achieve a compromise between processing time and accuracy. Three different forms of hierarchy were used:

- The hier(2,2,2) form, where the value of CONV=2 was used at each resolution. This means that two less than 1deg or mm iterations are required for the iteration loop to converge at all three resolution levels per transformation parameter.
- The hier(2,2,1) form, where the value of CONV=1 was used for the full resolution level. 2 less than 1 deg or mm iterations are required at quarter and half resolution and 1 at full resolution.
- The hier(2,1,1) where the value of CONV=1 was used for resolutions half and full. . 2 less than 1 deg or mm iterations are required at quarter resolution and 1 at half and full resolution.

Tables 3a-c give the AARE and AATE and the Relative Average Processing Time for each resolution for the 3 hierarchical forms. Each entry of tables 33-35 is the average of 10 registration experiments.

Table 33: AARE, AATE and Relative Average Processing Time for the "10 displacements" hierarchical SPECT-MR 3D registration experiments with the hier(2,1,1) scheme.

Resolution	**AARE (degrees)**	**AATE (mm)**	**APT/To**
Quarter	1.68	1.51	0.26
Half	1.22	0.73	0.9+0.26=1.16
Full	**0.94**	**0.46**	7.3+1.16=**8.46**

Table 34: AARE, AATE and Relative Average Processing Time for the "10 displacement" hierarchical SPECT-MR 3D registration experiments with the hier(2,2,1) scheme.

Resolution	**AARE (degrees)**	**AATE (mm)**	**APT/To**
Quarter	1.68	1.51	0.26
Half	0.96	0.56	1.63+0.26=1.89
Full	**1.04**	**0.46**	6.3+1.89=**8.19**

Table 35: AARE, AATE and Relative Average Processing Time for the "10 displacement" hierarchical SPECT-MR 3D registration experiments with the hier(2,2,2) scheme.

Resolution	AARE (degrees)	AATE (mm)	APT/To
Quarter	1.68	1.51	0.26
Half	0.96	0.56	1.63+0.26=1.89
Full	0.65	0.61	12.5+1.89=14.39

Tables 33-35 show that the hierarchical implementation reduced the processing time. The scheme (2,2,1) reduced the processing time by a factor of (1-8.19/19.3)=57.5% compared to the single-resolution method. The full hierarchical scheme hier(2,2,2) had the same accuracy as the single-resolution method while reducing the processing time by a factor of (1-14.39/19.3)=25.4%.

6.2.2 3D CT-MR registration

The CT and T2- MR data used, were obtained through "The Whole Brain Atlas" web page of the Harvard Medical School. The CT and MR studies came from a patient with acute stroke and are provided registered at the whole Brain Atlas web site. The "10 displacements" experimental protocol with the same transformations was used for the CT-MR experiments. The T2-MR study was considered as the reference study and the CT study was considered as the reslice study. The brain area of the CT images was extracted using the Live Wire Tool of the 3DVIEWNIX software system and it was used as a mask in order to define the brain area in the T2-MR images. The CT study brain was then rotated and translated using the standard "10 displacements" transformation set and then registered to the reference MR study brain.

The hierarchical registration algorithm forms hier(2,2,1) and hier(2,2,2) that gave respectively the best registration speed and accuracy during the SPECT-MR experiments were tried. Tables 4a-b give the AARE and AATE and the Average Processing Time for each resolution for the 2 hierarchical forms. Each entry of tables 36-37 is the average of the 10 registration experiments.

Table 36: AARE, AATE and Relative Average Processing Time for the "10 displacement" hierarchical CT-MR 3D registration experiments with the hier(2,2,1) scheme.

Resolution	**AARE (degrees)**	**AATE (mm)**	**APT/To**
Quarter	1.5	1.6	0.27
Half	0.82	0.83	1.5+0.27=1.77
Full	0.68	0.51	6+1.77=7.77

Table 37: AARE, AATE and Relative Average Processing Time for the "10 displacement" hierarchical CT-MR 3D registration experiments with the hier(2,2,2) scheme.

Resolution	**AARE (degrees)**	**AATE (mm)**	**APT/To**
Quarter	1.5	1.6	0.27
Half	0.82	0.83	1.5+0.27=1.77
Full	0.56	0.41	12+1.77=13.77

Tables 36-37 show that the hier(2,2,2) form gives the best accuracy for both rotations (0.56 deg) and translations (0.41 mm). Its processing time however, was almost double the time needed by the hier(2,2,1) form.

6.3 2D registration using 1D projections with reduced dimension images

In this Section we will present the 2D rigid registration experiments performed between medical images with non-overlapping segments. We cut (crop) the images at two different levels and register images with reduced dimension. We use 1D binary projections and we adjust the projection limits according to the cropped image in order to perform accurate registration. We use the variance of the weighted ratio as a registration function which we have shown is able to register 2D and 3D images more accurately and robustly than mutual information methods. The function is computed explicitly for n=5 Chebyshev points[5] in a [-9,+9] interval and it is approximated using Chebyshev polynomials for all other points. This iteration loop is the basic idea for all registration methods which are developed as part of this work. In this context, the motivation is the need to produce a well engineered registration system of methods for 3D-3D rigid body registration (volume and projection based), 2D- 3D registration and non-rigid body registration.

The images used are MR scans of the head. We crop one of the two scans at two different levels and we perform registration experiments of the full scan which is T2 weighted to the cropped scans which are proton density. We cut the noise using thresholding and a threshold of 40. The images show in figure 21.

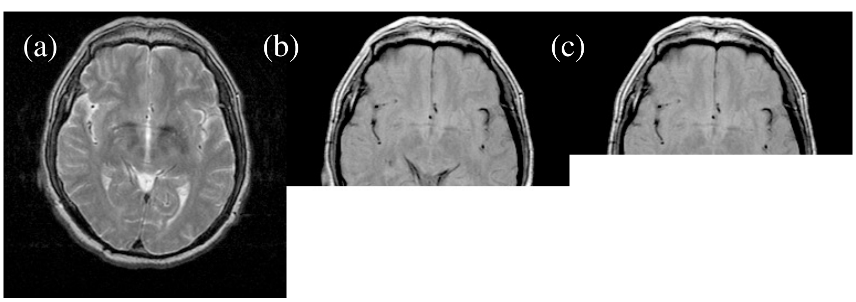

Fig. 21. Left (a): The reslice T2 weighted image. Middle(b): The reference image cut at a ydim=156/256. Right (c): The reference image cut at a ydim=128/256.

The registration function used is the variance of the weighted ratio. This function was first defined for the volume and area based registration [131,132,140]. We compute the voxel per voxel ratio of the two images and we set the ratios between signal and background voxels to a standard high value. Then we compute the variance of the ratios over the union of the non-background areas or volumes of the two images. We minimize this function with a Chebyshev polynomial approximation based iteration loop. We have used this method for 3D-3D volume based registration and showed the advantage of being accurate and robust. [132] The method is also able to register 3D medical images using 2D binary projections with greater accuracy and robustness compared to Mutual Information and Normalized Mutual Information methods. It also performs better than Mutual Information methods for 2D registration using 1D binary projections.

The 2D registration method using 1D projections and cropped images works in the following way:

After preprocessing, the contour pixels of the two images are projected along the x- and y-axes giving two sets of x- and y-projections. They are then rotated by θ degrees and projected onto the x-axis giving a set of θ degree projections. The projection of the reslice image is part of the iteration loop whereas the projection of the reference image is performed only once. Projections are incorporated into the geometric transformation function. The minimum and maximum values of x- and y-coordinates of the nonzero pixels of the geometrically transformed data set are computed and the 1D projections are created by padding the in-between ranges [xmin, xmax], [ymin, ymax], [xθmin, xθmax] with a standard non-zero value. The projections have double the dimension of the image in order to cope with the out-of-the-imaging area rotations and translations. For registration of translations the sum of x- and y-projections is used whereas for the registration of the xy-plane rotation the θ degree projections are used. The registration function is the 1D equivalent of the volume based definition given above. The way that we compute the projections allows us to avoid the use of interpolation within the geometric transformations. Instead of interpolation a computation of minimum and maximum x- and y-dimensions is performed.

The cropped image is defined as the reference image. The other image is aligned to the reference and is referred to as the reslice image because in the 3D registration case it has to be resliced after alignment

The main iteration loop is entered and one of the N=3 geometric transformation parameters is adjusted with each iteration.

For this parameter the reslice image is transformed at n=5 Chebyshev points in the transformation units interval [-A, +A] and for these points the registration function is computed explicitly. The transformation units are degrees for rotations and pixels for translations. The approximated function has a point of minimum which is considered as the adjustment value of the geometric transformation parameter. Using this value, the reslice image is transformed.

The adjustment values computed for each transformation parameter in different iterations are summed to give the final adjustment value. Convergence for a transformation parameter is achieved when two iterations which adjust this transformation parameter give adjustment values less than one transformation unit.

It is clear from the above that the value of θ which registers the 2D rotation is a parameter of the algorithm. Extensive experiments showed that the value is not steady for all initial transformations and should be varied and the registration results compared in order to get the best registration result. The range of the variation of this angle used for the results in this report is 40 to 50 degrees for the usual orientation of the reference image which is parallel to the y-axis. If the reference image is significantly rotated relative to the y-axis, then a measurement of the angle of the rotation of the axis of symmetry of the image is performed and the θ range is adjusted accordingly.

Eleven angles in the range 40-50deg separated by one degree (40, 41, 42,…,50) are used to evaluate the best θ.

The algorithm used is:

Algorithm 1: 2D image registration using binary projections and repetitive execution

For θ = 40,50 degs with step 1deg

Step 1 : Define A (cut image) as reference image and B as reslice image

Step 2: Compute x,y and θ deg projections for A

For each of xy rotation, x translation, y translation:

Step 3 : Transform B at n Chebyshev points positions.

Step 4 : For each Chebyshev point:

compute x , y and θ deg projection of B

compute the registration function in the common cut area.

End For (Chebyshev Points)

Step 5 : Approximate using Chebyshev polynomials and compute the point of minimum

Step 6 : Adjust reslice image to the point of minimum

Step 7 : With 2 less than one adjustments per transformation exit.

End For (transformations)

End For θ

Choose the best registration of all thetas.

From the beginning of this registration related work the evaluation of the accuracy is performed using a standard set of geometric transformation parameters. We de-register the reslice image and we bring it back into register using the registration algorithm. For volume based registration we have found that the method converges to the correct registration position with average accuracy of 0.36mms for translations and 0.36degrees for rotations. For 3D-3D rigid registration using 2D binary projections the method converges to the correct registration position with an accuracy of 0.27mms for translations and 0.24 degrees for rotations. The method has the ability to converge always to the correct position without suffering from local minima and it is more accurate than Mutual Information and Normalized Mutual Information methods. [47,6,13] For 2D registration using 1D binary projections and full images the method has an average accuracy of 0.46mms for translations and 0.32 degrees for rotations. It still does not converge to local minima and is more accurate than Mutual Information methods.

In this section we use a standard set of 10 2D rigid transformations for the evaluation of the accuracy. The limits of the transformations are -10 deg to +10 degs for rotations and -10 pixels to +10 pixels for translations. The set of transformations are shown in Table 38.

Table 38. Standard set of 10 2D rigid transformations

Transf #	**XY rotation(degrees)**	**X translation(pixels)**	**Y translation(pixels)**
1	7.35	2.35	1.44
2	-5.14	8.77	7.33
3	-8.67	-2.44	-2.66
4	8.33	7.11	-3.75
5	-0.95	-1.63	-3.14
6	-9.14	-9.21	8.42
7	-5.85	-6.87	-8.05
8	2.24	-3.92	5.63
9	-3.6	0.45	-2.97
10	4.1	9.23	8.05

After the image is de-registered we perform 11 registration experiments and we visually compare the final results in order to choose the most accurate one. This can also be done with the use of the full area criterion with the registered images. Table 39 gives an example of the results for all thetas for transformation # 1 and with the ydim=156.

Table 39. Example of choice of the θ (projection angle) which registers accurately the images with ydim=156.(transformation #1)

θ (degrees)	**XY rotation error(degrees)**	**X translation error(pixels)**	**Y translation error(pixels)**
40	-0.27	-0.06	-0.19
41	0.57	1	0.20
42	0.32	0.83	0.31
43	-2.4	-0.74	0.25
44	0.65	0.83	0.25
45	-0.49	0.6	0.25
46	-0.27	0.43	-0.24
47	0.93	0.88	-0.02
48	-2.43	-0.74	0.25
49	0.99	1.11	0.14
50	-0.6	0.38	0.25

Based on this result we chose the value of θ=40 to be the most accurate.

With more reduced value of ydim=128 the errors increase for all thetas. Table 40 gives an example of the results for all thetas for ydim=128 and transformation #1.

Table 40. Example of choice of the θ (projection angle) which registers accurately the images with ydim=128.(transformation #1)

θ (degrees)	**XY rotation error(degrees)**	**X translation error(pixels)**	**Y translation error(pixels)**
40	-0.55	1.22	0.03
41	0.45	2.23	0.03
42	-0.13	2.4	-0.24
43	-0.27	1.61	-0.3
44	0.26	2.01	0.03
45	0.13	2.4	-0.24
46	-0.07	2.01	-0.07
47	-0.44	1.95	0.14
48	-1	1.33	-0.13
49	-0.27	1.67	-0.24
50	0.54	2.57	0.25

Based on these results we chose the value of θ=40 for the correct result.

We perform the above experiments repetitively for all transformations. Tables 41 and 42 show the results for each transformation for ydim=156 and ydim=128 respectively. We get average rotational accuracy 0.3degrees and average translational accuracy 0.2pixels for ydim=156. For ydim=128 we get average rotational accuracy 0.69degrees and average translational accuracy 0.59pixels.

Table 41. Errors for ydim=156

Transf #	XY rotation(degrees)	X translation(pixels)	Y translation(pixels)
1	-0.27	-0.06	-0.19
2	-0.24	0.05	0.07
3	-0.63	0.09	-0.12
4	-0.67	-0.09	-0.09
5	0.2	0.39	0.23
6	0.28	0.35	-0.01
7	0.22	0.44	0.21
8	-0.06	0.58	-0.05
9	-0.5	0.22	-0.04
10	-0.00	0.51	0.23

Table 42. Errors for ydim=128

Transf #	**XY rotation(degrees)**	**X translation(pixels)**	**Y translation(pixels)**
1	-0.55	1.22	0.03
2	-0.24	0.05	0.07
3	-0.68	1.32	-0.12
4	-0.67	1.42	-0.09
5	-0.97	1.18	-0.10
6	-0.67	1.19	-0.01
7	-1.35	0.89	0.05
8	-0.57	1.31	0.00
9	0.39	1.12	0.01
10	-0.79	1.41	0.23

We run the experiments on a High Performance Computing server iceberg which is the Sheffield node of the White Rose Computing Grid. Iceberg has 96 Sun X2200 nodes. We use one node which has 4 cores and 16 Gbytes of RAM. The processing time per experiment per θ is between 0.3 and 1 sec.

6.4 Non-rigid body registration

Another aspect of our method that needs to be investigated in the future is how well it can perform non-rigid body registration. The non-rigid body registration algorithm has been presented in Chapter 4.

For non-rigid registration the 2D form of the method has been implemented. The MR scan was transformed using the local geometric transformation model and then registered using the method.

Figure 22 shows an example of the non-rigid registration experiment. The warped image symbolizes the crisis due to color incompatibilities. The white warped image reduces to the level the surface matches the shape of the head. The result is after 15 iterations per parameter of the registration algorithm but close results have been obtained after the 9th iteration.

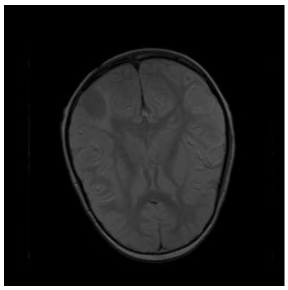

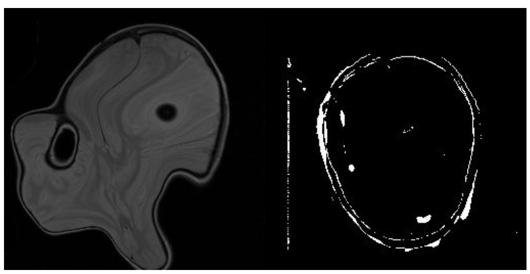

Fig.22 Top row: Reference image, Second row left: Reslice image before registration, Second row right: zero-areas of non-overlap after registration.

6.5 2d-3d registration

For 2d/3d registration the following algorithm is proposed:

- The surface points of the preoperative 3D volume are segmented and projected onto the fluoroscopic plane.

- The vertebrae areas of the X ray images are also segmented.

- The projected points are matched to the 2d areas iteratively using the Chebyshev polynomial based iteration loop.

Literature Information for the application of the algorithm in the future can be found in [24, 145,146,147,148,149,150,151,152].

6.5.1. 2D/3D Registration System using free head motion

We will present a demo in order to show a 3D medical imaging tool for manipulation of stereo and 3D medical images included in the European Project Panorama. The main tool that will be presented is a head tracker for manipulation of 3D medical images in mono or stereo mode that can be used by a surgeant or physician to take in a HANDS – FREE way different mono or stereo views of volumetric medical image data. The main media used during the demonstration were the following:

2 Silicon Graphics Workstations

1 SGI camera

An Intel PC

The 3D Viewnix Medical Image Processing Software running on both of the SGIs

3D MRI and CT medical images of the head.

Tools to be presented

Two different kind of tools will be presented. The tools created by the Medical Image Processing Group of the University of Pennsylvania [32] are being distributed with the 3D Viewnix Medical Image Processing Software System and also the tools for stereo and 3D medical image processing written at the Information Processing Laboratory and incorporated in the 3DViewnix System using the X- Windows based libraries provided by MIPG. A short description of the tools presented follows: (for tools provided by the MIPG some of the images and text are based on the 3DViewnix tutorial and user manual).

A1. Standard 3D Viewnix Tools

A1.1 Input raw medical image data using the EASYHEADER module.

The simplest way to import data into 3dviewnix is by using the EasyHeader module. This can be accessed by PORT-DATA ->IN->EasyHeader. Easy Header would allow you to generate a 3dviewnix gray data file interactively. Easy Header allows the user to read a series of 3D medical image scans which are saved in raw format and by providing manually the necessary information to create 3D Viewnix – compatible medical image volumes. When running Easy Header you will see the following fields (figure 23) that you have to set in the image window.

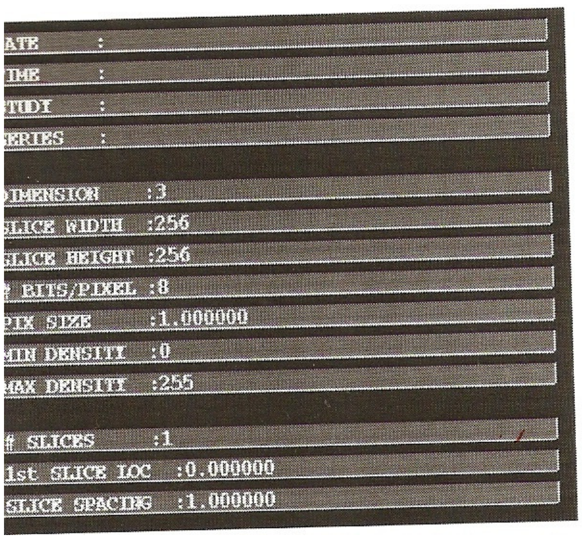

Figure 23: Fields of the 3D Viewnix Easy Header module that can be used to read serial medical studies in raw format.

A1.2. Surface rendering creation using Scene Operation – Segment – Threshold

The volume file created with Easy Header can be turned into a 3DViewnix compatible surface file using the Preprocess operation- Threshold that performs interactive thresholding of the histogram for the slices of the 3D volume and saves the output in a surface rendering compatible format.

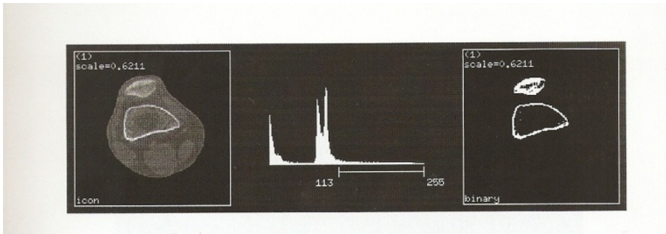

Figure 24 : Main window of the thresholding operation. The user is able to select interactively the areas of the histogram that are to be included in the surface rendering.

The visualization of the data can be done using the Manipulate – Move command which allows the user to see the surface he generated:

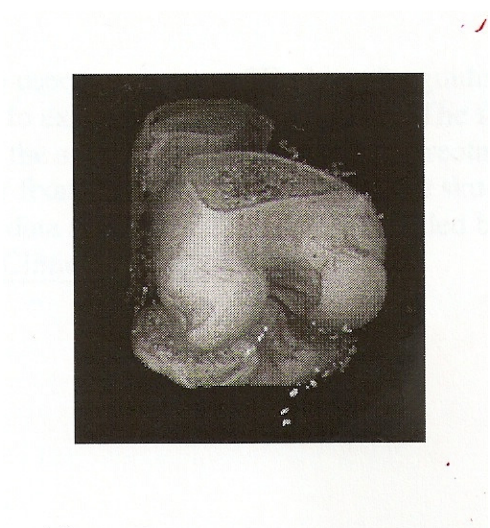

Figure 25: Surface rendering of a knee- joint.

6.5.1.1 Select slice tool

This tool allows the user to select with the cursor a slice at an arbitrary angle from a medical image volume using the surface rendering of the medical image data. The screen of interactively selecting the MR data along the desired direction shows in the following figure. The volume was originally created using axial t2-weighted MR data. (Provided by the Department of Radiology of The Cleveland Clinic Foundation).

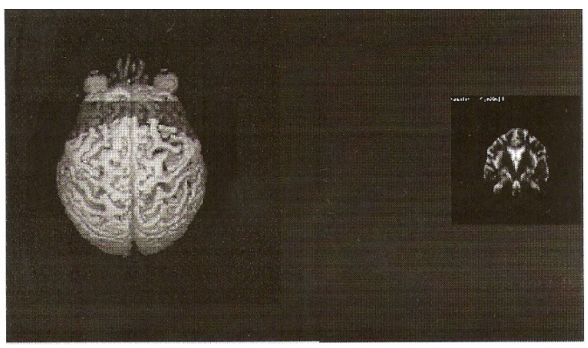

Figure 26: Select slice operation through the MR brain. The rendering was originally created using axial MR images.

6.5.1.2 Cut object tool

The cut object tool allows the user to separate a 3D object by guiding with the cursor a planar surface. In this way he is able to examine the inner structures. The following figure shows a surface rendering of a part of the skull of a patient with the stereotactic mask affixed rigidly on his skull. The screws used for fixation were separated from the skull. The original data are axial CT images. (Provided by the Department of Radiology of The Cleveland Clinic Foundation).

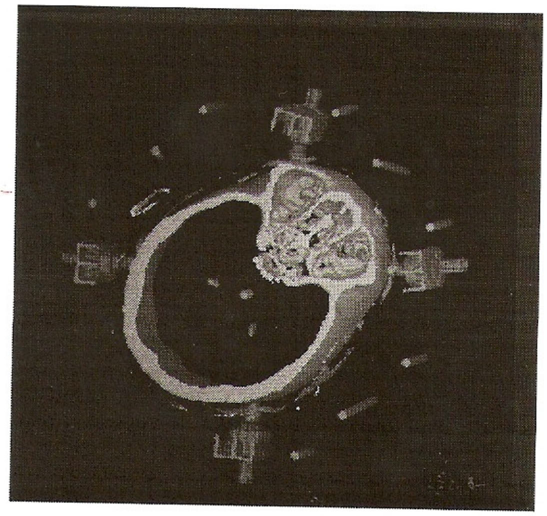

Figure 27: Cut Object tool used to separate and render a skull rendering created from stereotactic surgery CT data.

6.5.1.3 Move object tool

The move object tool exists in the standard configuration of the 3DViewnix and allows the user to rotate and translate 3D objects using the cursor. In this work we rotate the cursor with the motion of the head of the viewer. The following figure shows a rotated surface rendering of the brain using the cursor. (Original T2 MR images provided by the Department of Radiology of The Cleveland Clinic Foundation).

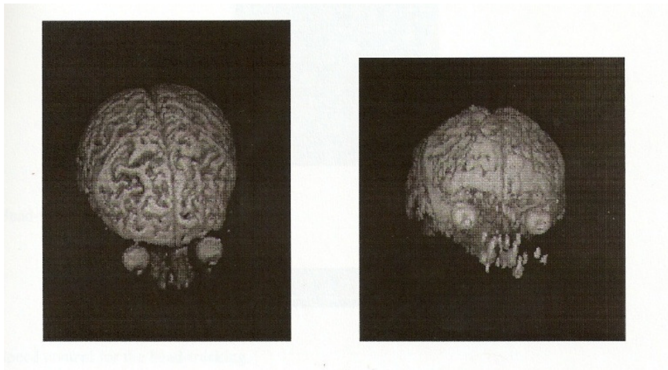

Figure 28: Surface rendering of an MR brain rotated at 2 different angles.

A2. Tools created and incorporated into 3D Viewnix

The tools allowed the user of the 3DViewnix system to perform some of the basic operations of 3DViewnix in a HANDS-FREE way by using the motion of the user's head as it is captured by a standard SGI camera. Additionally they extended the abilities of 3DViewnix by making it able to deal with stereoscopic 3D medical images. These tools are:

6.5.1.4 Head tracking rotation of 3D medical images

This tool allows the rotation of 3D medical objects using the motion of the head as it is captured by an SGI-camera. The algorithm uses a color segmentation scheme to identify the position of the viewer's head as it is captured by the SGI camera. The rotation of the 3D objects is then performed according to this position instead of the position of the cursor. The user enters the HANDS-FREE mode by pressing the HEAD-ON button in the button panel. When the user is in the HANDS-FREE mode , he is able to manipulate the 3D object using only his head. The user exits the HANDS – FREE mode by a simple motion of the mouse. The user is able to adjust interactively the SPEED of the rotation of the object related to the motion of the head (in order to be able to view smaller or greater 3D rotations using the same head motion). He is also able to MAGNIFY the rendering in order to examine smaller details. The following figures show the HEAD-TRACKING button panel, the SPEED control, and the details of a magnified rendering.

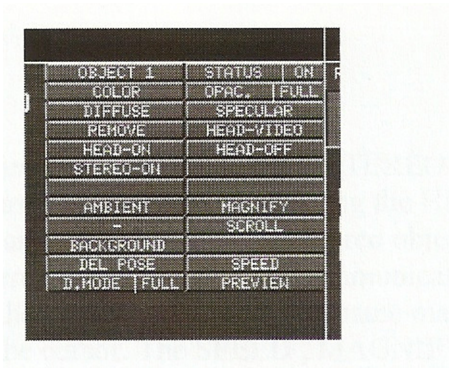

Figure 29: Head-tracking button panel

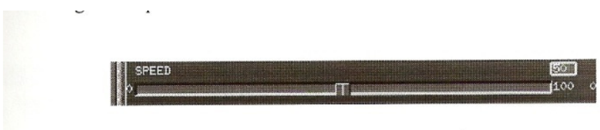

Figure 30 : Speed control for the head – tracking

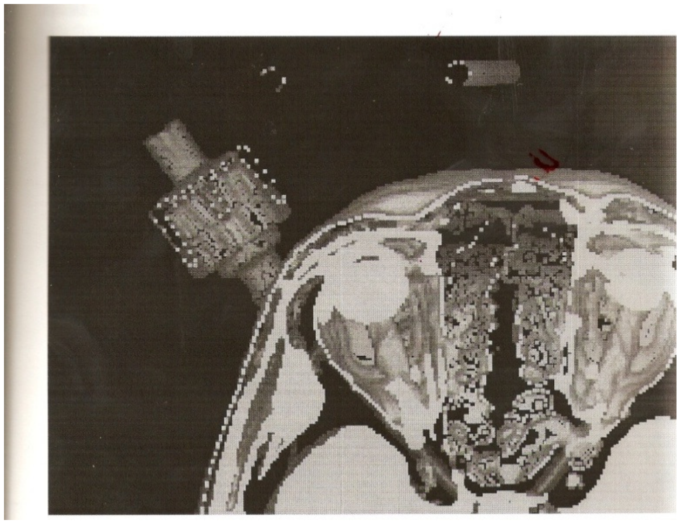

Figure 31: Use the Magnify operation in-order to view details of images.

6.5.1.5 Head tracking in Stereo Mode

The user is able to enter in the stereo mode by pressing the STEREO-ON button of the HEAD – TRACKING button panel (see figure above). Then by pressing the HEAD-ON button he is able to enter the HANDS FREE mode and manipulate the 3D stereo objects with the motion of his head. By using a pair of shutter stereoscopic glasses that communicate with a polarized beam combiner the user is able to view the stereo renderings. The same manipulation of stereo renderings can be done also with the cursor. The SPEED, MAGNIFY, and ROTATE options work in the STEREO mode also.

Description of the medical renderings : Three renderings of medical images were used. 2 renderings created using medical images provided by The Department of Radiology of The Cleveland Clinic Foundation and 1 standard 3DViewnix rendering. These renderings are shown in the following figures: the first is the rendering of a 3D brain created by T2 – weighted axial MR images with xy-lane resolution 3mm. The third is the rendering of a skull provided with the 3DViewnix software system .

Figure 32: Surface rendering of a brain created by axial T2-weighted MR images.

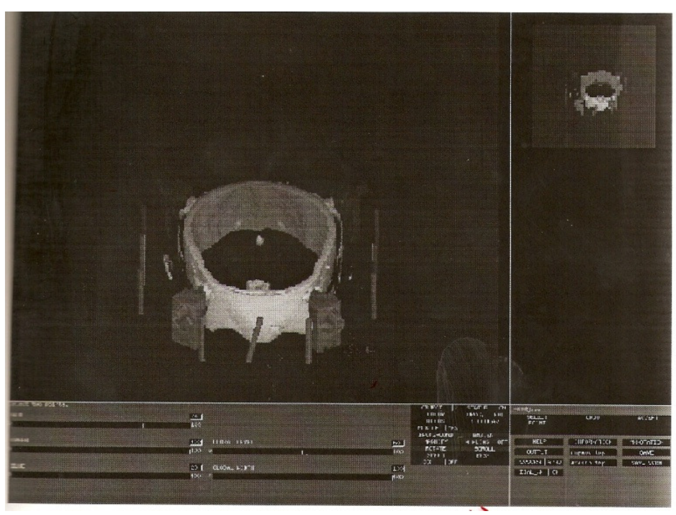

Figure 33: Surface rendering of a skull during stereotactic surgery.

Figure 34: Surface rendering of a skull. (Included in the 3D Viewnix Package of Medical Image Processing Group University of Pennsylvania).

6.6. Conclusions

We have presented an algorithm for two-dimensional registration of musculoskeletal radiographic examinations. The technique determines a best match of bone anatomy by rotating and translating portions of digitized radiographs. To align the two images the algorithm iteratively minimizes the variance of the weighted ratio of the two images. Ratios between signal and background pixels are amplified using an amplifier on the ratio image. Digitized x-rays of foot and knee phantoms were used to determine if this method could align bone structures taken in different degrees of rotation and translation. Clinical examples of spinal fusion were used to compare this new automated method and traditional manual methods.

We have also presented the application of a new automated feature-based method for the solution of the problem of cross-modality rigid registration of medical images. The method uses a Chebyshev polynomial approximation-based iteration loop to minimize a novel registration function which is defined as the mean-squared value of the weighted voxel-per-voxel mean ratio of the two images. Weighting is performed by setting the ratios between signal and background voxels to a standard high value. We used T2-weighted MR, SPECT and CT image studies of the head and performed 80 three-dimensional registration experiments in order to evaluate the accuracy of the method for cross-modality registration and also to test the performance of the hierarchical form of the algorithm. We found that the average error for SPECT to MR registration is 0.65 deg for rotations and 0.6mm for translations. For CT to MR registration the average errors are respectively 0.56deg and 0.41mm.

The dynamic behavior of the algorithm, as measured by the number of iterations taken for convergence, is not affected by the change in resolution. The hierarchical implementation improves the speed of the registration procedure by an average gain which is dependent on the hierarchical form used. The hier(2,2,2) form, which requires for convergence two iterations with adjustment values less than 1 transformation unit at all three resolution levels (quarter, half, full), retains the accuracy of the single-resolution method while improving the registration speed by 25.4 percent. The hier(2,2,1) form, which requires for convergence two less-than-1-unit iterations for quarter and half resolution and 1 less-than-1-unit iteration for full resolution, increased the registration speed by an average 57.5 percent.

In addition to providing excellent results, the proposed method is advantageous compared to cross-correlation techniques because it is independent of signal intensity distributions. It is also advantageous compared to least-squares based surface matching techniques because of its good behavior at lower resolutions and its tendency to avoid being trapped to local minima.

We have also presented a technique for registration of 2D reduced dimension (cut) images using 1D binary projections. The registration uses the variance of the weighted ratio as a registration function and achieves registration by minimizing this function using a Chebyshev polynomial based iteration loop. We avoid the use of interpolation with the use of a geometric transformation routine which does not incorporate interpolation. Instead we compute the minima and maxima of the transformed images along the lines of projections and we pad the in between values in order to compute the projections.

We have applied the method for the registration of cropped images. The modification with the use of cropped images is that we always use the cropped image as a reference and we limit the computation of the registration function based on the projections of the cropped image. In order to achieve acceptable accuracy we modify the projection angle θ between 11 values (40,41,42,…,50) we execute the program repetitively and we choose the most accurate result.

For the testing of the method we cut the reference image at two levels along y-dimension, at ydim=156 and ydim=128. We get accuracy better than 0.5degrees and 0.5pixels for ydim=156. The accuracy decreases for ydim=128.

We have also programmed a system for 2D/3D registration based on the image processing for video images of the forehead moving freely for 2D images and the Open GL interface with the 3DViewnix environment for connection with the 3D data. The method has been implemented in stereo mode.

CHAPTER VII

CONCLUSIONS AND FUTURE WORK

We have presented the main characteristics of the method for registration of 2D and 3D images rigidly using binary areas, volumes and projections . The method is independed to signal intensity methods and it is able to perform multimodality image registration. Compared to surface fitting methods the method is not affected by noise which allows an implementation with the incorporation of the 2D projection algorithm into a surface fitting registration scheme. The registration function works with non rigid giving a unique solution for small areas of local effect. Compared to Mutual Information methods for rigid registration the method has been shown not to be affected by misregistrations caused by local minima and to be able to maintain an accuracy of better than 0,5 degrees and 0,5 pixels. The method has also been shown to not be affected by resolution. For registration using linear projections the method uses minimal interpolation. The main points regarding the method that have been made in this thesis will be discussed in this chapter.

7.1 Introduction

In the field of digital image processing image registration is the process of using electronic hardware to geometrically align two images so that corresponding voxels/pixels can be superimposed on each other. With image registration methods , image processing methods which performe thresholding, segmentation, fuzzy classification, geometrical transformation in rigid and non rigid form have been developed. The speed of the image registration algorithm is related to the shape and volume of the object to be registered. Square objects are registered faster than the Mutual Information methods whereas the speed of medical image of the head registration is comparable to Mutual Information methods. In the medical field, image registration is used for diagnostic purposes when images of the same anatomical structure must be superimposed on each other. Registration methods have been developed which are used for combining computer tomography (CT) and magnetic resonance imaging data to obtain more complete information about the patient , for monitoring tumor growth, for treatment verification, for comparison of the patient's data with anatomic atlases. The image registration methods can be divided into rigid and non rigid . Rigid techniques adgust for rotations and translations only (six parameters for the 3D case) . This is the case with rigid brain scans. Non – rigid techniques assume a nonlinear transformation model and can adjust for image warping.

We have presented the steps of the algorithm which show that it belongs to Feature based methods. Feature based methods use the anatomic information inherent in the two image data sets. These techniques follow a general methodology with four steps:

a) extraction of features in each image

b) pairing of these features

c) choice of the geometric transformation and estimation of its parameters

d) application of this transformation.

2D/3D registration is a special case of registration which is of particular interest to surgeons. We presented a literature review of the methods used for 2D/3D registration. In chapter 6 we presented a technique to interface the 2D image processing algorithms with a 3D software package. With the help of 2D/3D registration methods surgical robots may be programmed using pre-surgical 3D dataset and a set of intraoperative fluoroscopic X-Ray image . In this way there is no need for fiducial markers.

The non rigid registration approach deals with the warping met in images and cannot be faced with the translational and rotational adjustment of the rigid case. The methods are divided into parametric and non parametric. We presented a parametric technique for registration of warped binary images of the head.

We have addressed different forms of the registration problem with the common logic of using the minimal information of the binary images. The main registration feature is the contour or the surface and for this reason we present the results in 3D with surface renderings. We have presented in these chapters several points which are considered novel in the field of medical image registration.

7.2 Novelty of the approach

We introduced a registration function , the weighted variance of the ratio and were able to make it work with areas and volumes from MR , Xray, Spect, CT images with 1 dimensional lines of projections and with small local areas for non rigid registration of binary images. The algorithm for minimization of the registration of the registration function is able to overcome local minima and it is working similar to Powell and simulated annealing methods. Starting with the idea of exploiting with wavelets the signal area information in compressed images which was presented in RSNA 1994 we have developed classification and segmentation schemes like the hierarchical fuzzy k – means to exploit the areas with greater information content. The convergence of the algorithm in some type of problems is faster than the Mutual Information methods. The accuracy with the use of projections is better than the Mutual Information methods. We have used reduced dimension images and also with the deterioration in resolution we maintained the accuracy. The volume based 3D registration method works efficiently with the presence of noise. The area based technique has been applied for rigid and for non rigid local registration. Compared to principal axes the method is accurate for the medical images of the head using the 1D projections and very fast for square objects since only x and y projections are used. The accuracy of the method for rigid registration is below 0,5 degrees and 0,5 voxels.

7.3 Theoretical aspects of literature in image registration

Medical image registration literature focuses on the solution of a wide range of problems for the solution to be applied for 2D-3D, rigid , non rigid image registration. We have presented the main categories of feature based techniques.

Correlation methods register medical images by maximizing a similarity or minimizing a disparity criterion between images. The similarity or disparity criterion used is signal intensity based , and it is maximized or minimized iteratively. The methods that are based on correlative criteria is an active research field. The cross correlation techniques use signal intensities have been reported to work well with monomodality image registration but the have recently incorporated in the solution of 2D to 3D registration, rigid and non rigid problems. The errors reported are less than 0,74degrees and 1mm. The ratio image uniformity criterion was introduced by Woods et al [35,36]. To align the two images , the algorithm calculates the ratio of one image to the other on a voxel per voxel basis and then iteratively minimizes the variance of this ratio. The method is based on the ideal assumption that in the case that the images are registered, the values of the voxels in one image , can result by multiplying the voxels in the other image with a constant multiplicative factor.

Surface matching methods register images by using the anatomic surface models of the two images. The surface matching methods have a high degree of sophistication but due to the sensitivity to noise they have been reported to work as preprocessing step to signal intensity based methods.

The principal axes transformation is known from the theory of rigid bodies. A rigid body may be located using the position of the center of its mass and the orientation of its principal axes with respect to its center of mass. The principal axes method is simple and fast and for this reason the are presented as a method of reference. They also have the characteristic of using axes as means of registration which is similar with the 1D projections used for the 2D registration in this thesis.

The Mutual Information is a measure of registration based on Entropy. Mutual Information is based on the fact that when two images are registered the joint histogram shows clusters of overlapping similar intensities with sharp edges. The Mutual Information method is in the general class of probabilistic models based methods and are used for rigid, non rigid and 2D to 3D registration. They have been implemented in parallel for non rigid registration.

7.4 Algorithm and experimental results for registration using areas and volumes

The subject of this thesis is the development of a novel iterative method for two and three dimensional image registration. The processing steps of the method use a fuzzy c-means classification algorithm, a trilinear interpolation routine, a thresholding routine, and an iteration loop based on Chebyshev's approximation theory. For the application of fuzzy c-means in this thesis an hierarchical form of the algorithm has been programmed. In order to create the cubic voxel intensities we programmed a trilinear interpolation routine. Thresholding is performed with the use of the centroids of the clusters computed by the fuzzy c-means classification. We programmed a novel iteration loop which works like the Powell method and also deregisters and and brings back orderly the images using the Chebyshev polynomials in a similar way to simulated annealing theoretical paradigm.

Using the algorithm for image registration , a total of 200 two dimensional experiments for alignment of a T2 to a T1 axial MR scan were performed. A standard experimental protocol with standard geometric transformations with a wide range of values was developed for the evaluation of the method. The three dimensional registration accuracy of the method was tested with a total of 240 three dimensional registration experiments. A protocol for the three dimensional experiments also includes a standard set of transformations with wide range of values in the 3D space.

We have presented the main characteristics of the method for registration experiments of 2D and 3D images rigidly using binary areas and volumes. We have chosen experimentally the number of Chebyshev points for 2D and 3D registration. We presented the registration function curves as they are extrapolated per iteration. We performed worst case registration analysis and we showed that the error is within the 1 degree and 1 voxel and below 0,5 degrees and 0,5 voxels on average. When an even number of Chebyshev points is used we apply the maximum iteration rule to define the final error which oscilates around the correct registration position. We described the main registration procedure as it was implemented in the department of Musculoskeletal Radiology of The Cleveland Clinic Foundation. We used surface renderings to present the final results of the correct registration position. We compared half with full resolution and we found out that the method works adequately in half resolution experiments compared to full resolution ones. We performed 2D non rigid body experiments and we showed that the method works locally with large elastic deformations of binary images.

The method has the advantage compared to signal intensity methods that it is able to perform multimodality image registration. Compared to surface fitting methods the method is not affected by noise which allows the incorporation of the 2D projection algorithm into a surface fitting registration scheme. The registration function works with non rigid giving a unique solution for small areas of local effect. Compared to Mutual Information methods for rigid registration the method has been shown not to be affected by misregistrations caused by local minima and to be able to maintain an accuracy of better than 0,5 degrees and 0,5 pixels. The method has also been shown to not be affected by resolution.

7.5 Algorithm and experimental results for registration using 1d and 2d projections

A new robust method for 2D and 3D rigid registration using binary projections was developed and tested using MR scans of the head.

For the 2D case the accuracy of the method is better than 1degree and 1 pixel. In most cases the error is less than 0.5 deg and 0.5 pixels. The preprocessing of the images must be careful not to produce non-registrable areas in the contours to be registered (avoid for example repetitive median filtering in one of the two images). No interpolation is necessary for 2D registration with the use of binary projections. The registration function is not dependent on signal intensity distributions. The method is directly applicable to binary images and contours. The method is fast with a typical time of 1-2sec running on an HP A6240 Intel Quad Core 2,4GHz PC with 2GByte ram.

The first results of a 3D projection based method have been given in this report. The accuracy of the method is better than 0.5 degrees for rotations and 0.5 voxels for translations. Compared to the full volume method the method takes more steps to converge towards the correct registration position but remains as accurate. Minimal preprocessing of the images prior to registration is needed. The method is more accurate and robust than standard MI methods. It converges to stable final positions independent of the initial misregistration.

7.6 Future work

Future work may include the following plans:

- 3D registration using 1D binary projections. We can use very few contour points in order to register the 3D images using the 1D projections.
- Production of a journal paper with reduced dimension images. We can experiment with curved cuts in order to register the images.
- Application of the non rigid registration method on the joint histogram. We can apply the registration function on the joint histogram in order to perform non rigid registration.
- 2D/3D application based on the 3D registration using 2D binary projections. We can use an international set database [24] in order to perform 2D/3D registration.

- Evaluation of the parallel performance of the algorithm as the algorithm scales from Chebyshev points to 1d projections. The algorithm shows tolerable scalability with the increase of the processors but further studies are needed for evaluation of the parallel performance of the method.
- Creation of a system which includes compression, segmentation, surface rendering , 2d and 3d registration. This requires GUI based programming for incorporation of the algorithms.

REFERENCES

[1] Zitova B, Flusser J, "Image Registration Methods: A Survey", Image and Vision Computing 21 (2003) pp977-1000.

[2] Maurer CR, Fitzpatrick JM. A review of medical image registration. In: Maciunas RJ, ed. Interactive Image-Guided Neurosurgery. Park Ridge, IL: American Association of Neurological Surgeons, 1994;17-44. Neurosurgical Topics.

[3] Toga AW, Banerjee PK. Registration revisited. J Neurosci Methods 1993;48(1-2):1-13.

[4] Evans AC, Peters TM, Collins DL, Neelin P, Gabe C. Image registration based on discrete anatomic structures. In: Maciunas RJ, ed. Interactive Image-Guided Neurosurgery. Park Ridge, IL: American Association of Neurological Surgeons 1994;63-80. Neurosurgical Topics.

[5] Weber DA, Ivanovic M. Correlative image registration. Semin Nucl Med 1994;24(4):311-323.

[6] Slomka PJ & Baum RP, "Multimodality Image Registration with Software: state-of-the-art", Eur J Nucl Med Mol Imaging (2009) 36 (Suppl 1):S44–S55.

[7] West J, Fitzpatrick JM, Wang MY, Dawant BM, Maurer CR et Al. "Retrospective Intermodality Registration Techniques for Images of the Head: Surface-based versus Volume-Based", IEEE Transactions on Medical Imaging, Vol. 18, No.2, February 1999, pp144-150.

[8] Bardera A, Feixas M, Boada I, and Sbert M. "High-Dimensional Normalized Mutual Information for Image Registration Using Random Lines", Third International Workshop on Biomedical Image Registration(WBIR) (2006),LNCS 4057, pp 264-271.

[9] Liao YL, Sun YN, Guo WY, Chou YH, Hsieh JC et Al, "A Comparison between the Surface-Based and Mutual-Information-Based Methods for Co-registering SPECT and MR Images" Proceedings of the 29th Annual International Conference of the IEEE EMBS, Cité Internationale, Lyon, France, August 23-26, 2007, pp 868-871

[10] Staring M, van der Heide UA, Klein S, Viergever MA, and Pluim JPW, "Registration of Cervical MRI Using Multifeature Mutual Information", IEEE Transactions on Medical Imaging, Vol. 28, No. 9, Sept 2009 pp. 1412-1421(electronic pre-publication)

[11] Pluim JPW, Maintz JBA, Viergever MA, " Image Registration by Maximization of Combined Mutual Information and Gradient Information" MICCAI 2000: 452-461

[12] Loeckx D, Slagmolen P, Maes F, Vandermeulen D, and Suetens P, "Nonrigid Image Registration Using Conditional Mutual Information", IEEE Transactions on Medical Imaging, Vol. 29, No. 1, Jan 2010 pp.19-29 (electronic pre-publication)

[13] Lu X, Zhang S, Su H, Chen Y," Mutual Information-Based Multimodal Image Registration Using a Novel Joint Histogram Estimation", Computerized Medical Imaging and Graphics 32 (2008) 202–209

[14] Roche A, Pennec X, Malandain G and Ayache N, "Rigid Registration of 3-D Ultrasound with MR images: A New Approach Combining Intensity and Gradient Information", IEEE Transactions on Medical Imaging, Vol 20, No. 10, October 2001, pp1038-1049.

[15] van de Kraats EB, Penney GP, Tomazevic D, van Walsum T and Niessen WJ, "Standardized Evaluation Methodology for 2D-3D Registration", IEEE Transactions on Medical Imaging, Vol. 24, No.9, Sept 2005, pp 1177-1189.

[16] McLaughlin RA, Hipwell J, Hawkes DJ, Noble JA, Byrne JV et. al. , "A Comparison of a Similarity-Based and a Feature-Based 2D-3D Registration Method for Neurointerventional Use", IEEE Transactions on Medical Imaging, Vol.24, No.8 August 2005, pp1058-1066.

[17] Maurer CR, Maciunas RJ, Fitzpatrick JM, " Registration of Head CT Images to Physical Space using a Weighted Combination of Points and Surfaces", IEEE Transactions on Medical Imaging, Vol. 17, No. 5, October 1998, pp. 753-761.

[18] Turkington TG, Jaszczak RJ, Pelizzari CA, Harris CC, MacFall JR, Hoffman JM, Coleman RE. Accuracy of registration of PET, SPECT and MR images of a brain phantom. J of Nucl Med 1993;34(9):1587-1594.

[19] Kall BA, Goerss SJ, Kelly PJ, Stiving SO. Three-dimensional display in the evaluation and performance of neurosurgery without a stereotactic frame: More than a pretty picture? Stereotact Funct Neurosurg 1994;63:69-75.

[20] Strother SC, Anderson JR, Xu XL, Liow JS, Bonar DC, Rottenberg DA. Quantitative comparisons of image registration techniques based on high-resolution MRI of the brain. J Comput Assist Tomogr 1994;18(6):954-962.

[21] Kapouleas I, Alavi A, Alves WM, Gur RE, Weiss DW. Registration of three-

dimensional MR and PET images of the human brain without markers. Radiology 1991;181:731-739.

[22] Pelizzari CA, Levin DN, Chen GTY, Chen CT. Image registration based on anatomic surface matching. In: Maciunas RJ, ed. Interactive Image-Guided Neurosurgery. Park Ridge, IL: American Association of Neurological Surgeons 1994;47-62. Neurosurgical Topics.

[23] Venot A, Lebruchec JF, Roucayrol JC. Anew class of similarity measures for robust image registration. Computer Vision, Graphics, and Image Processing 1984;28:176-184.

[24] Primož Markelj, Boštjan Likar, Franjo Pernuš, A New Image Database for 3D/2D Registration Based on the Visible Human Data Set, Biomedical Image Registration Lecture Notes in Computer Science Volume 6204, 2010, pp 151-160

[25] A. Guéziec, P. Kazanzides, B. Williamson, and R. H. Taylor,“Anatomybased registration of CT-scan and intraoperative X-rayimages for guiding a surgical robot,” IEEE Trans. Med. Imag., vol. 17,pp. 715–728, Oct. 1998.

[26] D. B. Russakoff, T. Rohlfing, A. Ho, D. H. Kim, R. Shahidi, J. R. AdlerJr., and C. R. Maurer Jr. et al., “Evaluation of intensity-based 2D-3D spine image registration using clinical gold-standard data,” in Lecture Notes in Computer Science, J. C. Gee et al., Eds. Berlin, Germany: Springer-Verlag, 2003, vol. 2717, WBIR 2003, pp. 151–160.

[27] M. Vermandel, N. Betrouni, G. Palos, J. Y. Gauvrit, C. Vasseur, and J. Rousseau, “Registration, matching, and data fusion in 2D/3D medical imaging: Application to DSA and MRA,” in Lecture Notes in Computer Science, R. Ellis and T. Peters, Eds: Springer-Verlag, 2003, vol. 2878,
Medical Image Computing and Computer Assisted Intervention – MICCAI 2003, pp. 778–785.

[28] J. V. Byrne, C. Colomina, J. Hipwell, T. Cox, J. A. Noble, G. P. Penney, and D. J. Hawkes, “An assessment of a technique for 2D-3D registration
of cerebral intra-arterial angiography,” Br. J. Radiol., vol. 77, no. 914, pp. 123–128, 2004.

[29] S. A. M. Baert, G. P. Penney, T. van Walsum, and W. J. Niessen, “Precalibration versus 2D-3D registration for 3D guide wire display in endovascular interventions,” in Lecture Notes in Computer Science, C. Barillot, D. Haynor, and P. Hellier, Eds. New York: Springer, 2004, pt. 2, vol.
3217, Medical Image Computing and Computer-Assisted Intervention- MICCAI 2004, pp. 577–584.

[30] R. A. McLaughlin, J. Hipwell, D. J. Hawkes, J. A. Noble, J. V. Byrne,and T. Cox, “A comparison of 2D-3D intensity-based registration and feature-based registration for neurointerventions,” in Lecture Notes in Computer Science, T. Dohi and R. Kikinis, Eds: Springer, 2002, pt. 2, vol. 2489, Medical Image Computing and Computer-Assisted Intervention– MICCAI 2002, pp. 517–524.

[31] Y. Masutani, T. Dohi, F. Yamane, H. Iseki, and K. Takakura, “Interactive virtualized display system for intravascular neurosurgery,” in Lecture Notes in Computer Science, J. Troccaz, W. Grimson, and R. Mösges, Eds: Springer, 1997, vol. 1205, CVRMed-MRCAS ’97, pp. 427–435.

[32] Medical Image Processing Group 3D Viewnix Software System University of Pennsylvania 2014

[33] Darko Zikic, Ali Kamen, Nassir Navab: Unifying Characterization of Deformable Registration Methods Based on the Inherent Parametrization. WBIR 2010: 161-172

[34] Herbin M, Venot A, Devaux JY, Walter E, Lebruchec JF, Dubertret L, Roucayrol JC. Automated registration of dissimilar images: Application to medical imagery. Computer Vision, Graphics, and Image Processing 1989;47:77-88.

[35] Woods RP, Cherry SR, Mazziotta JC. Rapid automated algorithm for aligning and reslicing PET images. J Comput Assist Tomogr 1992;16(4):620-633.

[36] Woods RP, Mazziotta JC, Cherry SR. MRI-PET registration with automated algorithm. J Comput Assist Tomogr 1993;17(4):536-546.

[37] Junck L, Moen JG, Hutchins GD, Brown MB, Kuhl DE. Correlation methods for the centering, rotation, and alignment of functional brain images. J Nucl Med 1990;31(7):1220-1226.

[38] Gerlot-Chiron P, Bizais Y. Definition and evaluation of a surface overlap criterion for medical image registration. Prog Clin Biol Res 1991;363: 429-442.

[39] Gerlot-Chiron P, Bizais Y. Registration of multimodality medical images using a region overlap criterion. Computer Vision, Graphics, and Image Processing: Graphical Models and Image Processing 1992;54(5):396-406.

[40] Non Rigid 2D-3D Medical Image Registration using Markov Random Fields Enzo Ferrante and Nikos Paragios 16th International Conference on Medical Image Computing and Computer Assisted Intervention MICCAI 2013 Nagoya : Japan (2013).

[41] Press WH, Teukolsky SA, Vetterling WT, Flannery BP. Numerical recipes in C. The art of scientific computing. 2nd ed. New York: Cambridge University Press, 1992.

[42] Pelizzari CA, Chen GT, Spelbring DR, Weichselbaum RR, Chen CT. Accurate three dimensional registration of CT, PET and/or MR images of the brain. J Comput Assist Tomogr 1989;13(1):20-26.

[43] Rusinek H, Tsui WH, Levy AV, Noz ME, de Leon MJ. Principal axes and surface fitting methods for three-dimensional image registration. J Nucl Med 1993;34(11):2019-2024.

[44] Turkington TG, Hoffman JM, Jaszczak RJ, MacFall JR, Harris CC, Kilts CD, Pelizzari CA, Coleman RE. Accuracy of surface fit registration for PET and MR brain images using full and incomplete brain surfaces. J Comput Assist Tomogr 1995;19(1):117-124.

[45] Alpert NM, Bradshaw JF, Kennedy D, Correia JA. The principal axes transformation - A method for image registration. J Nucl Med 1990;31(10):1717-1722.

[46] Slomka PJ, Hurwitz GA, Stephenson J, Cradduck T. Automated alignment and sizing of myocardial stress and rest scans to three-dimensional normal templates using an image registration algorithm. J Nucl Med 1995;36(6):1115-1122.

[47] Pluim JPW, Maintz JBA, Viergever MA, “Mutual-Information-Based Registration of Medical Images: A Survey”, IEEE Transactions on Medical Imaging, Vol. 22, No. 8, August 2003, pp986-1004.

[48] A Novel Subsampling Method for 3D Multimodality Medical Image Registration Based on Mutual Information Maryam Zibaeifard, Mohammad Rahmati Amirkabir/Rlectrical Engineering/Vol41/No1/Spring 2009/ Archive of SID www.sid.ir

[49] Parallel implementation of Total – FETI DDM with application to medical image registration. Michal Merta, Alena Vasatova, Vaclav Hapla and David Horak

[50] A Probabilistic Approach to Non Rigid Medical Image Registration , Ivor JA Simpson D.Phil Thesis University of Oxford 2012

[51] V.R.S Mani, Dr S. Arivazhagan , Survey of Medical Image Registration, Journal of Biomedical Engineering and Technology , 2013, Vol 1, No 2, 8-25.

[52] Fimmel E, Giannerini S, Gonzalez DL, Strüngmann L. Circular codes, symmetries and transformations. J Math Biol. 2014 Jul 10. [Epub ahead of print]

[53] Avants BB, Tustison NJ, Stauffer M, Song G, Wu B, Gee JC. . The Insight ToolKit image registration framework. Front Neuroinform. 2014 Apr 28;8:44

[54] Rigas G, Nikou C, Goletsis Y, Fotiadis DI. Hierarchical similarity transformations between Gaussian mixtures. IEEE Trans Neural Netw Learn Syst. 2013 Nov;24(11):1824-35

[55] Souza CE, Huguenin JA, Khoury AZ. Topological phase structure of vector vortex beams. J Opt Soc Am A Opt Image Sci Vis. 2014 May 1;31(5):1007-12

[56] Watanabe A, Slice DE. . The utility of cranial ontogeny for phylogenetic inference: a case study in crocodylians using geometric morphometrics. J Evol Biol. 2014 Jun;27(6):1078-92

[57] Gong RH, Güler Ö, Kürklüoglu M, Lovejoy J, Yaniv Z. Interactive initialization of 2D/3D rigid registration. Med Phys. 2013 Dec;40(12):121911

[58] Noorda YH, Bartels LW, Huisman M, Nijenhuis RJ, van den Bosch MA, Pluim JP. Registration of CT to pre-treatment MRI for planning of MR-HIFU ablation treatment of painful bone metastases. Phys Med Biol. 2014 Aug 7;59(15):4167-79.

[59] Luan S, Sun L, Hu L, Hao A, Li C, Tang P, Zhang L, Du H. Projective invariant biplanar registration of a compact modular orthopaedic robot. Biomed Mater Eng. 2014;24(1):511-8

[60] Gefen S, Kiryati N, Bertrand L, Nissanov J. , "Planar –to-Curved-Surface Image Registration" Conference on Computer Vision and Pattern recognition Workshop , pp 72 2006.

[61] Pilutti D, Strumia M, Hadjidemetriou S. Bi-modal Non-rigid Registration of Brain MRI Data with Deconvolution of Joint Statistics. IEEE Trans Image Process. 2014 Jul 8. [Epub ahead of print]

[62] Eckhard T, Eckhard J, Valero EM, Nieves JL. Nonrigid registration with free-form deformation model of multilevel uniform cubic B-splines: application to image registration and distortion correction of spectral image cubes. Appl Opt. 2014 Jun 10;53(17):3764-72.

[63] Toennies K, Rak M, Engel K. Deformable part models for object detection in medical images. Biomed Eng Online. 2014;13 Suppl 1:S1

[64] Gruslys A, Acosta-Cabronero J, Nestor P, Williams G, Ansorge R. A New Fast

Accurate Non-Linear Medical Image Registration Program Including Surface Preserving Regularisation. IEEE Trans Med Imaging. 2014 Jun 23. [Epub ahead of print]

[65] Deslee G, Klooster K, Hetzel M, Stanzel F, Kessler R, Marquette CH, Witt C, Blaas S, Gesierich W, Herth FJ, Hetzel J, van Rikxoort EM, Slebos DJ. Lung volume reduction coil treatment for patients with severe emphysema: a European multicentre trial. Thorax. 2014 Jun 2. [Epub ahead of print]

[66] Rodriguez A, Fernandez-Lozano C, Dorado J, Rabuñal JR. . Two-dimensional gel electrophoresis image registration using block-matching techniques and deformation models. Anal Biochem. 2014 Jun 1;454:53-9.

[67] Papiez BW, Heinrich MP, Risser L, Schnabel JA. Complex lung motion estimation via adaptive bilateral filtering of the deformation field. Med Image Comput Comput Assist Interv. 2013;16(Pt 3):25-32

[68] Kossert K, Grau Carles A, Nähle OJ. Improved Čerenkov counting techniques based on a free parameter model. Appl Radiat Isot. 2014 Apr;86:7-12.

[69] Chenoune Y, Bouaoune Y, Deléchelle E, Petit E, Garot J, Rahmouni A. MR/CT multimodal registration of short-axis slices in CT volumes. Conf Proc IEEE Eng Med Biol Soc. 2007;2007:4496-9.

[70] Parker JG, Mair BA, Gilland DR. Respiratory motion correction in gated cardiac SPECT using quaternion-based, rigid-body registration. Med Phys. 2009 Oct;36(10):4742-54.

[71] Rouhani M, Sappa AD. The richer representation the better registration. IEEE Trans Image Process. 2013 Dec;22(12):5036-49.

[72] Oliveira FP, Faria DB, Tavares JM. Automated segmentation of the incus and malleus ossicles in conventional tri-dimensional computed tomography images. Proc Inst Mech Eng H. 2014 Aug 1. pii: 0954411914546123. [Epub ahead of print]

[73] Lee J, Lyu I, Styner M. Multi-atlas segmentation with particle-based group-wise imageregistration. Proc Soc Photo Opt Instrum Eng. 2014 Mar 21

[74] Chen M, Lang A, Ying HS, Calabresi PA, Prince JL, Carass A. Analysis of macular OCT images using deformable registration. Biomed Opt Express. 2014 Jun 11;5(7):2196-214.

[75] Roy S, Carass A, Jog A, Prince JL, Lee J. MR to CT Registration of Brains using

Image Synthesis. Proc SPIE. 2014 Mar 21;9034. pii: spie.org/Publications/Proceedings/Paper/10.1117/12.2043954.

[76] Zikic D, Glocker B, Criminisi A.Encoding atlases by randomized classification forests for efficient multi-atlaslabel propagation.Med Image Anal. 2014 Jul 2. pii: S1361-8415(14)00104-2. doi: 10.1016/j.media.2014.06.010. [Epub ahead of print]

[77] Zhang Y, Chang L, Ceritoglu C, Skranes J, Ernst T, Mori S, Miller MI, Oishi K. A Bayesian approach to the creation of a study-customized neonatal brainatlas. Neuroimage. 2014 Jul 12;101C:256-267. doi: 10.1016/j.neuroimage.2014.07.001. [Epub ahead of print]

[78] Rusu M, Bloch BN, Jaffe CC, Genega EM, Lenkinski RE, Rofsky NM, Feleppa E, Madabhushi A. Prostatome: A combined anatomical and disease based MRI atlas of the prostate. Med Phys. 2014 Jul;41(7):072301. PMID:

[79] Reda FA, Noble JH, Labadie RF, Dawant BM. An artifact-robust, shape library-based algorithm for automatic segmentation of inner ear anatomy in post-cochlear-implantation CT. Proc Soc Photo Opt Instrum Eng. 2014 Mar 21;9034:90342V.

[80] Brouwer CL, Kierkels RG, van T Veld AA, Sijtsema NM, Meertens H. The effects of computed tomography image characteristics and knot spacing on the spatial accuracy of B-pline deformable image registrationin the head and neck geometry.Radiat Oncol. 2014 Jul 29;9(1):169. [Epub ahead of print]

[81] Pearlman PC, van Deurzen MH, Pluim JP, Grolman W. Coregistration of Preoperative Computed Tomography and Intraoperative Three-Dimensional Rotational X-Ray Images for Cochlear Implant Surgical Evaluation. Otol Neurotol. 2014 Jul 23. [Epub ahead of print]

[82] Stidd DA, Wewel J, Ghods AJ, Munich S, Serici A, Keigher KM, Theessen H, Moftakhar R, Lopes DK. Frameless neuronavigation based only on 3D digital subtraction angiography using surface-based facial registration.J Neurosurg. 2014 Jul 18:1-6. [Epub ahead of print]

[83] Pettersson A, Kero T, Söderberg R, Näsström K.Accuracy of virtually planned and CAD/CAM-guided implant surgery on plastic models. J Prosthet Dent. 2014 Jun 30. pii: S0022-3913(14)00262-5. doi: 10.1016/j.prosdent.2014.01.029. [Epub ahead of print]

[84] Roy S, Carass A, Jog A, Prince JL, Lee J. MR to CT Registration of Brains using Image Synthesis.Proc SPIE. 2014 Mar 21;9034. pii: spie.org/Publications/Proceedings/Paper/10.1117/12.2043954.

[85] Daga P, Pendse T, Modat M, White M, Mancini L, Winston GP, McEvoy AW, Thornton J, Yousry T, Drobnjak I, Duncan JS, Ourselin S.
Susceptibility artefact correction using dynamic graph cuts: Application to neurosurgery. Med Image Anal. 2014 Jul 5;18(7):1132-1142. doi: 10.1016/j.media.2014.06.008. [Epub ahead of print]

[86] Farnia P, Ahmadian A, Shabanian T, Serej ND, Alirezaie J.
Brain-shift compensation by non-rigid registration of intra-operative ultrasound images with preoperative MR images based on residual complexity.
Int J Comput Assist Radiol Surg. 2014 Jul 4. [Epub ahead of print]

[87] Ou Y, Akbari H, Bilello M, Da X, Davatzikos C. Comparative Evaluation of Registration Algorithms in Different BrainDatabases with Varying Difficulty: Results and Insights.IEEE Trans Med Imaging. 2014 Jun 13. [Epub ahead of print]

[88] Piella G.Diffusion maps for multimodal registration.
Sensors (Basel). 2014 Jun 16;14(6):10562-77. doi: 10.3390/s140610562.
PMID:

[89] Bueno JM, Skorsetz M, Palacios R, Gualda EJ, Artal PMultiphoton imaging microscopy at deeper layers with adaptive optics control of spherical aberration. J Biomed Opt. 2014 Jan;19(1):011007. doi: 10.1117/1.JBO.19.1.011007.

[90] Edwards AR, Chalam KV, Bressler NM, Glassman AR, Jaffe GJ, Melia M, Saggau DD, Plous OZ. Reproducibility of Spectral-Domain Optical Coherence Tomography Retinal Thickness Measurements and Conversion to Equivalent Time-Domain Metrics in Diabetic Macular Edema.
Diabetic Retinopathy Clinical Research Network Writing Committee, Bressler SB, JAMA Ophthalmol. 2014 Jul 24. doi: 10.1001/jamaophthalmol.2014.1698. [Epub ahead of print]

[91] Ramaswamy G, Lombardo M, Devaney N.Registration of adaptive optics corrected retinal nerve fiber layer (RNFL) images.Biomed Opt Express. 2014 May 22;5(6):1941-51. doi: 10.1364/BOE.5.001941. eCollection 2014 Jun 1.

[92] Zheng Y, Xiao R, Wang Y, Gee JC.A generative model for OCT retinal layer segmentation by integrating graph-based multi-surface searching and image registration. Med Image Comput Comput Assist Interv. 2013;16(Pt 1):428-35.

[93] Liu JJ, Grulkowski I, Kraus MF, Potsaid B, Lu CD, Baumann B, Duker JS, Hornegger J, Fujimoto JG. In vivo imaging of the rodent eye with swept source/Fourier domain OCT.Biomed Opt Express. 2013 Feb 1;4(2):351-63. doi: 10.1364/BOE.4.000351.

Epub 2013 Jan 29.

[94] Chang CH, Lei YN, Ho YH, Sung YH, Lin TS Predicting the holistic force-displacement relation of the periodontal ligament: in-vitro experiments and finite element analysis. Biomed Eng Online. 2014 Jul 30;13(1):107. [Epub ahead of print]

[95] Kang SH, Lee JW, Lim SH, Kim YH, Kim MK. Dental image replacement on cone beam computed tomography with three-dimensional optical scanning of a dental cast, occlusal bite, or bite tray impression. Int J Oral Maxillofac Surg. 2014 Jul 8. pii: S0901-5027(14)00224-0. doi: 10.1016/j.ijom.2014.06.009. [Epub ahead of print]

[96] Chandra A, Lin T, Tribble MB, Zhu J, Altman AR, Tseng WJ, Zhang Y, Akintoye SO, Cengel K, Liu XS, Qin L. PTH1-34 alleviates radiotherapy-induced local bone loss by improving osteoblast and osteocyte survival.
Bone. 2014 Jul 1;67C:33-40. doi: 10.1016/j.bone.2014.06.030. [Epub ahead of print]

[97] Pettersson A, Kero T, Söderberg R, Näsström K.
Accuracy of virtually planned and CAD/CAM-guided implant surgery on plastic models. J Prosthet Dent. 2014 Jun 30. pii: S0022-3913(14)00262-5. doi: 10.1016/j.prosdent.2014.01.029. [Epub ahead of print]

[98] Almukhtar A, Ju X, Khambay B, McDonald J, Ayoub A.
Comparison of the accuracy of voxel based registration and surface basedregistration for 3D assessment of surgical change following orthognathic surgery.PLoS One. 2014 Apr 2;9(4):e93402. doi: 10.1371/journal.pone.0093402. eCollection 2014.

[99] Hadjiiski L, Zhou C, Chan HP, Chughtai A, Agarwal P, Kuriakose J, Kazerooni E, Wei J, Patel S.Coronary CT angiography (cCTA): automated registration of coronary arterial trees from multiple phases.Phys Med Biol. 2014 Jul 31;59(16):4661-4680. [Epub ahead of print]

[100] Alizadeh Sani Z, Shalbaf A, Behnam H, Shalbaf R. Automatic Computation of Left Ventricular Volume Changes Over a CardiacCycle from Echocardiography Images by Nonlinear Dimensionality Reduction.J Digit Imaging. 2014 Jul 25. [Epub ahead of print]

[101] Hsieh MM, Fitzhugh CD, Weitzel RP, Link ME, Coles WA, Zhao X, Rodgers GP, Powell JD, Tisdale JF. Nonmyeloablative HLA-matched sibling allogeneic hematopoietic stem cell transplantation for severe sickle cell phenotype.
JAMA. 2014 Jul 2;312(1):48-56. doi: 10.1001/jama.2014.7192.

[102] Santos J, Chaudhari AJ, Joshi AA, Ferrero A, Yang K, Boone JM, Badawi RD. Non-rigid registration of serial dedicated breast CT, longitudinal dedicatedbreast CT and PET/CT images using the diffeomorphic demons method. Phys Med. 2014 Jul 9. pii: S1120-1797(14)00144-6. doi: 10.1016/j.ejmp.2014.06.040.

[103] Ebrahimi M, Siegler P, Modhafar A, Holloway CM, Plewes DB, Martel AL. Using surface markers for MRI guided breast conserving surgery: a feasibility survey. Phys Med Biol. 2014 Apr 7;59(7):1589-605. doi: 10.1088/0031-9155/59/7/1589. Epub 2014 Mar 10.

[104] Okamoto T, Onda S, Yanaga K, Suzuki N, Hattori A. Clinical application of navigation surgery using augmented reality in the abdominal field.Surg Today. 2014 Jun 6. [Epub ahead of print]

[105] Zhao Q, Chou CR, Mageras G, Pizer S.Local Metric Learning in 2D/3D Deformable Registration With Application in the Abdomen.IEEE Trans Med Imaging. 2014 Apr 22. [Epub ahead of print]

[106] Spinczyk D, Karwan A, Copik M.Methods for abdominal respiratory motion tracking.Comput Aided Surg. 2014;19(1-3):34-47. doi: 10.3109/10929088.2014.891657. Epub 2014 Apr 10.

[107] Neshat H, Cool DW, Barker K, Gardi L, Kakani N, Fenster A. A 3D ultrasound scanning system for image guided liver interventions. Med Phys. 2013 Nov;40(11):112903. doi: 10.1118/1.4824326.

[108] Yang W, Fraass BA, Reznik R, Nissen N, Lo S, Jamil LH, Gupta K, Sandler H, Tuli R. Adequacy of inhale/exhale breathhold CT based ITV margins and image-guided registration for free-breathing pancreas and liver SBRT. Radiat Oncol. 2014 Jan 9;9:11. doi: 10.1186/1748-717X-9-11.

[109] Velec M, Moseley JL, Brock KK. Simplified strategies to determine the mean respiratory position for liverradiation therapy planning. Pract Radiat Oncol. 2014 May-Jun;4(3):160-6. doi: 10.1016/j.prro.2013.07.001. Epub 2013 Aug 8.

[110] Seif M, Lu H, Boesch C, Reyes M, Vermathen P. Image registration for triggered and non-triggered DTI of the humankidney: Reduced variability of diffusion parameter estimation.J Magn Reson Imaging. 2014 Jun 25. doi: 10.1002/jmri.24671

[111] Hodneland E, Hanson EA, Lundervold A, Modersitzki J, Eikefjord E, Munthe-

Kaas AZ. Segmentation-driven image registration- application to 4D DCE-MRI recordings of the moving kidneys. IEEE Trans Image Process. 2014 May;23(5):2392-404.

[112] Schneider C, Nguan C, Longpre M, Rohling R, Salcudean S.Motion of the kidney between preoperative and intraoperative positioning.IEEE Trans Biomed Eng. 2013 Jun;60(6):1619-27. doi: 10.1109/TBME.2013.2239644. Epub 2013 Jan 11.

[113] Li G, Su H, Shang W, Tokuda J, Hata N, Tempany CM, Fischer GS.
A Fully Actuated Robotic Assistant for MRI-Guided Prostate Biopsy and Brachytherapy.Proc Soc Photo Opt Instrum Eng. 2013 Mar 12;8671:867117.

[114] Radtke JP, Kuru TH, Boxler S, Alt CD, Popeneciu IV, Huettenbrink C, Klein T, Steinemann S, Bergstraesser C, Roethke M, Roth W, Schlemmer HP, Hohenfellner M, Hadaschik BA.Comparative analysis of transperineal template-saturation prostate biopsy versus MRI-targeted biopsy with MRI-US fusion-guidance.
J Urol. 2014 Jul 28. pii: S0022-5347(14)04049-X. doi: 10.1016/j.juro.2014.07.098. [Epub ahead of print]

[115] Yamamoto H, Nir D, Vyas L, Chang RT, Popert R, Cahill D, Challacombe B, Dasgupta P, Chandra A. A Workflow to Improve the Alignment of Prostate Imaging with Whole-mount Histopathology.
Acad Radiol. 2014 Aug;21(8):1009-19. doi: 10.1016/j.acra.2014.04.015.

[116] Haq R, Aras R, Besachio DA, Borgie RC, Audette MA.,
3D lumbar spine intervertebral disc segmentation and compression simulation from MRI using shape-aware models.Int J Comput Assist Radiol Surg. 2014 Jul 5. [Epub ahead of print]

[117] Kotani T, Akazawa T, Sakuma T, Koyama K, Nemoto T, Nawata K, Yamazaki A, Minami S. Accuracy of Pedicle Screw Placement in Scoliosis Surgery: A Comparison between Conventional Computed Tomography-Based and O-Arm-Based Navigation Techniques. Asian Spine J. 2014 Jun;8(3):331-8. doi: 10.4184/asj.2014.8.3.331. Epub 2014 Jun 9.

[118] Reaungamornrat S, Wang AS, Uneri A, Otake Y, Khanna AJ, Siewerdsen JH.
Deformable image registration with local rigidity constraints for cone-beam CT-guided spine surgery.Phys Med Biol. 2014 Jul 21;59(14):3761-87. doi: 10.1088/0031-9155/59/14/3761. Epub 2014 Jun 17.

[119] Brazenor GA, Malham GM, Ballok ZE. Co-registration of isotope bone scan with CT scan and MRI in the investigation of spinal pathology.

J Clin Neurosci. 2014 May 2. pii: S0967-5868(14)00091-5. doi: 10.1016/j.jocn.2013.11.034. [Epub ahead of print]

[120] Peter R, Malinsky M, Ourednicek P, Lambert L, Jan J.
Novel registration-based framework for CT angiography in lower legs.
Med Biol Eng Comput. 2013 Oct;51(10):1079-89. doi: 10.1007/s11517-013-1085-y. Epub 2013 Aug 14.

[121] Matsuki K, Matsuki KO, Mu S, Kenmoku T, Yamaguchi S, Ochiai N, Sasho T, Sugaya H, Toyone T, Wada Y, Takahashi K, Banks SA.
In vivo 3D analysis of clavicular kinematics during scapular plane abduction: comparison of dominant and non-dominant shoulders.
Gait Posture. 2014;39(1):625-7. doi: 10.1016/j.gaitpost.2013.06.021. Epub 2013 Jul 18.

[122] Pizzagalli F, Auzias G, Delon-Martin C, Dojat M.
Local landmark alignment for high-resolution fMRI group studies: toward a fine cortical investigation of hand movements in human.
J Neurosci Methods. 2013 Aug 15;218(1):83-95. doi: 10.1016/j.jneumeth.2013.05.005. Epub 2013 May 31.

[123] Bezdek JC, Hall LO, Clarke LP. Review of MR image segmentation techniques using pattern recognition. Med Physics 1993;20(4):1033-1048.

[124] Hall LO, Bensaid AM, Clarke LP, Velthuizen RP, Silbiger ML, Bezdek JC. A comparison of neural networks and fuzzy clustering techniques in segmenting magnetic resonance images of the brain. IEEE Trans on Neural Networks 1992;2:672-683.

[125] Gonzalez RC, Woods RE. Digital image processing. Addison-Wesley Publishing Company, 1992.

[126] J.Kybic, P. Thevenaz, A. Nirkko, M.Unser, “Unwarping of unidirectionally distorted EPI images”, IEEE Transactions on Medical Imaging, vol.19, no.2, pp80-93, Feb. 2000.

[127] J. Kybic and M. Unser, “Fast parametric elastic image registration”, IEEE Transactions on Image Processing Vol 12, No 11, Nov 2003, pp 1427-1442

[128] Khamene A, Chisu R, Wein W, Navab N, Sauer F, “A Novel Projection-Based Approach for Medical Image Registration”, Third International Workshop on Biomedical Image Registration(WBIR) (2006) pp 247-256

[129] Chan HY, Chung ACS, “Efficient 3D-3D Vascular Registration Based on Multiple Orthogonal 2D Projections”, Second International Workshop on Biomedical Image Registration(WBIR) (2003), pp 301-310

[130] Cain SC, Hayat MM, Armstrong EE, “Projection Based Image Registration in the Presence of Fixed Pattern Noise”, IEEE Transactions on Image Processing, Vol. 10, No 12, December 2001, pp 1860-72.

[131] Kotsas P, Malasiotis S, Strintzis M, Piraino DW and Cornhill JF, “A Fast and Accurate Method for Registration of MR Images of the Head”, International Journal of Medical Informatics 52(1998) pp167-182.

[132] Kotsas P, “A New Automated Method for Three Dimensional Registration of MR Images of the Head”, Master’s Thesis, Dept. of Biomedical Engineering, The Ohio-State University.

[133] Kotsas P, “Non-Rigid Registration of Medical Images using an Automated Method”,EnformatikaVolume7,August2005,pp199-201

[134] Harvard University Medical Altlas 2014.

[135] Wong A, Orchard J, “Robust Multimodal Registration Using Local Phase Coherence Representations”, Journal of Signal Processing Systems, (2009)54,pp89-100.

[136] Yale University Bioimage Suite 2014

[137] Rohde GK, Aldroubi A, and Healy DM Jr, “Interpolation Artifacts in Sub-Pixel Image Registration”, IEEE Transactions on Image Processing, Vol. 18, No. 2, February 2009, pp333-345.

[138] Salvado O, Wilson DL, “Removal of Interpolation Artifacts in Similarity Surfaces”, Third International Workshop on Biomedical Image Registration(WBIR) (2006),LNCS 4057, pp43-49.

[139] Kotsas P, “2D Rigid Registration of MR Scans Using 1D Binary Projections” Enformatika Conference, Instabul Nov 2005, http://www.kotsas.gr

[140] Personal Site of Panos Kotsas: http://www.kotsas.gr 2014

[141] D.Marsh, “Applied geometry for computer graphics and CAD”, Second Edition, Springer(2005).

[142] G. P. Penney, J. Weese, J. A. Little, P. Desmedt, D. L. G. Hill, and D.J. Hawkes, “A comparison of similarity measures for use in 2-D-3-D medical image registration,” IEEE Trans. Med. Imag., vol. 17, no. 4, pp.586–595, Apr. 1998.

[143] J. H. Hipwell, G. P. Penney, R. A. McLaughlin, K. Rhode, P. Summers,T. C. Cox, J. V. Byrne, J. A. Noble, and D. J. Hawkes, “Intensity-based 2-D–3-D registration of cerebral angiograms,” IEEE Trans. Med. Imag., vol. 22, no. 11, pp. 1417–1426, Nov. 2003.

[144] Woods, Roger P.; Grafton, Scott T.; Watson, John D. G.; Sicotte, Nancy L.; Mazziotta, John C., Automated Image Registration: II. Intersubject Validation of Linear and Nonlinear Models Journal of Computer Assisted Tomography: January/February 1998 - Volume 22 - Issue 1 - pp 153-165

[145] J.Weese, G. P. Penney, P. Desmedt, T. M. Buzug, D. L. G. Hill, and D. J. Hawkes, “Voxel-based 2-D/3-D registration of fluoroscopy images and CT scans for image-guided surgery,” IEEE Trans. Inf. Technol. Biomed., vol. 1, no. 4, pp. 284–293, Dec 1997.

[146] H. Livyatan, Z. Yaniv, and L. Joskowicz, “Gradient-based 2-D/3-D rigid registration of fluoroscopic X-ray to CT,” IEEE Trans. Med. Imag., vol. 22, no. 11, pp. 1395–1406, Nov. 2003.

[147] J. Feldmar, N. Ayache, and F. Betting, “3D-2D projective registration of free-form curves and surfaces,” Comput. Vis. Image Understanding, vol.65, no. 3, pp. 403–424, 1997.

[148] Y. Kita, D. L. Wilson, and J. A. Noble, “Real-time registration of 3D cerebral vessels to X-ray angiograms,” in Lecture Notes in Computer Science, W. M. Wells, A. Colchester, and S. Delp, Eds. New York:Springer, 1998, vol. 1496, Medical Image Computing and Computer-Assisted
Intervention (MICCAI 98), pp. 1125–1133.

[149] S. Lavallée and R. Szeliski, “Recovering the position and orientation of free-form objects from image contours using 3D distance maps,” IEEE Trans. Pattern Anal. Mach. Intell., vol. 17, no. 4, pp. 378–390, Apr. 1995. [8] M. J. Murphy, “An automatic six-degree-of-freedom image registration algorithm for image-guided frameless stereotaxic radiosurgery,” Med. Phys., vol. 24, no. 6, pp. 857–866, 1997.

[150] MIT Slicer software package 2014.

[151] D. Tomazevic, B. Likar, T. Slivnik, and F. Pernus, “3-D/2-D registration of CT

and MR to X-ray images," IEEE Trans. Med. Imag., vol. 22, no. 11, pp. 1407–1416, Nov. 2003.

[152] G. P. Penney, P. G. Batchelor, D. L. G. Hill, D. J. Hawkes, and J.Weese,"Validation of a two- to three-dimensional registration algorithm for aligning preoperative CT images and intraoperative fluoroscopyimages," Med. Phys., vol. 28, no. 6, pp. 1024–1032, 2001.

[153]Intensity and Feature Based 3D Rigid Registration of Pre- and Intra-Operative MR Brain Scans Janneke Ansems (0535576) August, 2007 M.Sc. Thesis Technische Universiteit Eindhoven Department of Biomedical Engineering

[154] Kotsas P, Dodd TJ. Rigid registration of medical images using the 1D and 2D binary projections , Journal of Digital Imaging, Oct. 2011, Vol 24, Issue 5, pp913-925

[155] Moghe AA, Singhai J. Image Registration: A review of elastic registration methods applied to medical imaging. International Journal of Computer Applications Vol.70-No7,May2013,pp 6-11.